2003

Transmission of electromagnetic power through a biological medium

Ripan Das
Louisiana State University and Agricultural and Mechanical College

TRANSMISSION OF ELECTROMAGNETIC POWER THROUGH A BIOLOGICAL MEDIUM

A Thesis

Submitted to the Graduate Faculty of the
Louisiana State University and
Agricultural and Mechanical College
in partial fulfillment of the
requirements for the degree of
Master of Science in Electrical Engineering

in

The Department of Electrical and Computer Engineering

by
Ripan Das
B.Tech., Indian Institute of Technology, Kanpur, India, 2001
December, 2003

To my parents and teachers for their love and encouragement.

ACKNOWLEDGEMENTS

I would like to express my sincere thanks to all persons who directly or indirectly contributed to completion of my study here at Louisiana State University.

I would like to express my sincere gratitude and respect to my major professor, Dr. Pratul Ajmera for his technical guidance and support. His constructive criticism and advice are gratefully acknowledged.

I am thankful to the committee members, Dr. Martin Feldman and Dr. Ashok Srivastava for giving their valuable time to serve in the examination committee.

I would also like to thank all of my colleague in Integrated Microsystems Group at Louisiana State University for their suggestions and help.

Partial support for this work is received from NSF EPSCoR program through Louisiana Board of Reagents through grant # 0092001. Any opinions, findings and conclusions or recommendations expressed here are those of the author and do not necessarily reflect the views of NSF. The author sincerely acknowledges their support. Author acknowledges teaching assistantship support from the Department of Electrical and Computer Engineering at LSU.

TABLE OF CONTENTS

ACKNOWLEDGEMENTS…… iii

LIST OF TABLES……. vi

LIST OF FIGURES…… vii

SYMBOLS AND CONVENTION USED……. xii

ABSTRACT…… xiii

CHAPTER

1. INTRODUCTION……. 1
   - 1.1 Background……... 1
   - 1.2 Scope of Work……... 2
   - 1.3 Literature Review……. 4
   - 1.4 Organization of Thesis……... 6

2. BRIEF REVIEW OF INTERACTION OF EM WAVES WITH A BIOLOGICAL MEDIUM……... 7
   - 2.1 Overview……... 7
   - 2.2 EM Wave Effects on Biological Tissues at the Molecular Level……. 9
   - 2.3 Relative Permittivity, Conductivity and Their Dependence on Frequency……. 9
   - 2.4 Absorption and Reflection of EM Waves in Body Tissues…….. 12
   - 2.5 Energy in EM Radiation……... 18
   - 2.6 Important Observations on Absorption…… 20
   - 2.7 Reflection and Refraction of EM Waves in Dielectric and Conductive Mediums…….. 22
   - 2.8 Reflection and Refraction at a Plane Surface……... 22
   - 2.9 Snell's Law and Angle of Refraction in Different Mediums……... 27
   - 2.10 S Parameters and Calculation of Reflection from Simulations…… 28

3. SELECTION OF OPTIMUM FREQUENCY OF OPERATION……. 30
   - 3.1 Introduction…….. 30
   - 3.2 Laws for Optimum Frequency of a Receiver –Transmitter Coupled Coil……... 30
   - 3.3 Radar Theory Consideration for Optimum Transmission and Reception 33
   - 3.4 Wave Propagation through a Guided Medium……. 34
   - 3.5 Absorption and Reflection Consideration…… 35

4. ABSORPTION OF ELECTROMAGNETIC RADIATION IN A HUMAN BODY: ANALYTICAL AND SIMULTED RESULTS FROM LITERATURE…… 38

4.1 Simulated Results on Absorption in a Human Body……... 38
4.2 Simulated and Analytical Results on EM Radiation Absorption by Different Models for a Human Body…… 47
4.3 Non-Thermal Effects of EM Radiation on a Human Body…….. 54

5. MODELING AND SIMULATION OF TRANSMITTER-RECEIVER COUPLING FOR BIO-IMPLANTABLE SENSOR APPLICATIONS……..... 59
5.1 Development of a Simplified Model for Simulation Using Finite Element Technique……... 59
5.2 Goals for the Model……. 61
5.3 Software Package Used and Its Working Principle……. 62
5.4 Dimensions for the Circular Model……. 64
5.5 Model Justification…….. 66
5.6 Excitation Method…… 67
5.7 Description of EM Fields Induced in the System…… 68
5.8 Edge Based Finite Element Technique (EBFET)…… 69

6. SIMULATION AND RESULTS…… 75
6.1 Simulation Cases…… 75
6.2 Results…… 77
6.3 Summary and Conclusion of Chapter 6……. 106

7. CONCLUSION AND SUGGESTIONS FOR FURTHER RESEARCH…….. 107
7.1 Summary and Conclusions…… 107
7.2 Suggestions for Future Research……... 109

REFERENCES…….. 111

APPENDIX A: A SAMPLE *PROBLEM_EFEM* FILE…… 113

APPENDIX B: A SAMPLE *PROBLEM.G* FILE……. 125

APPENDIX C: PERMISSION FROM IEEE TO REPRINT…….. 134

VITA…….. 135

LIST OF TABLES

3.1. Skin depth (α^{-1}) of Cu at different frequencies, calculated by using the equation (3.8) and values from [16]…….35

6.1. Values of parameters taken from reference [16] used for simulation at different frequencies for the current density plots ……...94

6.2 Dimension of the elliptical model……101

LIST OF FIGURES

2.1. Electrical model for a tissue. Only one layer of cells is shown above. Output of a layer is connected to the input of the next layer to build the whole tissue. R_{ext}, C_{int}, and R_{int} belong to each cell membrane and they are connected in a parallel structure to build a single cell layer ……11

2.2. Geometry of the fat-muscle interface [3]. EM waves propagate along Z direction. Thickness of the fat layer is 2 cm and muscle layer is assumed very thick such that all EM power that enters the muscle layer is absorbed.……...14

2.3. Relative heating at the fat-muscle interface simulated at frequencies, (a) 433.2 MHz (b) 750 MHz (c) 918.8 MHz (d) 1200 MHz (e) 2 GHz and (f) 2.45 GHz. Different curves are for heating at different distances from the interface. (Printed with permission from reference 3, © 2003 IEEE).....15

2.4. Reflection and refraction at planar surface. Here angle of incidence = θ_i, angle of reflection = θ_r, and angle of transmission = θ_t. n is the normal to interface S-S. …23

2.5. Two port network. Above figure shows the two port network where E_{i1} and E_{i2} are incident fields at port 1 and port 2 respectively whereas E_{r1} and E_{r2} are the reflected fields at port 1 and port 2 respectively……..29

3.1 Secondary Coil. Figure shows the receiver coil with an inductance of L_S and coil resistance R_S and self capacitance C_s. C and R are the receiver load capacitance and resistance respectively. In all the analysis, self capacitance has been neglected……..32

3.2 Coupled transmitter-receiver coils. L_P and L_S are transmitter and receiver inductances respectively, R_S and R_P are transmitter and receiver resistances and I_P and I_S are transmitter and receiver currents respectively. M is the mutual coupling between the coils. C_S and C_P are the self capacitances of the secondary and primary coils respectively and they are neglected in this analysis……...32

3.3 Distance (α^{-1}) at which E or H field magnitude attenuates inside dry skin to e^{-1} times its value at the surface plotted as a function of frequency. It has been calculated with the equation (3.9 and using the data from reference [16]. Losses due to displacement current are not included here…….…….37

4.1 Absorption by a human body at different frequency: This figure shows whole body averaged SAR in $W.Kg^{-1}$ for models of a human body for incident fields of $1mW.cm^{-2}$ for frequencies upto 514.3 MHz. Each of the curves is drawn for parallel orientation of E, H and propagation vector k to the longest dimension of the

human body model. (Printed with permission from reference 3, copyright@IEEE.).....39

4.2 Experimental values of EM absorption for a monkey phantom model, [Printed with permission from reference 8]. Experimental values of absorbed power by a cylindrically symmetrical model for a monkey are plotted upto 100 MHz…….....40

4.3 Experimental values of EM absorption for a human phantom model. [Printed with permission from reference 8]. Experimental values of absorbed power by a cylindrically symmetrical model for a human body is plotted upto 100 MHz……..41

4.4 Relative absorption as function of λ^{-1} for a spherical model for a human body, Results are obtained with conductivity κ = 10 $s.m^{-1}$, for the spherical model. (Printed with permission from reference [2], © 2003 IEEE).....43

4.5 Relative absorption as function of λ^{-1} for a spherical model for a human body. Results are obtained with conductivity κ = 1 $s.m^{-1}$, for the spherical model. Printed with permission from reference [2], © 2003 IEEE);.....44

4.6 Spherical multilayered model, [printed with permission from reference 10]. Six region model of the human head. 1 – brain, 2-cerebrospinal fluid, 3-membrane, 4-bone, 5-fat, 6-skin, 7-surrounding medium……..49

4.7 Absorption for four different frequencies for the spheroid model in Fig. 4.6, [printed with permission from reference 10]. Shows normalized power density (NPD), (a) f = 433 MHz, no absorption in the core, (b) f = 915 MHz, core NPD = 0.12, (c) f = 2.45 GHz, core NPD = 0.06 (d) f = 5.8 GHz, no absorption in the core……50

4.8 Absorption in different planes of the spheroid model shown in Fig. 4.6, [printed with permission from reference 10]. Normalized power density (NPD) for a sphere of radius 3.3 cm at different planes, (a) plane x = 0, maximum NPD in the core is 0.10, (b) plane x=1.6 cm, maximum NPD in the core is 0.06, (c) plane x=2.4 cm, maximum NPD in the core 0.06, (d) plane x= 3.2 cm, maximum NPD in the core is 0.14……...52

4.9 Absorption for different radii of the brain core for the spheroid model in Fig. 4.6, [printed with permission from reference 10]**.** It shows NPD for simulations at 3 GHz and different radii, (a) radius = 1.1 cm, peak NPD = 0.78, (b) radius = 1.65 cm, peak NPD = 0.55, (c) radius = 3.3 cm, peak NPD = 0.18, (5d) radius = 6.6 cm, peak NPD is almost zero……....53

4.10 Absorption for different values of conductivities of the brain for the spheroid model in Fig. 4.6, [printed with permission from reference 10]. It shows E field and NPD

for simulation at 3 GHz and different conductivity (σ) values of brain core. (a) Normalized E field peaks are 1.88, 0.64 for σ = 0.5 mho.m^{-1}, (b) NPD peaks are 0.39, 0.21 for σ = 0.5 mho.m^{-1}, (c) Normalized E field peak is 0.28 for σ = 3.0 mho.m^{-1} and (d) NPD peaks are 0.42, 0.18 for σ=3mho.m^{-1}……55

4.11 NPD for different values of relative permittivity for the brain core, [printed from reference 10]. It shows NPD for simulation at 3 GHz with different values of relative permittivity (ε_r) for brain, (a) ε_r = 29, peak NPD = 0.29, (b) ε_r = 42, peak NPD = 0.55, (c) ε_r = 55, peak NPD = 0.98, (d) ε_r = 68, peak NPD = 1.2……....56

5.1 Geometry of a simplified model for simulation of human body with the implanted receiver. The implanted receiver is modeled as a cube as shown in (b), transmitter is modeled as an annular Cu conductor wrapped around the lower portion of the human body model and it is in layer 2. Layer 1 models the upper portion of a human body and layer 3 is an insulation between the ground plane and the upper portion of the model……60

5.2 The receiver – transmitter position in the model. It shows position of the receiver in layer 2. ……...61

5.3 Triangular mesh in the layer 2 cross-sectional plane of the model in Fig. 5.1. It also shows dimension of different annular regions. It can be seen that x axis passes through port 1 and port 2. Orientation of the model and its position with respect to the coordinate system is also obvious in the above figure…….65

5.4 Simulated E field around port 1 in the X-Y cross sectional plane. Resulting E fields at port 2 are not shown here. It shows vectors whose directions are along the E fields and lengths are proportional to magnitudes of E fields. All other E field magnitudes are shown relative to the E field magnitude around the port 1 located around 0.25 m……70

5.5 Triangular nth element in the mesh created in the cross sectional plane of a given problem geometry. N_1^n, N_2^n and N_3^n are the interpolation functions along the edges 1, 2 and 3 respectively……...73

5.6 Definition of the area coordinates. P is a point which can be anywhere inside the triangle. Clearly maximum value of $L_1^n = \frac{\Delta_1}{\Delta}$ is 1 and it is obtained when P is at 1…….73

6.1 Receiver to transmitter region energy density ratio vs. frequency (1 kHz to 9 GHz). Each one of the points corresponds to a different simulation and each one of these simulations has been done utilizing values of σ and ε_r appropriate for that frequency of simulation…….80

6.2 Receiver to transmitter region electric field ratio vs. frequency (1 kHz to 9 GHz). Each one of the points corresponds to a different simulation and each one of these simulations has been done utilizing values of σ and ε_r appropriate for that frequency of simulation……81

6.3 Resonance cavity formed by the transmitter and receiver regions, distance between A and B is16.5 cm. The lowest frequency corresponding to resonance would be when half-wavelength is equal to 16.5 cm……82

6.4 Input reflection coefficient (S_{11}) vs. frequency (1 kHz to 9 GHz), shows that reflection decreases steadily till approx. 30 MHz. Reflection is nearly unity around 1 GHz. Here also each one of the points corresponds to a different simulation and each one these simulations has been done utilizing values of σ and ε_r appropriate for that frequency of simulation……...84

6.5 Input reflection coefficient (S_{11}) vs. frequency (50 kHz to 100 kHz), shows steady decrease in S_{11} in this frequency zone as found in Fig. 6.3. Simulation has been done on the input file with values of σ and ε_r valid for 50 kHz……..….86

6.6 Input reflection coefficient (S_{11}) vs. frequency (6.3 MHz to 63 MHz), shows steady increase in S_{11} in this frequency zone as found in Fig. 6.3. Simulation has been done on the input file with values of σ and ε_r valid for 10 MHz……87

6.7 Input reflection coefficient (S_{11}) vs. frequency (1 GHz to 10 GHz), shows numerous resonance between these frequencies. Simulation has been done on the input file with values of σ and ε valid for 2 GHz……....88

6.8 Current density vs. frequency for the frequency range 1 kHz to 9 GHz, for a transmitter current density of 3.2×10^6 A.m^{-2}. It shows that for the secondary coil current requirement of 100 mA, induced current densities are far below the safe limit……..91

6.9 Induced power density in different layers vs. frequency (1 kHz to 9 GHz), for a transmitter current density of 3.2×10^6 A.m^{-2}. It shows that induced power densities are well below the safe limit……92

6.10 2D current density plot in the layer 2 of the model in Fig. 5.1. Simulation frequency is 1 kHz and parameters used are also for 1 kHz. This plot is in conformity with the relative current densities shown in Fig. 6.8. Values for current density in different areas can be found using equation (6.3). Cu marks Current density at the transmitter port 1……96

6.11 2D current density plot in the layer 2 of the model in Fig. 5.1. Simulation frequency is 50 kHz and parameters used are also for 50 kHz. Central core conductivity is

overwritten with value 0 $s.m^{-1}$. Values for current density in different areas can be found using equation (6.3). Cu marks current density at the transmitter port 1……..97

6.12 2D current density plot in the layer 2 of the model in Fig. 5.1. Simulation frequency is 50 kHz and parameters used are also for 50 kHz. Central core conductivity is 0.0002 $s.m^{-1}$ as mentioned in Table 6.1. Values for current density in different areas can be found using equation (6.3). Cu marks current density at the transmitter port 1……..98

6.13 2D current density plot in the layer 2 of the model in Fig. 5.1. Simulation frequency is 2 MHz and parameters used are also for 2 MHz. But central core conductivity is overwritten with 0 $s.m^{-1}$. Values for current density in different areas can be found using equation (6.3). Cu marks current density at the transmitter port 1…….99

6.14 2D current density plot in the layer 2 of the model in Fig. 5.1 for elliptical dimension. Simulation frequency is 1 kHz and parameters used are also for 1 kHz. But the inner core conductivity of 0.00059 $s.m^{-1}$ has been used. Cu marks current density at the transmitter port 1. Values for current density in different areas can be found using equation (6.3)…….102

6.15 2D current density plot in the layer 2 of the model in Fig. 5.1 for elliptical dimension. Simulation frequency is 100 kHz and parameters used are also for 100 kHz as shown in Table 6.1. Cu marks current density at the transmitter port 1. Values for current density in different areas can be found using equation (6.3)…….103

6.16 2D current density plot in the layer 2 of the model in Fig. 5.1 for elliptical dimensions. Simulation frequency is 2 MHz and parameters used are also for 2 MHz as shown in Table 6.1. Cu marks current density at the transmitter port 1. Values for current density in different areas can be found using equation (6.3)…….104

6.17 2D current density plot in the layer 2 of the model in Fig. 5.1 for elliptical dimension. Simulation frequency is 5.3 MHz and parameters used are for 5 MHz as shown in Table 6.1. Cu marks current density at the transmitter port 1. Values for current density in different areas can be found using equation (6.3)…….105

SYMBOLS AND CONVENTION USED

- Complex permittivity: $\varepsilon^* = \varepsilon + j\varepsilon'' = \varepsilon_r(\varepsilon_0 + j\frac{\varepsilon''}{\varepsilon_r})$, where ε_r is relative permittivity and ε_0 is permittivity value for free space.
- For all plots and simulations ε_r value is used for both dielectric and conductive mediums which would make permittivity value equal to ε.
- σ : Conductivity
- For a dielectric medium dielectric conductivity σ' includes both conductive and displacement current component.
- μ : Permeability
- E : Electric field
- H : Magnetic field.
- Variables (V) with an $e^{-j\omega t}$ time variation are shown as $\widetilde{V}$ and their rms values are shown as V. While V is used in a vector context, then it is written in bold faced letter, **V.** Phasors are denoted as $\overline{\mathbf{V}}$.
- EM : Electromagnetic
- EMT: Electromagnetic Transmission
- TEM: Transverse Electromagnetic
- EMF: Electromotive Force
- $j = \sqrt{-1}$
- ω denotes angular frequency of EM waves.
- f denotes frequency of EM waves.

ABSTRACT

Primary goal of this work is to study transmission of EM power through a multilayered biological medium. For a particular case study, EM power transmission from an external transmitter to a coupled receiver implanted inside a biological medium simulating a human body is studied to find solutions for factors such as optimum transmission frequency and excitation current. Different aspects of interaction of EM waves with biological bodies and tissues are discussed. Two major factors that may affect transmission of EM power through a biological body are absorption and reflection of EM waves. A simulation in which exact Maxwell's equations are solved to find E field distribution in cross-sectional planes of a human body with the implanted receiver takes into account both absorption and reflection accurately. A simplified model for a human body with an implanted receiver and an external transmitter is developed here. Main motivation is to find E field distribution throughout the model and find energy density coupling between the transmitter and the receiver regions. Edge based finite element simulations are carried out on the model for a number of frequencies between 1 kHz and 9 GHz and frequency dependent values for EM properties such as relative permittivity and conductivity of biological tissues are used for all the simulations. Energy density coupling, E field coupling and S parameters showing reflection at the excitation port are obtained from the simulated results. Energy coupling is found to be almost constant with values near 0.01 between 1 kHz and 500 MHz. Current densities are below the thermal safe current density level even for an excitation current density of 3×10^6 $A.m^{-2}$ in the transmitter. Although model used for simulation is simplistic, the results obtained are useful to study EM power losses in a multilayered biological medium. Results can be

applied to find safe limits of excitation current density for transmitting EM power through a biological medium such as a human body without causing any damage due to heating.

CHAPTER 1

INTRODUCTION

1.1 Background

Substantial amount of research has been going on for developing ultra-small biomedical sensors that can be implanted inside an animal or a human body. Usually batteries are needed as power supply for the sensor circuitry to perform various important functions. But once the implanted battery discharges, its replacement requires surgery. There is always an accompanying risk of infection or other complications with any surgical operation. An alternative way is to deliver power by external sources through a wired or wireless transmission. The first approach requires penetration of the wires through the body for connecting to an external power source. The latter approach usually utilizes EM power transmission via a transmitter-receiver system. There is another approach that combines the previous two approaches. Here a rechargeable battery can be used as a power source for a bio-implantable microsystem and the battery can be charged using a power source external to the body. Transmitting power from an external source through the body to the battery charging circuitry using wireless power transmission is hence a useful mechanism that avoids skin penetration of wires.

In his PhD dissertation [1], Von Arx has described a system that consists of a spiral wire transmitter coupled to an on-chip spiral receiver for powering the sensor circuitry in the bio-implanted microsystem. That particular system was designed to operate at 4 MHz which is the resonance frequency for both the transmitter and the receiver. Main purpose obviously was to increase power coupling and to reduce losses. Selection of frequency of operation was such that both the transmitter and the receiver

had optimum Q factor and there was low absorption of transmitted EM power by the intervening human tissues. Circuit laws were used to theoretically determine operating frequency and voltage of the transmitter – receiver system. But this work did not involve any detailed quantitative or qualitative study of absorption of the transmitted energy by biological tissues. A clear understanding of absorption of the transmitted power by different biological tissues and other related EM phenomena is important for designing an efficient wireless powered bio-implantable microsystem. Using circuit laws to obtain the received power for a given transmitted power for such a system does not take into account the frequency dependent absorption of EM energy by biological tissues in a human body. It also does not account for the reflection of EM fields by biological tissues. At the transmitter excitation port, part of the transmitted energy gets reflected. As the transmitted energy propagates through a biological medium, part of it is absorbed and a portion of it is only available to the receiver. So the circuit laws used by Von Arx [1] can be used, if the absorbed and reflected energy parts are also properly accounted for.

1.2 Scope of Work

This thesis mainly focuses on developing a model for estimating absorption and reflection of EM waves traveling through a biological medium. It also discusses both the thermal and non-thermal effects of EM waves on a human body. Various important EM properties of biological tissues, which have profound effect on both absorption and reflection of EM waves, are also discussed. Dependence of properties of body tissues on frequency of operation and tissue water content is also discussed with a physical model. A simplified model for a multilayered body is presented and the edge-based finite element technique is used to simulate EM field propagation in this multilayered biological body. Different tissue layers present in a human body have been used in the

model. In this work, energy density coupling between the transmitter and the receiver is found for a wide range of frequencies. Two-dimensional current density plots in the cross sectional planes of the model for a multilayered body are obtained for a wide range of frequencies. S parameter values which essentially give percentage of reflected field at the port of excitation are obtained for a range of frequencies**.** For all the simulations carried out, values for conductivities and dielectric constants for different tissue layers and conductors appropriate for that particular frequency of simulation have been used. A discussion on relationship between transmitter – receiver size and frequency of operation for efficient power coupling is given. Main objective is to determine optimum condition such as frequency of operation and magnitude of excitation current density for designing an efficient wireless solution for remote transmission of power for applications such as charging the battery or circuitry in an implantable bio-medical system, at the same time avoiding any radiation related hazards to the biological body. An optimum frequency or a range of optimum frequencies would be suggested at which there will be maximum coupling of the transmitted power to the implanted receiver. Possible magnitudes of electric field that might be induced in the body will be obtained from simulation results and will be compared with the limiting values of electric field which can cause any hazardous effect in the body. Magnitudes of induced current densities as well as induced power densities in the different tissues of the model for the multilayered body will be plotted against frequency and those values will be compared to the safe limits [2] of current density or power exposure that the body can sustain without any damage. Techniques utilized here can be used for studying interaction of EM waves with other multilayered inhomogeneous medium.

1.3 Literature Review

There has been significant amount of work [2-7] related to modeling absorption and interaction of EM waves with a human body. Some of the work report simulation results as well. Schwan [2] discussed variation of relative permittivity value of biological tissues with frequency. He also discussed depth of penetration of EM waves inside biological tissues and explained different non-thermal effects of EM waves on a human body. Guy [3] discussed relative heating patterns in different tissues and also reported simulation results on a bi-layered tissue model which shows dependence of relative heating on frequency of operation. Guy's simulation was carried out only for six frequencies. Johnson et al. [5] have reported biological effects of electromagnetic waves from the lower radio frequencies up through the optical spectrum. The problem of microwave penetration into the body with resultant internal power absorption was approached from both the theoretical and experimental viewpoints [5]. Gandhi [6] discussed about variation of absorption in men and animals with frequency. He also discussed dependence of absorption on polarization of EM fields. Gandhi also had a brief discussion on multilayer effects of human body and its frequency dependence. Allen et al. [8] reported experimental results on absorption of EM radiation by a human body. Massoudi et al. [9] used perturbation technique to derive analytical expressions for estimating absorbed power in the human body for different polarization of the incident E field. Authors in references [2-7] have discussed different theoretical aspects briefly. Neudar et al. [10] showed simulated energy and electric fields in a multilayered spherical model of a human head. One of the important considerations not addressed by their work is that their simulations at different frequencies did not take into account the frequency dependence of the properties such as conductivity and relative permittivity. Also

frequencies at which simulations were done were spaced far apart. Dielectric properties vary substantially with frequency. It will be seen from the simulated results in this thesis that a small change in dielectric constant or conductivity with change in frequency can cause substantial change in various EM phenomena such as reflection and absorption.

Appropriate literature is also reviewed in chapter 2, 3 and 4.

In this work, theoretical basis for numerical modeling and simulation of interaction of EM waves with the human body have been explained clearly especially with respect to the impacts of different important factors such as conductivity, permittivity and frequency of operation. In all the simulations that have been carried out, frequency dependent values of dielectric constant and conductivity have been used. Simulations have been carried out for more than twenty different frequencies by using values of σ and ε_r appropriate for the simulation frequency. Also the simulation technique used is *Edge Based finite Element Method* which is very accurate [11] in solving EM field in an inhomogeneous medium. This technique does not produce any spurious results which are known to happen occasionally in node based finite element technique. Accuracy of the results is hence expected to be high [11].

1.4 Organization of Thesis

In chapter 2, relevant theoretical aspects of interaction of EM fields with a biological medium have been covered. It starts with a discussion on limiting EM fields that can cause harm to a human body and then discusses electrical properties such as dielectric constant and conductivity of biological tissues and the factors on which their values depend. Different types of currents induced in biological tissues are also discussed. Absorption, reflection and refraction of EM waves in biological tissues have been explained and described quantitatively with equations.

In chapter 3, different considerations which are important for the selection of an optimum frequency for the coupled transmitter-receiver system to be used in a bio-implantable microsystem are discussed. Related phenomena are explained with analytical expressions.

In chapter 4, theoretical and simulation results from different works in literature on interaction of EM waves with biological bodies are discussed and some of them are compared with the analytical expressions in chapter 2.

In chapter 5, a simplified model for the human body with the transmitter – receiver system is presented. Purpose and motivation behind the model is stated. Different parts of the model are explained. Similarity of the excitation current with that in a real system is discussed. Edge based finite element technique used here for simulation is also discussed briefly.

Chapter 6 describes the simulation results and chapter 7 gives the conclusions and recommendations for further work.

Symbols and notations used for various quantities frequently used are defined and explained on page xii.

CHAPTER 2

BRIEF REVIEW OF INTERACTION OF EM WAVES WITH A BIOLOGICAL MEDIUM

2.1 Overview

Interaction of non-ionizing EM waves with biological bodies and tissues results in thermal heating as well as non-thermal effects such as field-force effect, polarization and depolarization of body cell membranes. Maximum recommended safe power limit for long-term human exposure has been specified as 10 $mW.cm^{-2}$ in the US [5]. Yet use of power densities up to 590 $mW.cm^{-2}$ is common in routine diathermy treatments [5]. So it is important to understand the limits of EM power exposure that human body can sustain without any crucial biological damage.

In the frequency range of 1 MHz to 300 GHz, wave lengths of EM waves are in the range of 300 m to 1 mm and are larger compared to the cell size. Hence there is little scattering of EM waves by a human body in this frequency range. Normal laws of reflection and transmission of waves can be applied in this range. As EM waves propagate through a human body, propagating EM energy can get absorbed by muscles and tissues producing localized heating. Fields in the EM waves also may cause other non-thermal effects such as electromechanical field force in the cells and polarization and depolarization of cell membranes. The heating in tissues possibly results from both ionic conduction and vibration of the dipole molecules of the water and the protein in tissue cells. Continuous temperature rise leading to severe damage of tissues can happen if the absorbed power is greater than the normal metabolic output of a human body. The normal metabolic heat production for a 70 kg man on a 2500 Calorie diet is around $4x10^{-4}$ calorie per gram per second [12]. Maximum power density, safe for long term exposure to the

human body was decided to be 10 $mW.cm^{-2}$ [12]. Higher values for radiation power density can be used if exposure time is brought down [12]. Based on the maximum power density, Schawn [2] estimated current density that can be induced inside a human body without causing any thermal hazard. Assuming an exposed area of 1 m^2, total power received for a 10 $mW.cm^{-2}$ radiation exposure is $100W = I^2R = J^2\rho A^2.L.A^{-1}$. Here A is exposed area, I is current, J is current density, L is thickness of a human body = 10 cm and ρ is resistivity of human body. It can be seen that $J^2\rho = 1\ mW.cm^{-3}$. For ρ = 100 ohm-cm [2], $J \approx 3\ mA.cm^{-2}$. Apparently resistivity of the human body tissue is frequency dependent and decreases with frequency. So 3 $mA.cm^{-2}$ limit will go up at the higher frequencies. Therefore, current density of 3 $mA.cm^{-2}$ can be taken as a safe upper limit for induced current density to avoid damaging body heating due to long term exposure of a human body to EM radiation. It is also found that induced electric field inside a human body can depolarize the cell membranes if it is greater than a certain threshold value. It is reported that induced electric field strength greater than 500 $kV.cm^{-1}$ can polarize or depolarize body cell membranes [2].

Heating due to EM power absorption in human body is non-uniform. Heating inside a particular tissue depends on the dielectric and conductive properties of that tissue. High water content tissues normally have high conductivity, whereas those with low water content have low conductivity. Absorption is high and depth of penetration is low in tissues of high water content. Standing wave pattern causing severe hot spots has been reported to result in the interface of muscles and fat. Section 2.3 shows the relative heating produced at and near the fat-muscle interface. Skin burns and even deep burns of the tissues under the skin have been found in test animals [3]. Heating of body tissues called diathermy by using RF power to give a therapeutic temperature rise in the range of

43^{o} C to 45^{0} C has been in practice. But this temperature range is very close to the temperature range where a little increase in temperature may lead to destructive damage of body tissues [12].

There are non-thermal effects of EM radiation as well. EM waves can result in alignment of cells, because of the induced dipole charges in those cells. Frequency at which this effect is important may be different for different cells. Also intense microwave field can cause polarized side chains of macromolecules to line up with the direction of the E field, leading to possible breakage of hydrogen bonds and to alterations of the hydrogen zone. Such effects can cause denaturizing or coagulation of molecules [2]. This effect is also known as field force effect. Different muscle movements in the human or an animal body is caused by depolarization and polarization of cell membranes. Induced electric field can result in substantial potential difference to develop across cell membranes causing unwanted polarization and depolarization.

2.2 EM Wave Effects on Biological Tissues at the Molecular Level

EM waves cause two types of effects at the molecular level. One is the oscillation of the free charges or ions and the other is the rotation of dipole molecules at the frequency of the incident wave. First one gives rise to conduction current and the second one causes displacement current with an associated loss due to viscosity. Conductivity and dielectric properties of a tissue decide which current would dominate in that tissue. Conductive current is higher in conductors whereas displacement current (charging and discharging current) is higher in tissues with high relative permittivity values.

2.3 Relative Permittivity, Conductivity and Their Dependence on Frequency

Both dielectric property and conductivity of a medium depend significantly on the frequency of the EM wave. Tissues can be modeled as shown in Figure 2.1, where only

one layer of membrane cells is shown. Each cell has C_{int} as its internal capacitance and R_{int} as its internal resistance. R_{ext} is the resistance of the paths which connects the cells to each other. R_{ext} is much higher than R_{int}. The dash line shows repetition of the same cell structure till the end path.

At low frequencies, the cell membranes with C_{int} of approximately 1 uF.cm^{-2} [2] act as an insulator causing current to flow only in the extra-cellular region through R_{ext}. This accounts for a high resistance or in other words a low conductivity of the tissues. At low frequencies, the charging time is high enough for the cell capacitance to get completely charged and discharged and this may explain high value for tissue dielectric constant. This is because dielectric constant value of a medium is basically an indicator of charge storing capability of the medium. Higher value of dielectric constant indicates high charge storing capability of the medium. Increase in frequency results in decreasing capacitive reactance of the cells causing more currents in the intracellular region which results in higher conductance of the tissue. Increase in frequency also results in partial charging or discharging of the membranes, which explains decrease in dielectric constant value of biological tissues at higher frequencies. Dielectric constant and conductivity variation with frequency can be theoretically explained with the help of the well-developed models for polar mediums [2]. In all the tissues, these properties changes with frequency because of their water content. The electric polarity of water rotates with applied field below certain critical frequency. The following models [2] for ε_r and σ, which hold for a polar medium, can also be applied for predicting conductivity and dielectric properties of different biological tissues.

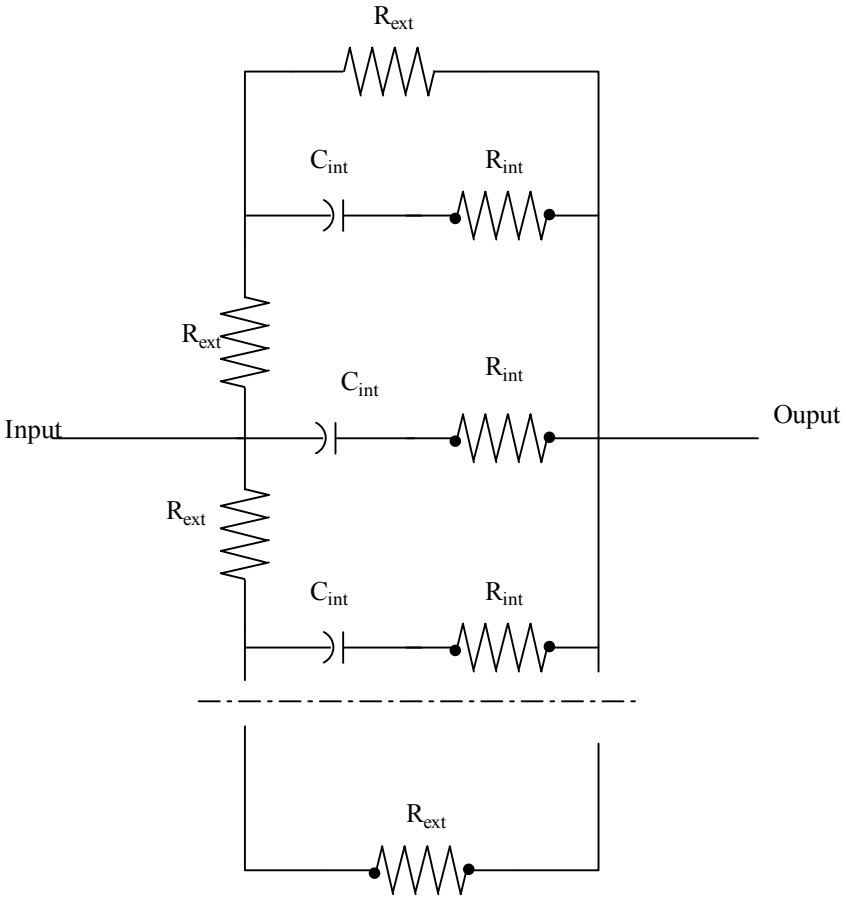

Figure 2.1: Electrical model for a tissue. Only one layer of cells is shown above. Output of a layer is connected to the input of the next layer to build the whole tissue. R_{ext}, C_{int}, and R_{int} belong to each cell membrane and they are connected in a parallel structure to build a single cell layer.

Subscript 0 and ∝ refer to points far below and far above critical frequency.

$$\varepsilon_r = \varepsilon_{r\infty} + \frac{\varepsilon_{r0} - \varepsilon_{r\infty}}{1 + \left(\frac{f}{f_{cr}}\right)^2} \tag{2.1}$$

$$\sigma = \sigma_0 + (\sigma_\infty - \sigma_0)\frac{\left(\frac{f}{f_{cr}}\right)^2}{1 + \left(\frac{f}{f_{cr}}\right)^2} \tag{2.2}$$

Here ε_r is relative permittivity of the medium, σ is the conductivity of the medium, f stands for frequency and f_{cr} stands for critical frequency of the medium.

2.4 Absorption and Reflection of EM Waves in Body Tissues

Absorption of power in different layers of body tissues depends on the conductive and dielectric properties of the tissues. It also depends on the frequency of the incident wave. Due to presence of plenty of nerve cells on the body surface, surface heating resulting in temperature rise can send warning signals to the body. But deep heating of tissues can cause damage without even being noticed. Standing wave formation due to reflection of field at the interface of the tissues with substantial difference in permittivity values may result in significant deep heating of one of the tissues [3]. Standing wave formation and the resulting relative heating in tissues occurring next to each other have a crucial dependence on frequency of the incidence EM wave. Guy reported substantial relative heating at the muscle-fat interface [3]. Results obtained by Guy in reference [3] are discussed below. Figure 2.2 is drawn to explain the geometry of the fat-muscle interface as discussed by Guy.

Figure 2.3 shows relative heating in fat and muscle. It can be seen from Fig. 2.3 that heating or absorption of power is maximum around the interface of the fat-muscle

layer. Maximum relative heat in muscle is taken as 1 and relative heating decreases with frequency [3]. Ratio of muscle to fat heating is highest at frequency 433 MHz and least at 2450 MHz. But at the same time with increase in frequency, relative heating increases in area perpendicular to the direction of propagation of radiation as can be seen from plot (f) in Fig. 2.3, where a second peak is observed for z = 2 cm in the muscle layer from the interface at x ≈ 5 cm.

As EM waves propagate through body tissues, it induces E field which generates current in the tissues. Body tissues are basically comprised of dielectric medium. Two types of currents, namely conduction current and displacement current are generated by EM waves**.** Loss in a dielectric medium can be shown as an effective conduction loss defined as *dielectric conductivity*.

2.4.1 Losses in a Dielectric Medium and Definition of Dielectric Conductivity

Theory of currents in a dielectric medium can be developed from the basics of currents in a capacitor. For a parallel plate capacitor with plate area A and the insulating lossy dielectric medium having complex dielectric constant ε^*, let a time varying voltage ($\tilde{v}$) be applied across its two parallel plates. It follows that $\varepsilon^* = \varepsilon + j\varepsilon'' = \varepsilon_r(\varepsilon_0 + j\frac{\varepsilon''}{\varepsilon_r})$, where ε is the real part, ε'' is the imaginary part of ε^*, ε_0 is permittivity of free space and ε_r is the relative permittivity of the medium. Total current in the capacitor can be written as, $\tilde{I} = \tilde{I}_{conduction} + \tilde{I}_{displacement} = G\tilde{v} - j\omega C\tilde{v}$. Here G is the conductance of the capacitor between its two plates. Capacitance can be given as, $C = \frac{\varepsilon}{\varepsilon_o}C_o$, where $C_o = \frac{\varepsilon_o A}{d}$, d is the thickness of the dielectric insulator of the parallel plate capacitor and

$\varepsilon = \varepsilon_r \varepsilon_0$. Incorporating this in the total current equation, total current can be written as,

$\tilde{I} = G\tilde{v} - (j\omega\varepsilon)\frac{C_o}{\varepsilon_o}\tilde{v}$. We can write, Current density, $\tilde{J} = \frac{\tilde{I}}{A}$.

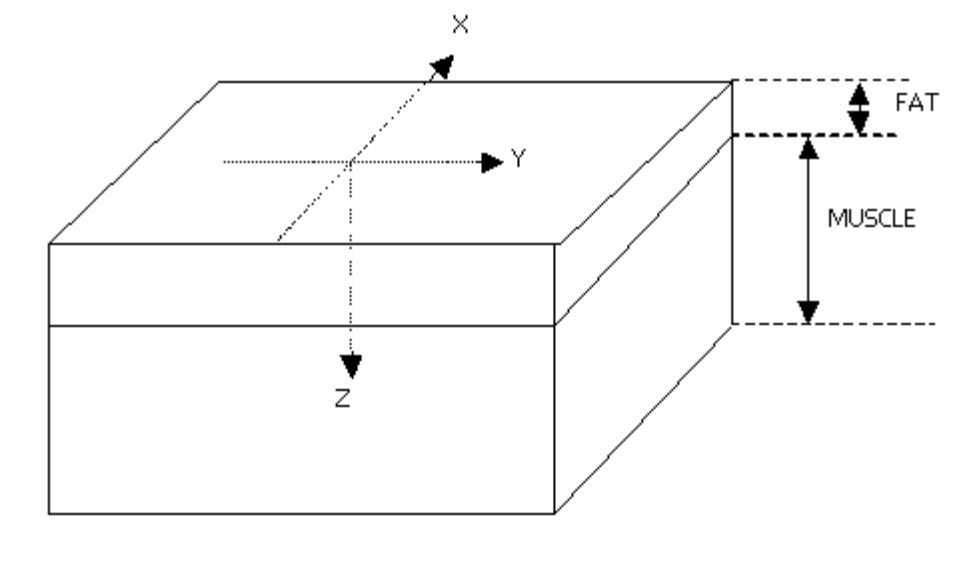

Figure 2.2: Geometry of the fat-muscle interface [3]. EM waves propagate along Z direction. Thickness of the fat layer is 2 cm and muscle layer is assumed very thick such that all EM power that enters the muscle layer is absorbed.

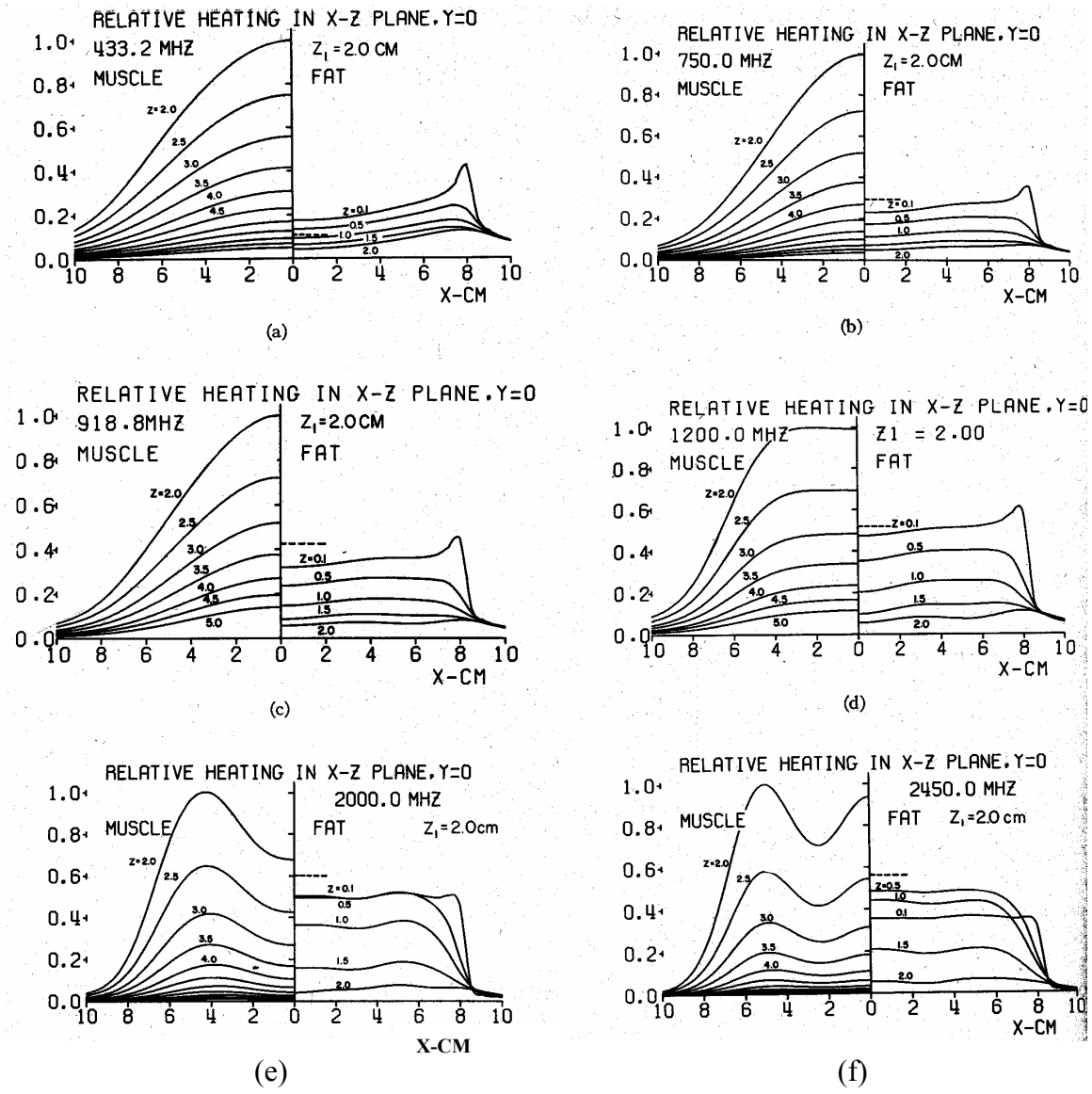

Figure 2.3: Relative heating at the fat-muscle interface simulated at frequencies, (a) 433.2 MHz (b) 750 MHz (c) 918.8 MHz (d) 1200 MHz (e) 2 GHz and (f) 2.45 GHz. Different curves are for heating at different distances from the interface. (Printed with permission from reference 3, © 2003 IEEE).

$$\tilde{J} = G\frac{\tilde{v}}{A} - j\omega\varepsilon\frac{C_o}{\varepsilon_o A}\tilde{v} = G\frac{d}{A.}\cdot\frac{\tilde{v}}{d} - j\omega\varepsilon\cdot\frac{\frac{\varepsilon_o A}{d}}{\varepsilon_o A}\tilde{v}\text{, or} \qquad \tilde{J} = \sigma\tilde{E} - j\omega\varepsilon\tilde{E}. \tag{2.3}$$

Here σ is the conductivity of the medium. From Maxwell's equations [7], total current density in a dielectric medium with complex dielectric constant $\varepsilon^* = \varepsilon + j\varepsilon''$ can also be written as, $\tilde{J} = \varepsilon^*\frac{\partial\tilde{E}}{\partial t} = \omega\varepsilon''\tilde{E} - j\omega\varepsilon\tilde{E}$. Comparing this expression with equation (2.3), it can be seen that effective conductivity of a lossy dielectric medium is $\omega\varepsilon''$. This is called *dielectric conductivity* σ' [7] and includes losses due to displacement current. In this thesis, $\sigma' = \omega\varepsilon''$ will be used to represent *dielectric conductivity* for all dielectric mediums.

2.4.2 Physics of Absorption of EM Radiation in Biological Tissues

For a linearly polarized EM wave propagating along z direction with its E field polarized along x direction and H field polarized along y direction, E and H field can be written as, [13]

$$E_x = E_{oX}\exp[-\alpha z + j(\beta z - \omega t + \theta)] \tag{2.4}$$

$$H_Y = H_{oY}\exp[-\alpha z + j(\beta z - \omega t + \theta + \gamma)] \tag{2.5}$$

$$\frac{H_{oY}}{E_{oX}} = \frac{\sqrt{\alpha^2 + \beta^2}}{\mu\omega} \tag{2.6}$$

Here α is the attenuation factor; β is the propagation constant, θ is the initial delay and γ is the phase lag between the H and E field defined by $\tan\gamma = \frac{\alpha}{\beta}$. The medium of propagation is a real medium with finite conductivity σ, permittivity ε and permeability μ. Here E_{oX} and H_{oY} are magnitudes of E and H field at the surface of the medium in the x and y directions respectively. Electric and magnetic fields are assumed to be

periodic sinusoidal in time. Analysis will still remain valid for any arbitrary periodic wave, because it can be shown that any function with arbitrary periodic time dependence can be written as a Fourier series expansion of sinusoidal components.

The constants α and β characterize properties of EM wave propagation in a medium. It can be seen from the equation (2.4) that a larger value of α rapidly attenuates the magnitude of field inside the medium along the direction of propagation. Phase and group velocity values of the wave depend on β. Values of α and β can be calculated from the definition of the complex propagation factor k, where distance and time dependence of EM waves are given by the term $e^{-j(\kappa x+\omega t)}$. k is related to α and β by the equation $-jk = -\alpha + j\beta$ and $k^2 = \mu\varepsilon\omega^2 + j\mu\sigma\omega$. (2.7)

Equation (2.7) can be solved for α and β to give [13],

$$\alpha = \omega\left[\frac{\mu\varepsilon}{2}\left(\sqrt{1+\frac{\sigma^2}{\varepsilon^2\omega^2}}-1\right)\right]^{\frac{1}{2}} \tag{2.8}$$

and

$$\beta = \omega\left[\frac{\mu\varepsilon}{2}\left(\sqrt{1+\frac{\sigma^2}{\varepsilon^2\omega^2}}+1\right)\right]^{\frac{1}{2}}. \tag{2.9}$$

2.4.3 Attenuation Factor

The depth inside a medium at which magnitude of E or H field becomes e^{-1} of its value at the surface is given by α^{-1}, where α is the attenuation factor as defined in section 2.4.2. Schwan [2] has shown that for biological tissues (skin, muscle etc.) with high water content, this depth can be analytically given by,

$$\frac{1}{\alpha} \approx \frac{1}{17}\sqrt{\frac{\lambda}{\sigma}} \approx \frac{1}{\sqrt{f}}, \quad \text{for} \quad \frac{f\varepsilon}{\sigma} < 60v_G \tag{2.10}$$

and $\frac{1}{\alpha} \approx \frac{\sqrt{\frac{\varepsilon}{\sigma}}}{377} \approx \frac{1}{f^2}$, for $\frac{f\varepsilon}{\sigma} > 60 v_G$, (2.11)

where $v_G = \frac{d\omega}{d\beta}$ is known as the group velocity of the propagating wave. These equations were derived mathematically with due consideration of the conductivities and dielectric constants and are in excellent agreement with the experimental values [2].

2.5 Energy in EM Radiation

Mean value of energy flow or energy crossing per unit area in the propagation direction is given as the real component of the complex Poynting vector which is defined as

$$\tilde{\mathbf{S}} = \frac{1}{2}\tilde{\mathbf{E}} \times \tilde{\mathbf{H}}^* . \quad (2.12)$$

For the EM wave propagating in the z direction as described in section 2.4.2, energy propagating in the z direction is given by

$$\mathrm{Re}(\tilde{S}_Z) = \mathrm{Re}(\frac{1}{2}\tilde{E}_X . \tilde{H}_Y{}^*) . \quad (2.13)$$

where $\mathrm{Re}(\frac{1}{2}\tilde{E}_X . \tilde{H}_Y{}^*)$ denotes real part of $\frac{1}{2}\tilde{E}_X . \tilde{H}_Y{}^*$ and $\tilde{S}_Z$ is the z component of $\tilde{\mathbf{S}}$.

Substituting the values of E_x and H_y from equation (2.4) and (2.5) into equation (2.13) we get average energy propagating in the z direction as $\mathrm{Re}\left[E_{oX}^2 \frac{\sqrt{\alpha^2 + \beta^2}}{2\mu\omega} \exp(-2\alpha z - j\gamma) \right]$.
For the EM wave propagating in z direction having E field polarized along x direction and H field polarized along y direction, the mean energy S_Z in the z direction can be given as,

$$S_Z = E_{oX}^2 \frac{\sqrt{\alpha^2 + \beta^2}}{2\mu\omega} \exp(-2\alpha z)\cos(\gamma) , \quad (2.14)$$

where $S_Z = \mathrm{Re}(\widetilde{S}_Z), E_{oX}$ is electric field at the surface and E_X is the E field at any distance z inside the medium. We know that $\tan\gamma = \frac{\alpha}{\beta}$ and $\cos\gamma = \frac{\beta}{\sqrt{\alpha^2+\beta^2}}$.

Substituting in equation (2.14) gives,

$$S_Z = E_{oX}^2 \frac{\beta}{2\mu\omega}\exp(-2\alpha z). \tag{2.15}$$

Here the mean energy flow is in the z direction and is given by S_Z. So energy transformed into heat per unit volume per second in the z direction is given by $-\frac{\partial S_Z}{\partial z}$.

Substituting value for S_Z from equation (2.15), energy lost as heat in the direction of propagation per unit volume per second is obtained as $-\frac{\partial S_Z}{\partial z} = \frac{\alpha\beta}{\mu\omega}E_{oX}^2\exp(-2\alpha z)$.

From equation (2.8) and (2.9), we can write,

$$\alpha\beta = \frac{\omega^2\mu\varepsilon}{2}\left[\left(\sqrt{1+\frac{\sigma^2}{\varepsilon^2\omega^2}}\right)^2 - 1\right]^{\frac{1}{2}} = \frac{\omega^2\mu\varepsilon}{2}.\frac{\sigma}{\varepsilon\omega} = \frac{\sigma\mu\omega}{2}.$$

So $\frac{\alpha\beta}{\mu\omega}E_{oX}^2\exp(-2\alpha z) = \frac{\sigma}{2}E_{oX}^2\exp(-2\alpha z)$ is the amount of energy transformed into heat and is the energy absorbed by the medium and is applicable for any medium. Therefore,

$$\text{Absorbed Energy} = \frac{\sigma}{2}E_{oX}^2\exp(-2\alpha z). \tag{2.16}$$

Equation (2.16) shows that the total exact EM energy transformed into heat per unit volume per unit second in the direction of propagation is product of conductivity of the medium and mean square value of the electric field. Total energy absorbed can be found by integrating the above function over the length of the path of propagation in the medium. Absorption goes down exponentially along the direction of propagation because

of the finite value of α. We have already noted that α^{-1} is defined as the skin depth of the medium.

2.6 Important Observations on Absorption

A number of useful observations can be made about energy absorption in a dielectric or a conductive medium from the above derived equations on absorption of energy and skin depths.

1. For the same amplitude of electric field we can see that for a given value of z when αz >> 1, absorbed energy along the direction of propagation decreases. This is because absorbed energy at a depth z inside the medium decays proportional to $\exp(-2\alpha z)$ and decreases with increase in the value of α. Absorbed energy also depends on the conductivity of the medium. Total mean absorbed energy per unit cross sectional area in the direction of propagation can be given as $\int_0^Z \frac{\sigma}{2} E_{oX}^2 \cdot e^{-2\alpha z} dz$. These results agree to the experimental and theoretical observations in reference [5].
2. Attenuation of a propagating wave inside a medium depends on the conductivity and dielectric properties of the medium. Total current density in a medium is given by $\widetilde{J} = \sigma\widetilde{E} + \varepsilon\frac{\partial\widetilde{E}}{\partial t} = (\sigma - j\omega\varepsilon)\widetilde{E}$. For conductors, $\sigma/\varepsilon\omega >> 1$ and conductive current component is much greater than the displacement current. In the case of dielectric mediums $\sigma/\varepsilon\omega << 1$ and displacement current is larger than the conductive current. As has been derived in section 2.4.1, for dielectric mediums, absorbed energy will be calculated using dielectric conductivity $\sigma' = \omega\varepsilon''$.

3. For dielectric mediums, $\sigma^2 / \varepsilon^2 \omega^2 << 1$ and it can be shown from (2.8) that $\alpha = \frac{\sigma}{2}\sqrt{\frac{\mu}{\varepsilon}} = \frac{\omega\varepsilon''}{2}\sqrt{\frac{\mu}{\varepsilon_r \varepsilon_0}}$. For a dielectric medium attenuation factor (α) of EM waves increases linearly with frequency if ε'' does not vary significantly with frequency. The attenuation factor α decreases inversely proportional to square root of relative permittivity value of the medium.

4. For a good conductor $\sigma^2 / \varepsilon^2 \omega^2 >> 1$ and from equation (2.8) the attenuation factor can be written as $\alpha = \sqrt{\frac{\omega\mu\sigma}{2}}$. The above assumption $\sigma^2 / \varepsilon^2 \omega^2 >> 1$ is easily justified for typical conductors like Cu with conductivity = 6.66 x 10^{+7} $s.m^{-1}$ for any practical and realizable frequency of EM waves. For a good conductor, attenuation factor (α) decreases as the square root of frequency and conductivity. Normally, permeability for all non-magnetic conductors is approximately the same.

5. Energy crossing a good conductor per unit area per second along the direction of propagation from equation (2.15) is,

$E_{oX}^2 \frac{\beta}{2\mu\omega}\exp(-2\alpha z) = \frac{E_{oX}^2}{2}\sqrt{\frac{\sigma}{2\mu\omega}}\exp(-\sqrt{2\omega\mu\sigma}\, z)$, as $\alpha = \beta = \sqrt{\frac{\omega\mu\sigma}{2}}$ for a good conductor. Energy per unit area per unit second propagating in the forward direction is expected to decrease with increase in frequency.

6. For a dielectric medium the same equation for electromagnetic energy crossing per unit area in the direction of propagation can be written as,

$$E_{oX}^2 \frac{\sqrt{\varepsilon}(1+\frac{\sigma'^2}{8\varepsilon^2\omega^2})}{2\sqrt{\mu}} \exp(-\sigma'\sqrt{\frac{\mu}{\varepsilon}}z) \quad \text{as} \quad \beta = \omega\sqrt{\mu\varepsilon}(1+\frac{\sigma'^2}{8\varepsilon^2\omega^2}) \quad \text{and} \quad \alpha = \frac{\sigma'}{2}\sqrt{\frac{\mu}{\varepsilon}}$$

for a dielectric medium [13]. Here dielectric conductivity $\sigma' = \omega\varepsilon''$ as discussed in section 2.4.1 has been used. It can be seen that with increase in frequency, energy flow inside the dielectric medium reduces even more compared to a conductor if operated at a high enough frequency where dielectric thickness is large for the attenuation to start becoming significant.

2.7 Reflection and Refraction of EM Waves in Dielectric and Conductive Mediums

Energy that gets reflected at the transmitter excitation port and at interfaces between different layers has to be reduced, in order to increase the amount of energy received by the receiver. Part of the incident energy, that gets reflected depends on the properties of the mediums such as relative dielectric constant and conductivity values. Laws of reflection and refraction of EM waves as derived in EM theory are applicable in biological tissue and bodies as long as the wavelengths of incident EM waves are greater than the cell dimensions. If wavelengths are smaller than the cell size, the incident wave undergoes scattering by the tissue cells.

2.8 Reflection and Refraction at a Plane Surface

Reflection and refraction of incident E field at the interface of two isotropic mediums with electrical properties ε_1, μ_1, σ_1 and ε_2, μ_2, σ_2 respectively as shown below in Figure 2.4 will be discussed here. Medium 2 is where the incident and the reflected beams are available and medium 1 is the one which has the transmitted beam. E_i is the incident E field polarized normal to the plane of incidence, E_r is the reflected E field and E_t is the transmitted E field. Values of the reflected and transmitted fields can be given as [13],

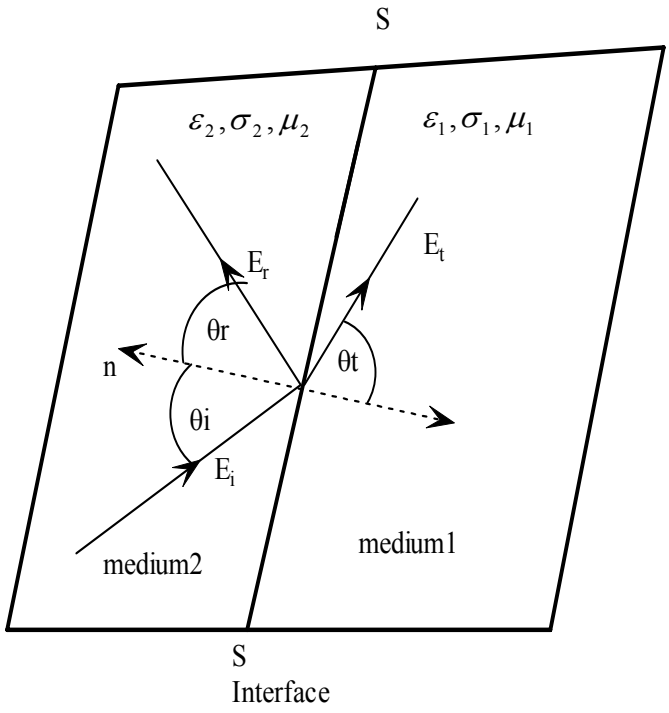

Figure 2.4: Reflection and refraction at planar surface. Here angle of incidence = θ_i, angle of reflection = θ_r, and angle of transmission = θ_t. n is the normal to interface S-S.

$$E_t = \frac{\mu_1 \kappa_2 (\cos\theta_r + \cos\theta_i)}{\mu_1 \kappa_2 \cos\theta_r + \mu_2 \kappa_1 \cos\theta_t} E_i \tag{2.17}$$

and $$E_r = \frac{\mu_1 \kappa_2 \cos\theta_i - \mu_2 \kappa_1 \cos\theta_t}{\mu_1 \kappa_2 \cos\theta_r + \mu_2 \kappa_1 \cos\theta_t} E_i , \tag{2.18}$$

where angle of incidence = θ_i, angle of reflection = θ_r, and angle of transmission = θ_t. All of these angles are taken with respect to the normal to the interface shown in Fig. 2.4. Eliminating angle of refraction and angle of transmission from the above equation with the help of Snell's law given below, simplified equation can be written in terms of θ_i as [13]:

$$E_t = \frac{2\mu_1 \kappa_2 \cos\theta_i}{\mu_1 \kappa_2 \cos\theta_i + \mu_2 \sqrt{\kappa_1^2 - \kappa_2^2 \sin^2\theta_i}} E_i \tag{2.19}$$

$$E_r = \frac{\mu_1 \kappa_2 \cos\theta_i - \mu_2 \sqrt{\kappa_1^2 - \kappa_2^2 \sin^2\theta_i}}{\mu_1 \kappa_2 \cos\theta_i + \mu_2 \sqrt{\kappa_1^2 - \kappa_2^2 \sin^2\theta_i}} E_i \tag{2.20}$$

Here κ_1 and κ_2 are the complex propagation factors of medium 1 and 2 respectively. Both κ_1 and κ_2 are given by $k^2 = \mu\varepsilon\omega^2 + j\mu\sigma\omega$. Equation (2.19) and (2.20) are derived using 1) $\theta_r = \theta_i$ and 2) $\kappa_1 \sin\theta_t = \kappa_2 \sin\theta_i$.

For propagation direction normal to the plane of incidence $\theta_i = 0$ and then the reflected and transmitted E fields, for perpendicular E field polarization, can be written from equation (2.19) and (2.20) as:

$$E_t = \frac{2\mu_1 \kappa_2}{\mu_1 \kappa_2 + \mu_2 \kappa_1} E_i \tag{2.21}$$

$$E_r = \frac{\mu_1 \kappa_2 - \mu_2 \kappa_1}{\mu_1 \kappa_2 + \mu_2 \kappa_1} E_i \tag{2.22}$$

For normal incidence, fields are identical for both normal and parallel polarization. Equation (2.21) and (2.22) can be further simplified for different properties of mediums of incidence and transmission.

2.8.1 Dielectric to Dielectric

For a dielectric medium with the assumption that σ is very small, it can be written from equation (2.7) that $\kappa = \sqrt{\mu\varepsilon}\omega$ and the above equations can be simplified to,

$$E_t = \frac{2}{1+\sqrt{\frac{\mu_2\varepsilon_1}{\mu_1\varepsilon_2}}} E_i \tag{2.23}$$

and

$$E_r = \frac{1-\sqrt{\frac{\mu_2\varepsilon_1}{\mu_1\varepsilon_2}}}{1+\sqrt{\frac{\mu_2\varepsilon_1}{\mu_1\varepsilon_2}}} E_i. \tag{2.24}$$

2.8.2 Dielectric to Conductor

In this case, because of the complex values of the propagation factor κ, amplitudes of the reflected and transmitted field components are complex in nature. Reflected component of the E field can be written as $E_r = \rho \exp(-i\delta) E_i$, where ρ is called the coefficient of reflection and δ is the associated phase. For incident E field polarization normal to the plane of incidence and dielectric to conductor incidence of EM waves, it has been shown by Stratton [13] that,

$$\rho^2 = \frac{(1-\frac{\mu_1\beta_2\cos\theta_i}{\mu_2\beta_1})^2 + 1}{(1+\frac{\mu_1\beta_2\cos\theta_i}{\mu_2\beta_1})^2 + 1} \tag{2.25}$$

and $\tan\delta = \frac{\mu_1\beta_2}{\mu_2\beta_1}\frac{2\cos\theta_i}{(\frac{\mu_1\beta_2}{\mu_2\beta_1})^2(\cos^2\theta_i - 1)}$. (2.26)

Defining [13] P = $\frac{\mu_1\beta_2}{\mu_2\beta_1} = \frac{\mu_1\omega\sqrt{\mu_2\varepsilon_2}}{\mu_2\sqrt{\frac{\omega\mu_1\sigma_1}{2}}} = \sqrt{\frac{2\mu_1\omega\varepsilon_2}{\mu_2\sigma_1}}$, where $\beta_2 = \omega\sqrt{\mu_2\varepsilon_2}$ since medium 2 is a dielectric and $\beta_1 = \sqrt{\frac{\omega\mu_1\sigma_1}{2}}$ because medium 1 is a conductor in this particular case. Then for frequency range $f << \frac{\sigma_1}{2\varepsilon_2}$, it can be seen that P<<1 and it can be written from equation (2.25) and (2.26) that $\rho^2 \approx 1 - 2P\cos\theta_i$ and $\tan\delta = -2P\cos\theta_i$ [13]. As discussed above value of P is much smaller than 1 for $f << \frac{\sigma_1}{2\varepsilon_2}$, so it can be said that for dielectric to conductor incidence of EM waves, reflection coefficient (ρ) is almost independent of the angle of incident and is close to 1 for frequencies $f << \frac{\sigma_1}{2\varepsilon_2}$. To decrease reflection to a local minimum, values of P should be increased. It can be seen from the expression for P that it can be increased by increasing frequency. Also if relative permittivity of the dielectric medium goes up, P increases and reflection decreases. On the other hand if conductivity of the conductor goes up, reflection increases as P decreases.

2.8.3 Conductor to Dielectric

For this case it can be shown that reflection coefficient (ρ) is independent of frequency for sufficiently high frequency range [13], $E_r = [\frac{1-\sqrt{\frac{\mu_2\varepsilon_1}{\mu_1\varepsilon_2}}}{1+\sqrt{\frac{\mu_2\varepsilon_1}{\mu_1\varepsilon_2}}}]^2 E_i$. As the dielectric constant value of the dielectric medium goes down with increase in frequency, reflection coefficient

is expected to increase, because variation of dielectric constant value of a conductor with frequency is negligible. So to decrease reflection at this interface, lower frequencies might be used.

2.9 Snell's Law and Angle of Refraction in Different Mediums

Snell's law is given by the following equation, where κ_1 and κ_2 are the complex propagation factors of medium 1 and 2 respectively and θ_t, θ_i are the angle of refraction and incidence respectively.

$$\sin\theta_t = \frac{\kappa_2}{\kappa_1}\sin\theta_i \tag{2.27}$$

2.9.1 Dielectric to Dielectric Incidence

It can be shown from equation (2.27) that $\sin\theta_t = \sqrt{\frac{\varepsilon_2}{\varepsilon_1}}\sin\theta_i$. For incidence from a medium with lower value of dielectric constant to a biological medium (For example from air to human skin), immaterial of the angle of incidence, the refracted field will be almost normal to the plane of incidence even for grazing incidence, because biological mediums have very high values for relative permittivity.

2.9.2 Dielectric to Conductor Incidence

For this case, it can be shown [13] that $\sin\theta_t = \sqrt{\frac{2\omega\mu_2\varepsilon_2}{\mu_1\sigma_1}}\sin\theta_i$. It is evident that for all practical usable frequency values, the angle of refraction would differ very little from zero. So the refracted field will be normal to the conductor.

2.9.3 Conductor to Dielectric Incidence

The above law may be used to find angle of refraction in a dielectric medium for the EM wave incident from a conductor medium. It can be seen that all real angles of refraction

will be approximately right angles. So the refracted beam will be parallel to the dielectric medium.

2.10 S Parameters and Calculation of Reflection from Simulations

The reflection and forward transmission of EM fields in a system can be very well described with the S parameter representation of the system. The system is defined by its two port representation. For the two port system shown in Figure 2.5, its S parameters can be described with the following equations.

$$E_{r1} = S_{11}E_{i1} + S_{12}E_{i2} \tag{2.28}$$

$$E_{r2} = S_{21}E_{i1} + S_{22}E_{i2} \tag{2.29}$$

The above equations show the relation between S parameters (S_{11}, S_{12}, S_{21}, and S_{12}) and the different components of E field at the two ports. If the output port 2 is driven with the load termination equal to Z_o (characteristic impedance of the two port network), then E_{i2} becomes zero and S_{11} can be written as in the following equation. Γ_1 is also known as the input coefficient of reflection [14].

$$S_{11} = \frac{E_{r1}}{E_{i1}} = \Gamma_1 \tag{2.30}$$

This is simply input reflection coefficient. In the simulated results for S parameter, S_{11} will give percentage of reflection at the input port for the problem.

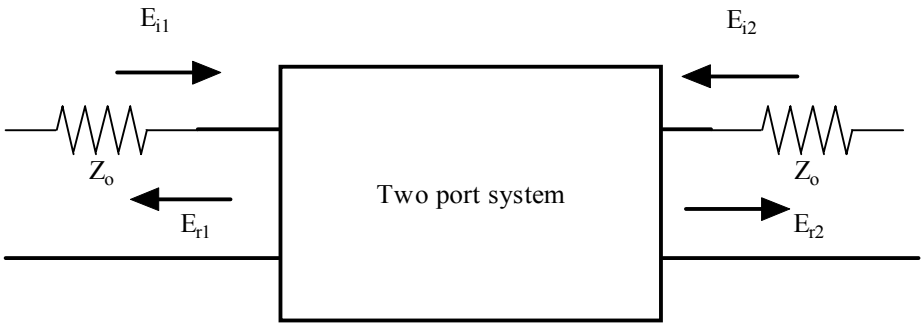

.

Figure 2.5: Two port network. Above figure shows the two port network where E_{i1} and E_{i2} are incident fields at port 1 and port 2 respectively whereas E_{r1} and E_{r2} are the reflected fields at port 1 and port 2 respectively.

CHAPTER 3

SELECTION OF OPTIMUM FREQUENCY OF OPERATION

3.1 Introduction

Choice of a frequency of operation for the transmitter – receiver system for an implantable biomedical system depends on a number of factors. It has to be chosen such that the system operates at a maximum possible power coupling. At that frequency, absorption of the transmitted energy by biological tissues also should be as low as possible. Reflection of incident field by the body should also be small. In the following sub-sections all of these have been discussed in detail.

3.2 Circuit Laws for Optimum Frequency of a Receiver–Transmitter Coupled Coil

Without any consideration of the transmitter, electromotive force (EMF) induced in the receiver shown in Figure 3.1, for a harmonic ($e^{-j\omega t}$) time varying magnetic field produced by the transmitter can be calculated from Faraday's law. Induced EMF is given by, $-\frac{d\tilde{\Phi}}{dt} = j\omega\tilde{\Phi}$. Here $\tilde{\Phi}$ is the magnetic flux induced at the secondary coil due to the transmitter coil. Magnitude of induced EMF is $\omega\Phi$. Then the power delivered to the receiver load R at resonance is given by:

$$P_L = \left(\frac{\omega\Phi}{R_S + R}\right)^2 R, \tag{3.1}$$

where R_S is the secondary coil resistance and R is the load resistance. Here coil self-capacitances are neglected. It can be seen from equation (3.1) that the maximum value of the power delivered at resonance to the receiver is proportional to ω^2. At very low frequencies, we would expect lower values of power coupling between the receiver and

transmitter coils. To get an idea of efficiency of transmitter – receiver system, both the transmitter and the receiver losses have to be taken into account.

For the coupled transmitter – receiver coil shown in Figure 3.2, neglecting both coil self capacitances C_P and C_S and following kirchoff's law we can write for the secondary side at resonance, $0 = \bar{I}_P j\omega M + (R + R_S)\bar{I}_S \Rightarrow \bar{I}_P = -\frac{(R + R_S)\bar{I}_S}{j\omega M}$. RMS value of secondary coil current $\bar{I}_S$ can be written as, $I_S = (\frac{P_L}{R})^{1/2}$, since P_L is the power loss in the load resistance R, RMS magnitude of primary current can be written as, $I_P = \frac{(R + R_S)\sqrt{\frac{P_L}{R}}}{\omega M}$. Therefore, power loss P_P in the primary coil is given as:

$$P_P = I_P^2 R_P = \frac{P_L}{Q_P Q_S \kappa^2}(m + 2 + \frac{1}{m}), \tag{3.2}$$

where $Q_P = \frac{\omega L_P}{R_P}$, $Q_S = \frac{\omega L_S}{R_S}$ and $M = \sqrt{L_S L_P}\kappa$, κ is known as the coefficient of coupling and $m = \frac{R}{R_S}$. Q_P and Q_S are known as Q factors of the transmitter and the receiver coils respectively. Secondary coil power loss P_S is given by $I_S^2 R_S = \frac{P_L}{m}$. Efficiency η of the coupled system at secondary coil resonance can be defined as, $\eta = \frac{P_L}{P_L + P_P + P_S}$. Substituting the values for P_P, P_S in the above equation for efficiency, one can obtain:

$$\eta = \frac{1}{1 + \frac{1}{m} + \frac{1}{Q_P Q_S \kappa^2}(m + 2 + \frac{1}{m})} \quad . \tag{3.3}$$

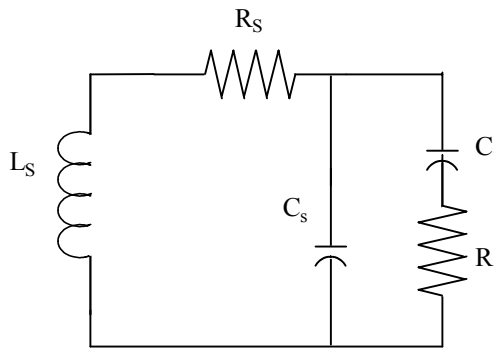

Figure 3.1: Secondary Coil. Figure shows the receiver coil with an inductance of L_S and coil resistance R_S and self capacitance C_s. C and R are the receiver load capacitance and resistance respectively. In all the analysis, self capacitance has been neglected.

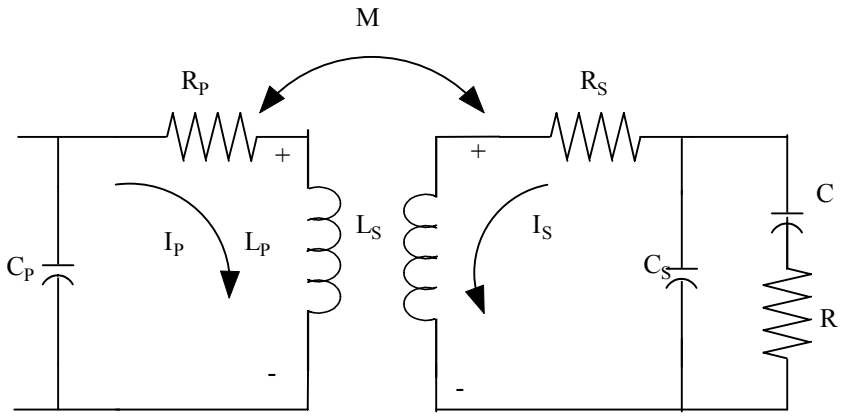

Figure 3.2: Coupled transmitter-receiver coils. L_P and L_S are transmitter and receiver inductances respectively, R_S and R_P are transmitter and receiver resistances and I_P and I_S are transmitter and receiver currents respectively. M is the mutual coupling between the coils. C_S and C_P are the self capacitances of the secondary and primary coils respectively and they are neglected in this analysis.

Equation (3.3) indicates that efficiency should go up with frequency and becomes independent of ω at very high frequency. In real coils, self resonance factors will limit application of the above result at higher frequencies.

3.3 Radar Theory Consideration for Optimum Transmission and Reception

From radar theory, power received at the receiver P_r is given as [15]:

$$P_r = \left(\frac{P_t G_t}{4\pi r^2}\right)\left(\frac{\sigma_A}{4\pi r^2}\right)\left(\frac{G_r \lambda^2}{4\pi}\right), \tag{3.4}$$

where, r is the distance of the receiver from the transmitter, P_t is transmitter power, G_t is the gain of the transmitter, G_r is the gain of the receiver, σ_A is effective area of the receiver in the direction perpendicular to the propagation of incident power and λ is wavelength of the incident wave. Equation (3.4) is applicable under the assumptions that no large obstacles intervene between antenna and target along an optical line of sight, no alternate transmission path exists via a reflecting surface, the intervening atmosphere is homogeneous with respect to index of refraction at the frequency used and the intervening atmosphere is transparent, i.e., does not absorb energy from the wave. It can be seen from equation (3.4) that for a given constant cross section and receiver gain, received power is proportional to square of the incident frequency or,

$$P_r \propto f^2 \quad . \tag{3.5}$$

It is also necessary to maintain certain level of beam sharpness for any reasonable gain for a transmitter or a receiver. The sharpness of a beam passing through an aperture of given size depends on the ratio of the diameter of the aperture to the wavelength of the radiation in the beam. For an antenna of given size, the breadth of the beam produced is proportional to the wavelength. So ratio of antenna size to wavelength should be large for beam sharpness. Antenna size should be chosen such that it is greater than wavelength of

EM waves for acceptable beam sharpness. For reasonable antenna efficiency, the size of an antenna should be greater than $\lambda/4$ [15]. So the frequency has a lower threshold for maintaining this upper-threshold of wavelength. However control of beam width shape may become a problem when the antenna size exceeds several wavelengths [15].

Form the above discussion, two points can be noted. First, from equation (3.5) we can see that, received power is proportional to the square of frequency. So low frequencies may lead to inadequate received power. Second, as antenna size cannot be made arbitrarily larger in a practical implantable system, so wavelength of the transmitted wave also cannot be greater than a certain value. This restricts lower limit of frequency of transmission to maintain the beam sharpness.

3.4 Wave Propagation through a Guided Medium

Excitation of EM waves to propagate through a guided medium is not possible under a certain threshold frequency. For an EM wave traveling in z direction in a waveguide with width a and height b, if it is assumed that the cross-section of the wave-guide is lying in the XY plane and wave propagates along z direction, then the frequency f_C of excitation corresponding to the lowest mode is given as [13]:

$$f_C = \frac{v_g}{2a} \quad \text{for a > b} \tag{3.6}$$

where v_g is the group velocity of the wave in that medium [13]. The lowest mode of excitation by definition corresponds to the lowest frequency of excitation. If the frequency is below the one specified above by equation (3.6), that wave would not propagate along the waveguide. This is a problem of realizing EM power transmission at low frequencies with a practical size waveguide

3.5 Absorption and Reflection Consideration

It has been discussed in section 2.5 that absorbed energy in a medium can be given as, $\frac{\sigma}{2}E_{oX}^2 \exp(-2\alpha z)$ from equation (2.16). The attenuation factor α depends on dielectric and conductive properties of the medium. It also depends on the frequency of operation. From the derivations in section 2.6, attenuation factors for a conductor and a dielectric medium can be given as:

$$\alpha_{CONDUCTOR} = \sqrt{\frac{\omega\mu\sigma}{2}} \tag{3.8}$$

$$\text{and } a_{DIELECTRIC} = \frac{\sigma'}{2}\sqrt{\frac{\mu}{\varepsilon_r\varepsilon_0}} \tag{3.9}$$

respectively. These two equations show that value of α always increases with frequency and so attenuation always increases with frequency for both dielectric and conductors. Following table shows skin depth (α^{-1}) of Cu at different frequencies.

Table 3.1: Skin depth (α^{-1}) of Cu at different frequencies from equation (3.8).

Frequency (Hz)	10^2	10^3	10^4	10^5	10^6	10^7	10^8
Skin-depth (m)	$1.55\text{x}10^{-2}$	$4.9\text{x}10^{-3}$	$1.5\text{x}10^{-3}$	$4.9\text{x}10^{-4}$	$1.5\text{x}10^{-4}$	$4.9\text{x}10^{-5}$	$1.5\text{x}10^{-5}$

In the Figure 3.3, thickness inside dry skin at which E or H field will be attenuated to a value of e^{-1} times their magnitude at the surface are plotted for a wide range of frequencies. As discussed in section 2.6, at lower frequencies, absorption in the skin and peripheral layers would increase with increase in frequencies, because dielectric conductivity $\sigma' = \omega\varepsilon''$, increases with frequency [13]. But equation $\frac{\sigma}{2}E_{oX}^2 \exp(-2\alpha z)$

also shows that at higher frequencies, when attenuation factor starts being significant, absorption at a depth z in the medium actually starts decreasing due to the exponentially decreasing term. Ideally very low absorption is expected at low frequencies and as such very good transmission efficiency should be possible. But the other constraints as discussed in sections 3.1 to 3.4 should also be taken into consideration. The frequency of operation should be chosen in such a way that absorption in the different layers be as small as possible. Efficiency of power transmission is low at low frequencies as discussed in section 3.1. Equation (2.16) for absorption shows absorption due to local electric field which does not include the reflected energy at the port of excitation. So reflection and refraction have also to be considered. Therefore, we need to choose the lowest frequency for which,

(a) There is minimum reflection of the incident wave. This can be decided by looking at the S parameter values.

(b) It is feasible to generate the transmission.

(c) Absorption in the medium should be as low as possible, and

(d) Efficiency of the transmitter – receiver coil system is high.

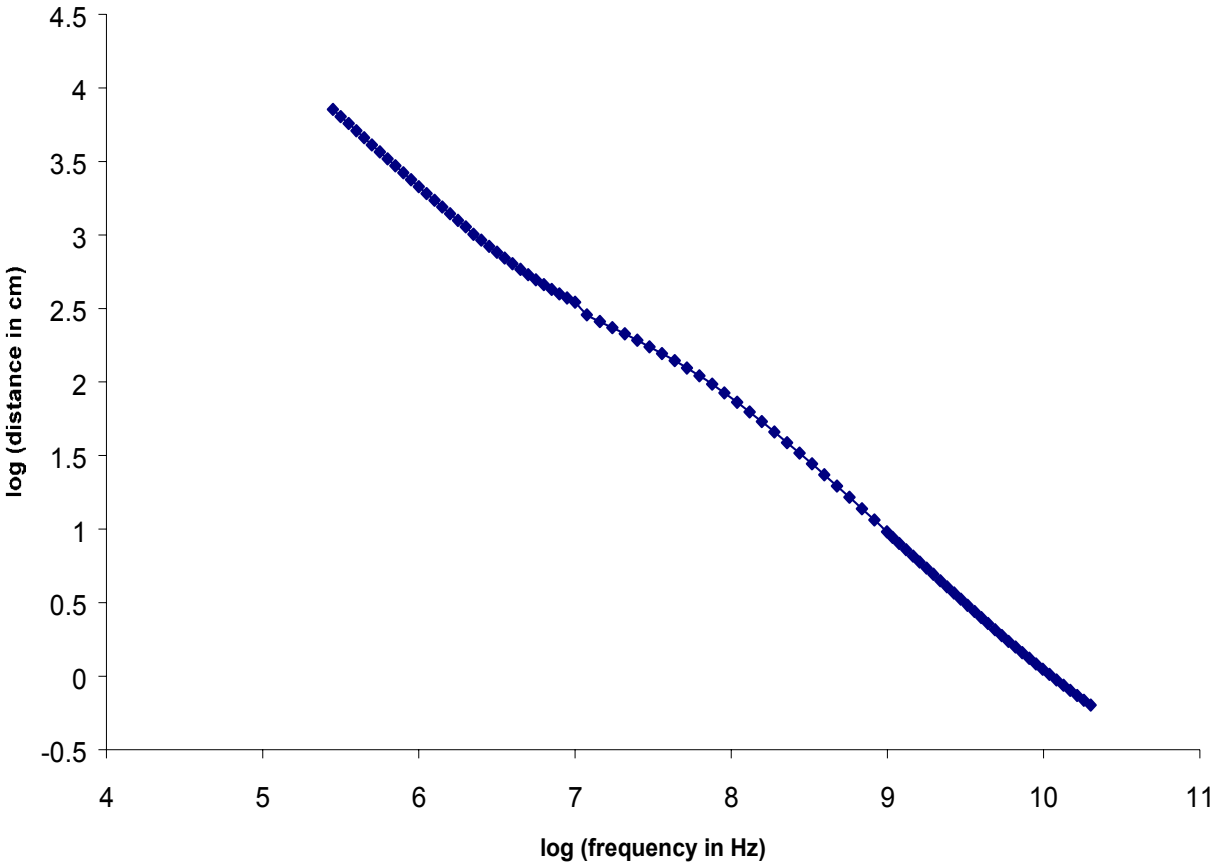

Figure 3.3: Distance (α^{-1}) at which E or H field magnitude attenuates inside dry skin to e^{-1} times its value at the surface plotted as a function of frequency. It has been calculated with the equation (3.9) and using the data from reference [16]. Losses due to displacement current are not included here.

CHAPTER 4

ABSORPTION OF ELECTROMAGNETIC RADIATION IN A HUMAN BODY: ANALYTICAL AND SIMULTED RESULTS FROM LITERATURE

4.1 Simulated Results on Absorption in a Human Body

A number of experimental as well as simulation works [8– 10, 17-18] are available which discuss absorption of EM radiation by a human body. A number of results from the discussion of physics of absorption in sections 2.5 and 2.6 and reflection of EM waves in sections 2.8 and 2.9, can be directly applied to study these results and to draw conclusions. Absorbed power in any biological medium depends on the frequency of the incident EM wave and properties of the medium; its size, shape and orientation with respect to the incident field polarization. Interior structure and EM properties such as relative permittivity, loss tangent and conductivity of the medium also play an important role. Figure 4.1 shows variation of free space specific absorption rate (SAR) by a human body vs. frequency [6]. In Fig. 4.1, curve A is for E polarization parallel to the length of the human body model and propagation direction from arm to arm, curve B is for propagation direction parallel to the length of the human body model and E field polarized along arm to arm and curve C is for H field polarization along the length of the human body model and propagation direction from front to back of the human body. Figure 4.2 shows experimental values of absorbed power vs. frequency [8] for a phantom (cylindrical) model of a monkey. Figure 4.3 shows experimental values of absorbed power vs. frequency [8] for a phantom (cylindrical) model of a human body.

In the simulations carried out in this thesis, excitation EM wave is TEM as will be discussed in chapter 5 and so cross-polarization results in both Fig. 4.2 and Fig. 4.3,

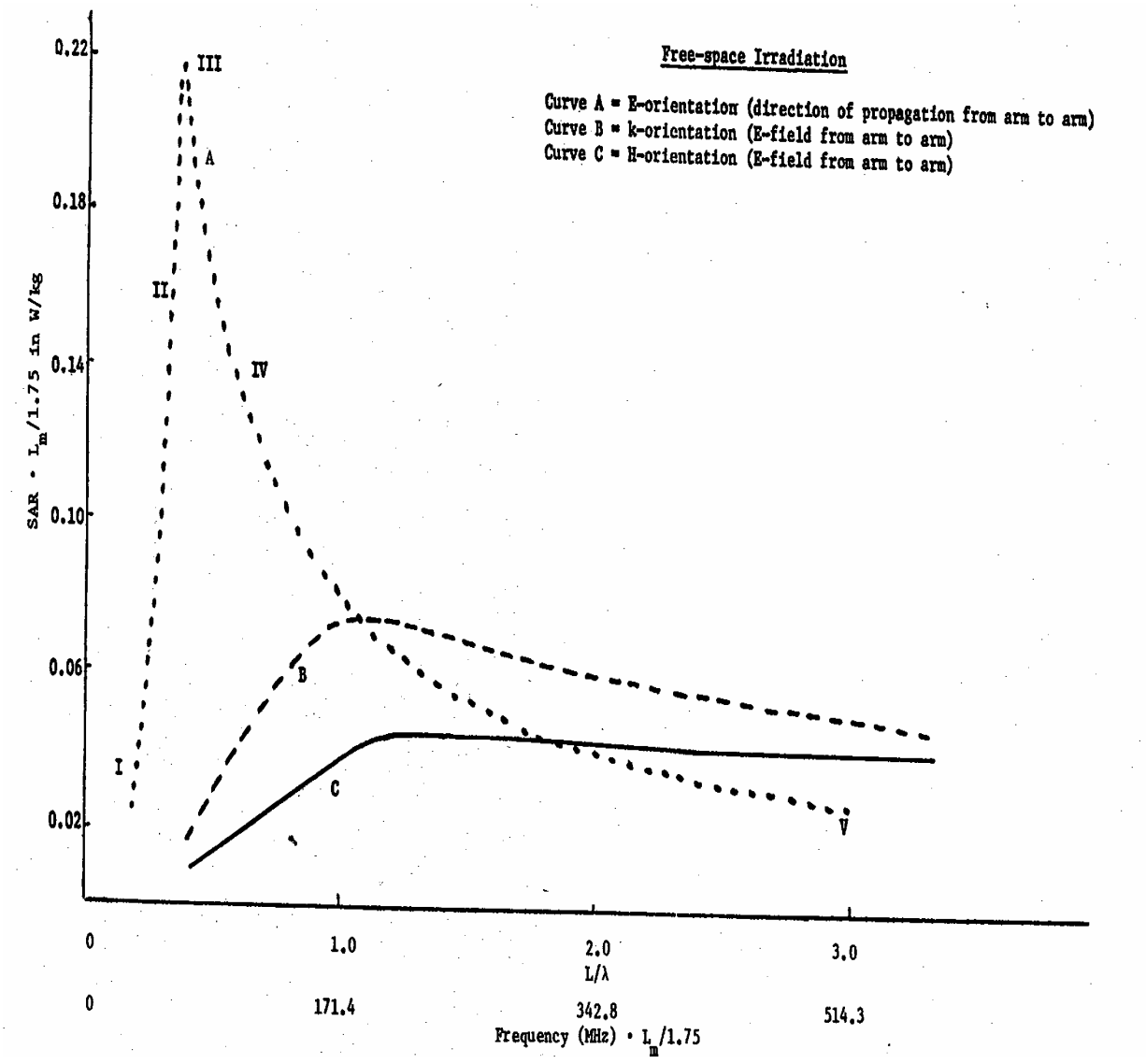

Figure 4.1 Absorption by a human body at different frequencies, showing whole body averaged SAR in $W.Kg^{-1}$ for models of a human body for incident fields of $1mW.cm^{-2}$ for frequencies upto 514.3 MHz. (Printed with permission from reference 6, © 2003 IEEE.)

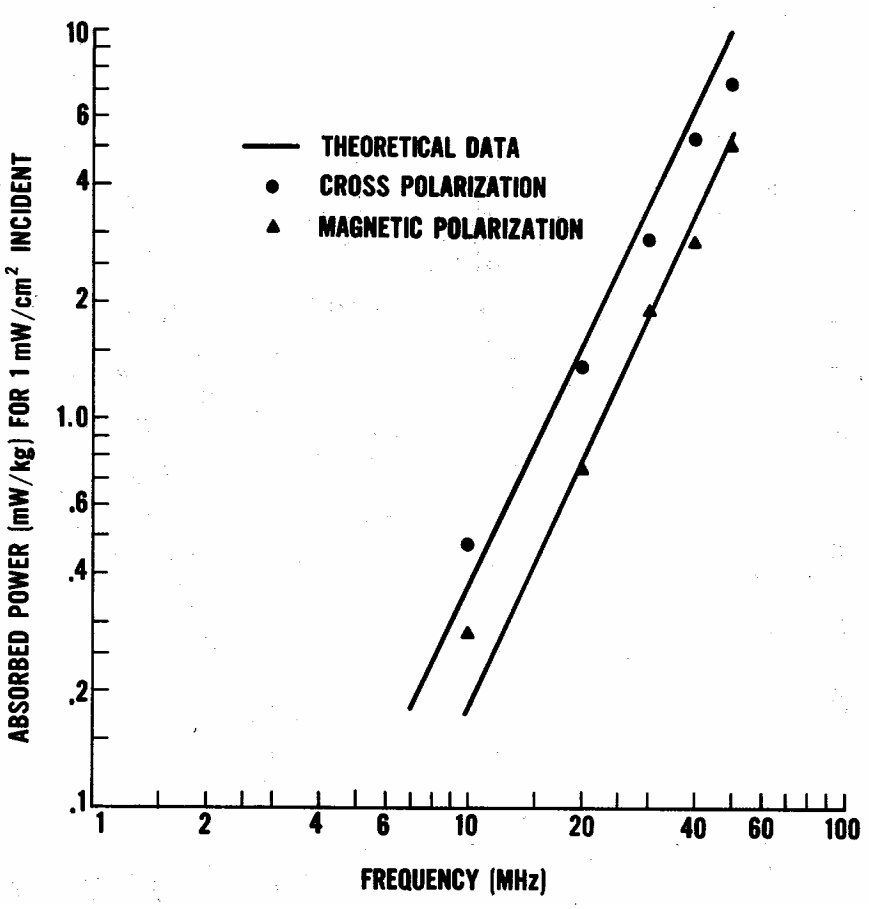

Figure 4.2: Experimental values of EM absorption for a monkey phantom model, [Printed with permission from reference 8]. Experimental values of absorbed power by a cylindrically symmetrical model for a monkey are plotted upto 100 MHz.

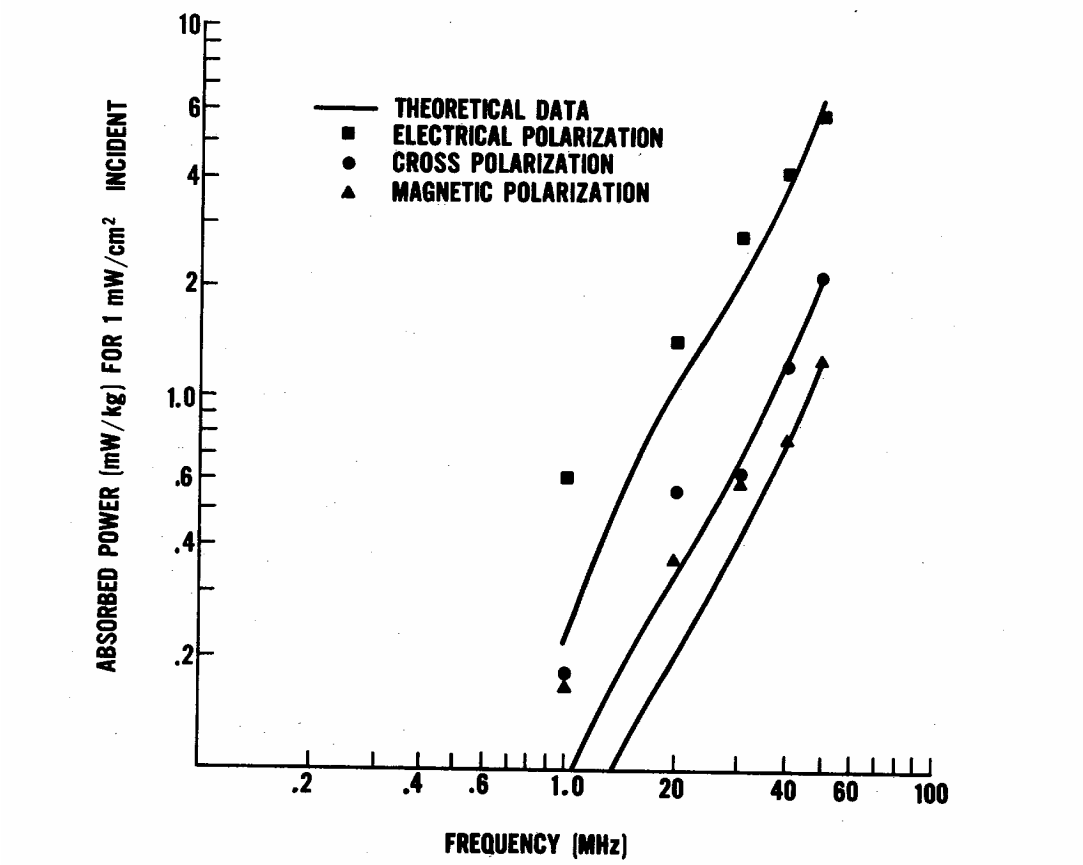

Figure 4.3: Experimental values of EM absorption for a human phantom model, [Printed with permission from reference 8]. Experimental values of absorbed power by a cylindrically symmetrical model of a human body are plotted upto 100 MHz.

(where both E and H fields are normal to the direction of propagation) may be applicable to our model. The low frequency absorption till 100 MHz as shown by Fig. 4.1 is confirmed by the experimental results in Figures 4.2 and 4.3.

Some observations:

1. From Fig. 4.1 highest absorption is found to occur at a frequency at which dimension of human body (L_m) is related to wavelength (λ) by $L_m \sim 0.4\lambda$ [6]. This condition is known as resonance. At resonance absorbed energy cross section is greater than unity. This implies that influence of body to the incident radiation extends beyond geometrical boundaries. Resonance frequency is a function of the size, shape and dielectric properties of the body. Resonance may arise when the dimension of the body becomes exact multiples of the half wavelength of the incident EM wave. Inside a human tissue, wavelengths of the propagating EM waves depend on its dielectric and conductive properties and also on its shape. At resonance no energy is lost if the enclosing structure is made out of an ideal conductor or dielectric. Wave travels back and forth in the enclosed structure. But there are conductor losses and dielectric losses as well in a real structure like human body and amplitude of the standing wave pattern will eventually die down. Figures 4.4 and 4.5 show variation of relative absorption (defined as the ratio of absorbed energy to the transmitted energy) vs. $a.\lambda^{-1}$ for a spherical model of a human body, where λ is the wavelength of the incident radiation and a stands for the sphere radius. While Fig. 4.4 shows results for conductivity $\kappa = 10$ s.m^{-1}, Fig. 4.5 shows the same for conductivity $\kappa = 1$ s.m^{-1} and it is observed that absorption at resonance goes down with increase in conductivity.

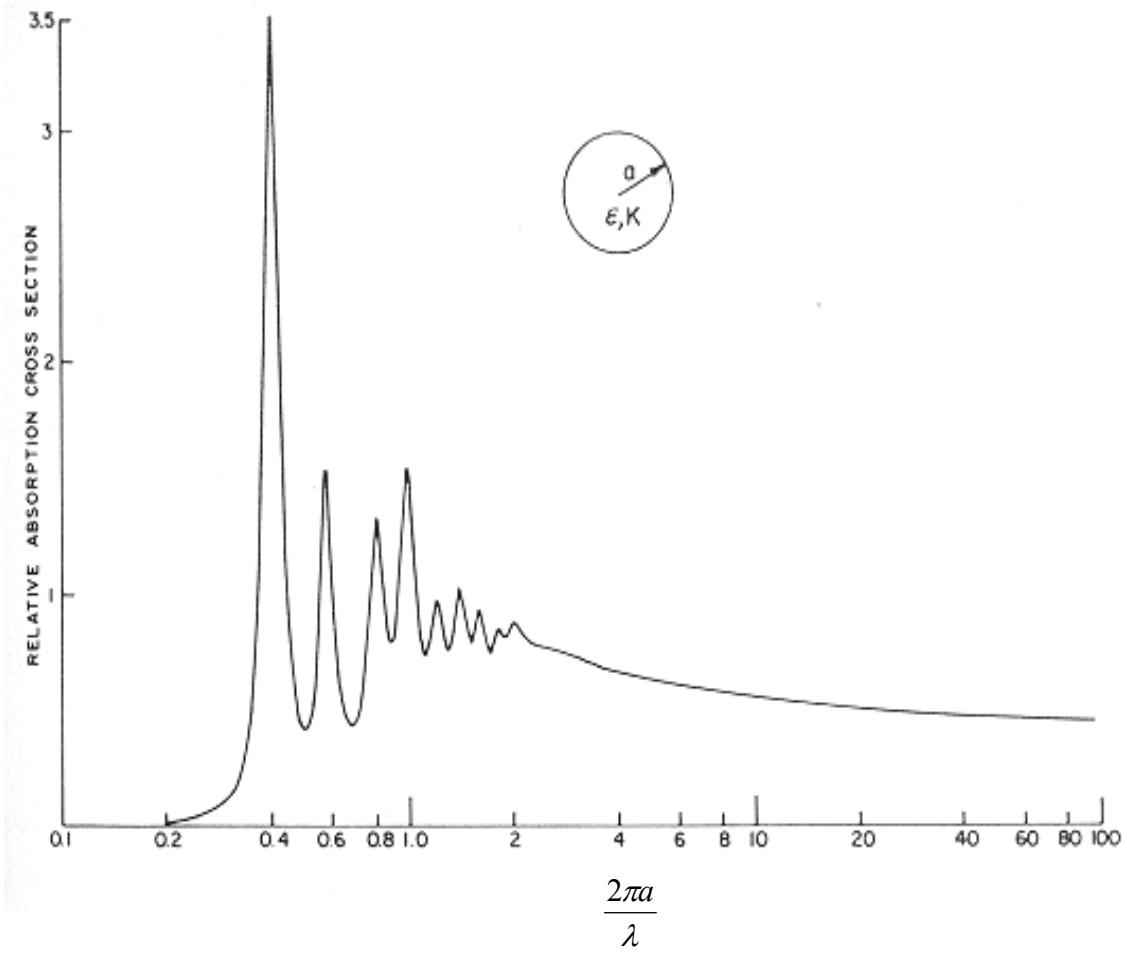

Figure 4.4: Relative absorption as function of λ^{-1} for a spherical model for a human body, Results are obtained with conductivity κ = 10 s.m^{-1}, for the spherical model. Printed with permission from reference [2], © 2003 IEEE.

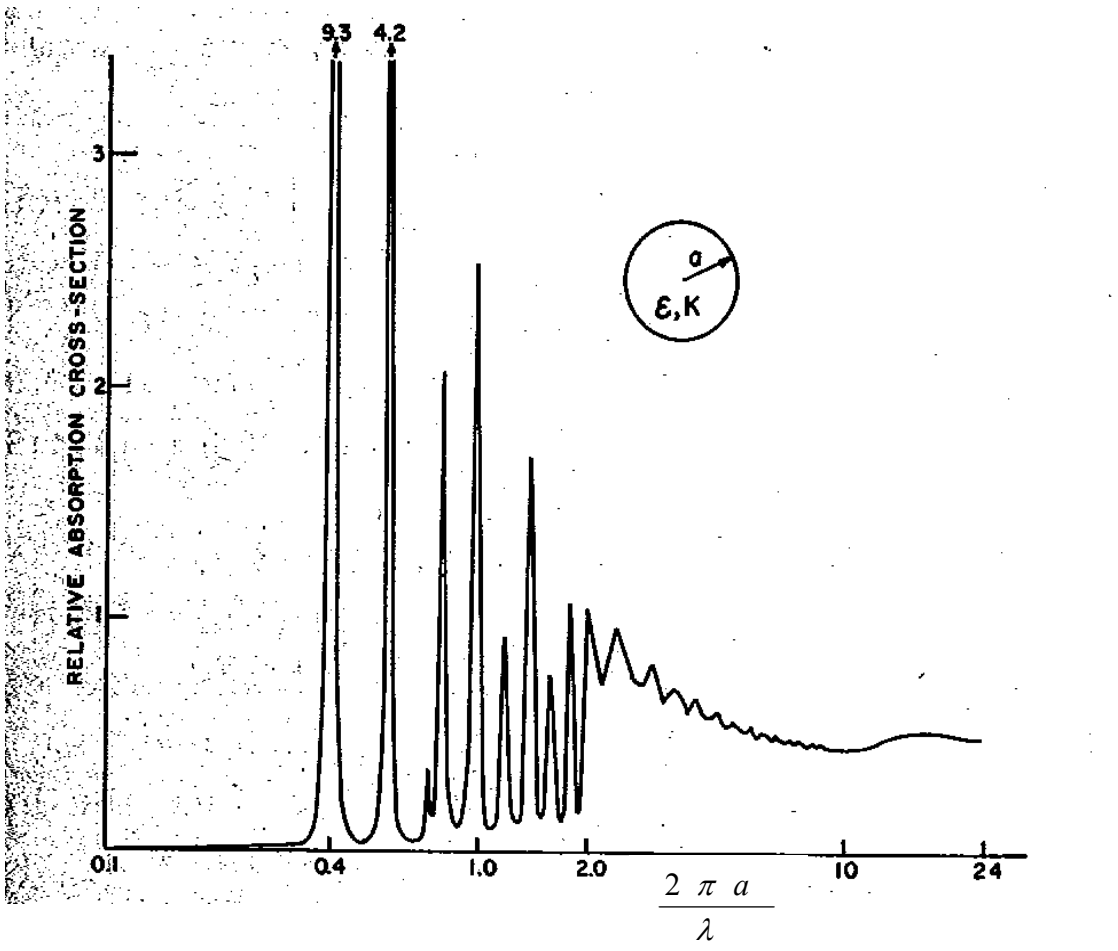

Figure 4.5: Relative absorption as function of λ^{-1} for a spherical model for a human body. Results are obtained with conductivity κ = 1 s.m^{-1}, for the spherical model. Printed with permission from reference [2], copyright@IEEE);

Comparison of Figure 4.4 and Figure 4.5 shows that as conductivity increases, magnitude of relative absorption goes down at resonance. Also it can be observed that in both cases, at higher values of ($\frac{a}{\lambda}$) resonance dies down.

2. Absorption depends on the orientation of human body, propagation direction and electric field polarization. Figure 4.1 shows that it is the maximum when electric field polarization is parallel to the longest dimension of human body and propagation direction of the EM wave is from arm to arm.

3. From Fig. 4.1, we can see that absorption goes up with frequency till it reaches a resonance frequency. This dependence has been experimentally confirmed as f^2 [9]. It then starts decreasing and this dependency has been found to be proportional to f^{-1} [6]. Decrease in absorption at frequencies higher than the resonance frequency as shown in figure 4.1 can be explained with the help of theoretical results on EM radiation absorption in a medium as discussed in section 2.6. Absorption per unit volume per unit time inside a medium at a depth z is given by $\frac{\sigma}{2} E_{oX}^2 \exp(-2\alpha z)$. As derived in section 2.6, for a dielectric medium, absorbed energy per unit time per unit volume in the direction of propagation can be written as $E_{oX}^2 \frac{\omega\varepsilon''}{2} \exp(-\sigma' \sqrt{\frac{\mu}{\varepsilon}} z)$. A human body is mostly dielectric and it can be written that absorption by the tissues in a human body is proportional to $\omega \exp(-\sigma')$, where $\sigma' = \omega\varepsilon''$. Absorption is expected to decrease exponentially with frequency, but this happens only at higher frequencies where $\exp(-2\alpha z)$ is significant. At lower frequencies, it is negligible because as shown in Fig. 3.1 α^{-1} for human skin is 20 m at 1 MHz which implies that inside a biological medium with properties of human skin at z = 20 cm, the exponential factor will have a value of $e^{-0.02} \sim 1$ and there would be negligible effect of the factor $\exp(-2\alpha z)$ on the value of absorption at 1 MHz. So at lower frequencies,

absorption in a biological medium increases with increase in frequency. This result is in congruence to the results shown in Fig. 4.2 and 4.3. From the values of attenuation distance calculated for dry skin in Figure 3.3, it can be seen that for frequencies around 505 MHz, distance for e^{-1} times attenuation is approximately 16 cm and from that point onwards it can be said that $\exp(-2\alpha z)$ becomes significant inside a biological medium of thickness 20 cm with properties similar to dry skin. So at frequencies above 500 MHz for this biological medium absorption would go down exponentially with frequency.

4. Results of EM radiation absorption obtained for a planar medium can be approximated to be valid for arbitrary shaped and non-planar mediums as long as radius of curvature of that shape is greater than wavelength λ of the incident EM wave [18]. Also for EM waves passing through air to human body, with the help of the analytical theories discussed in section 2.8, it can be seen that angle of refraction is very close to zero because of high relative permittivity value of the human body and as such transmitted field is always normal to the human body immaterial of the angle of incidence. So shape does not matter as long as there is no scattering, because the transmitted component of field will be approximately normal to the human body.

5. It has also been experimentally verified [18] that only between a range of frequencies, the human body shows multilayer properties to EM radiation. It has been shown [18] that below certain frequency, EM radiation is transparent throughout human body as attenuation of EM fields is very small and in the high frequency range when attenuation is significant, E and H fields are restricted to

skin itself. So at those low and high frequencies, response of the human body to EM radiation can be analyzed by assuming a homogenous model for a human body. Only in the intermediate range of frequencies the multilayered human body needs to be assumed for analysis.

4.2 Simulated and Analytical Results on EM Radiation Absorption by Different Models for a Human Body

As mentioned earlier, orientation of the spherical model with respect to polarization of the incident EM field may make an order-of-magnitude difference in the EM power absorption. EM power absorption by a prolate spheroid model of a human body has been analytically found using the perturbation theory as shown in the following equations [9].

Power absorbed for E field polarized parallel to the major axis of the prolate spheroid =

$$\frac{1}{2c^2}\sigma E^2 4\pi^2 f^2 [A_e^2 + \frac{a^2 b^2}{5(a^2+b^2)\eta\eta^*}] \ . \tag{4.1}$$

All the notation are defined in reference [9] and are also mentioned below.

$A_e = -\ 1/\sigma\eta_o g_{\|}$, where $\eta_o = 377$ ohms, known as the characteristic impedance of free space, σ conductivity of a human body (a homogenous model for the human body has been assumed), $g_{\|} = (u_{10}^2 - 1)[\frac{u_{10}}{2}\ln\frac{u_{10}+1}{u_{10}-1} - 1]$, $A_h = -\ 1/\sigma\eta_o g_{\perp} = A_C$,

$g_{\perp} = \frac{u_{10}(u_{10}^2-1)}{2}[\frac{u_{10}}{u_{10}^2-1} - \frac{1}{2}\ln\frac{u_{10}+1}{u_{10}-1}]$, $u_{10} = \frac{a}{\sqrt{a^2-b^2}}$ where a and b are the lengths of the semi major and semi minor axis of the prolate spheroid. Power absorbed for H field polarized perpendicular to the major axis = $\frac{1}{2c^2}\sigma E^2 4\pi^2 f^2 [A_h^2 + \frac{b^2}{10\eta\eta^*}]$. (4.2)

Power absorbed for both H and E field polarized perpendicular to the major axis =

$$\sigma E^2 4\pi^2 f^2 [A_C^2 + \frac{a^2 b^2}{5(a^2 + b^2)\eta\eta^*}] \ . \tag{4.3}$$

Equations (4.1) to (4.3) are valid under the following assumptions:

1. The spheroid dimensions are small compared to the wavelength, ($a/\lambda < 0.1$), which basically ensures no resonance.
2. Real part of the complex dielectric constant is small compared to the imaginary part.

An important result that was stated earlier without any proof that below resonance frequency EM power absorption by biological tissues increases proportional to f^2 can be verified with these equations.

In another analytical as well as simulated study [10] done for a six layered spheroid representing the human head reveals some interesting features about absorption of EM wave radiation by a layered dielectric body. Six different layers namely, cerebrospinal fluid, membrane, bone, subcutaneous fat and skin were defined in that model for a human head. The surrounding region was taken as air. Model is shown in Figure 4.6.

4.2.1 Variation of Absorption with Frequency

Figure 4.7 shows absorbed energy at four different frequencies; 433 MHz, 915 MHz, 2.45 GHz and 5.8 GHz. Figure 4.7 shows absorbed normalized power densities (NPD) for the plane x = 0. Radius of the outer layer in the sphere is taken as 6.6 cm. It is clear that with frequency increase from 433 MHz to 915 MHz, there is only a slight increase in the absorbed power in the outer layers, but a substantial increase in absorption in the core is observed. At a higher frequency of 2.45 GHz, deposition within the core diminishes, but there is an increase in the absorption in the side layers. At 5.8 GHz, absorption

diminishes in the side layers and is approximately zero in the core. For frequency near 100 MHz, no absorption was seen, as wavelength was too big compared to the size of the sphere and wave passes through the sphere.

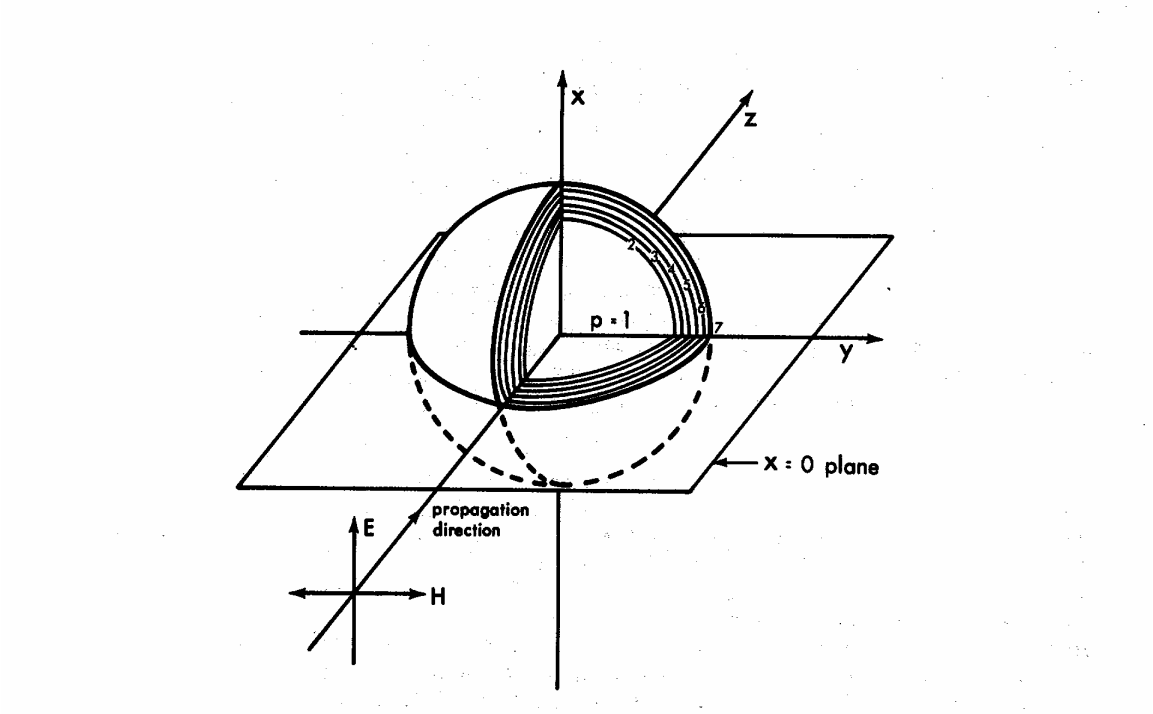

Figure 4.6: Spherical multilayered model for a human head, [printed with permission from reference 10]. Six region model of the human head. 1 – brain, 2-cerebrospinal fluid, 3-membrane, 4-bone, 5-fat, 6-skin, 7-

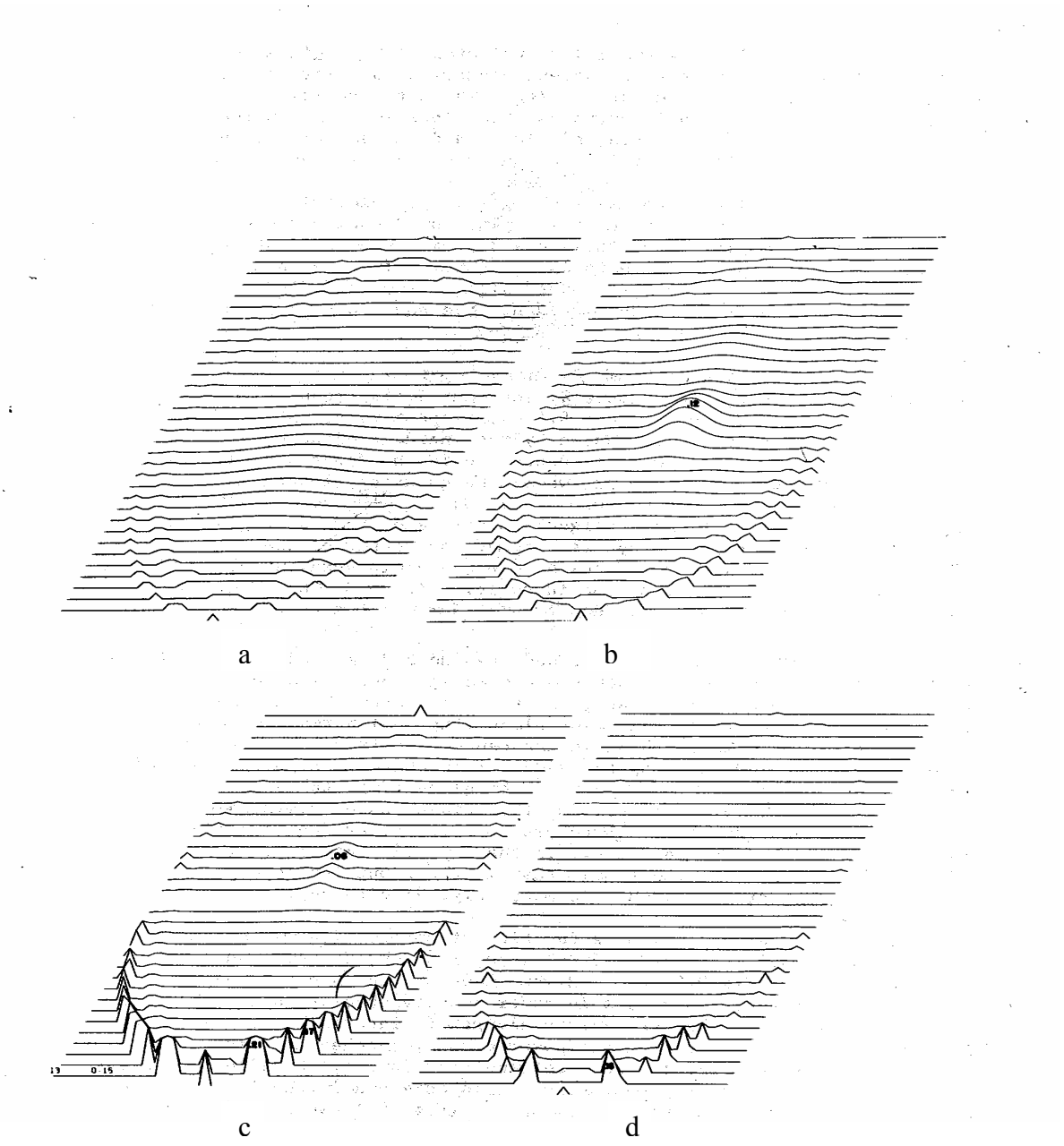

Figure 4.7: Absorption for four different frequencies for the spheroid model in Fig. 4.6, [printed with permission from reference 10]. Shows normalized power density (NPD), (a) f = 433 MHz, no absorption in the core, (b) f = 915 MHz, core NPD = 0.12, (c) f = 2.45 GHz, core NPD = 0.06 (d) f = 5.8 GHz, no absorption in the core.

These results are in accordance with the previously stated results that absorption increases first with frequency below resonance and then it starts decreasing due to very high attenuation. Large amount of absorption occurs in the outer side layers. This result is in agreement with our finding about attenuation depth (α^{-1}) starting to become dominant for frequencies around 500 MHz for skin.

4.2.2 Absorption at Different Positions

Figure 4.8 from reference [10] shows variation in the energy deposition at the planes corresponding to different values of x in Fig. 4.6 for an incident field at 3 GHz. As can be seen from Figure 4.8, deposition in the sides increases and deposition in the central core decreases as ones moves up from the plane x = 0 to x = 2.4 cm **.** But for the layer x = 3.2, there is no sideways deposition and there is a sharp increase in deposition in the core region. We may say that core deposition decreases with increase in height, and then becomes very high at the top pole, since core and surface becomes the same at the pole.

4.2.3 Variation in Absorption with Size of the Sphere

Figure 4.9 from reference [10] shows variation of absorption as the radius of the sphere is increased from 1.1 cm to a maximum of 6.6 cm. Frequency of the EM radiation is 3 GHz and the internal wavelength is 1.5 cm. It is evident that absorption increases as the size of the sphere becomes comparable to the wavelength. It was stated in discussion in section 4.1 that resonance corresponding to maximum absorption occurs near ($\frac{a}{\lambda} \approx 0.5$). Results shown in Figure 4.9 agree to this statement.

4.2.4 Absorption Variation Dependence on EM Properties of the Human Body

With change in conductivity, electric field induced in a medium changes substantially, but there is only negligible change in the values of absorbed energy [10].

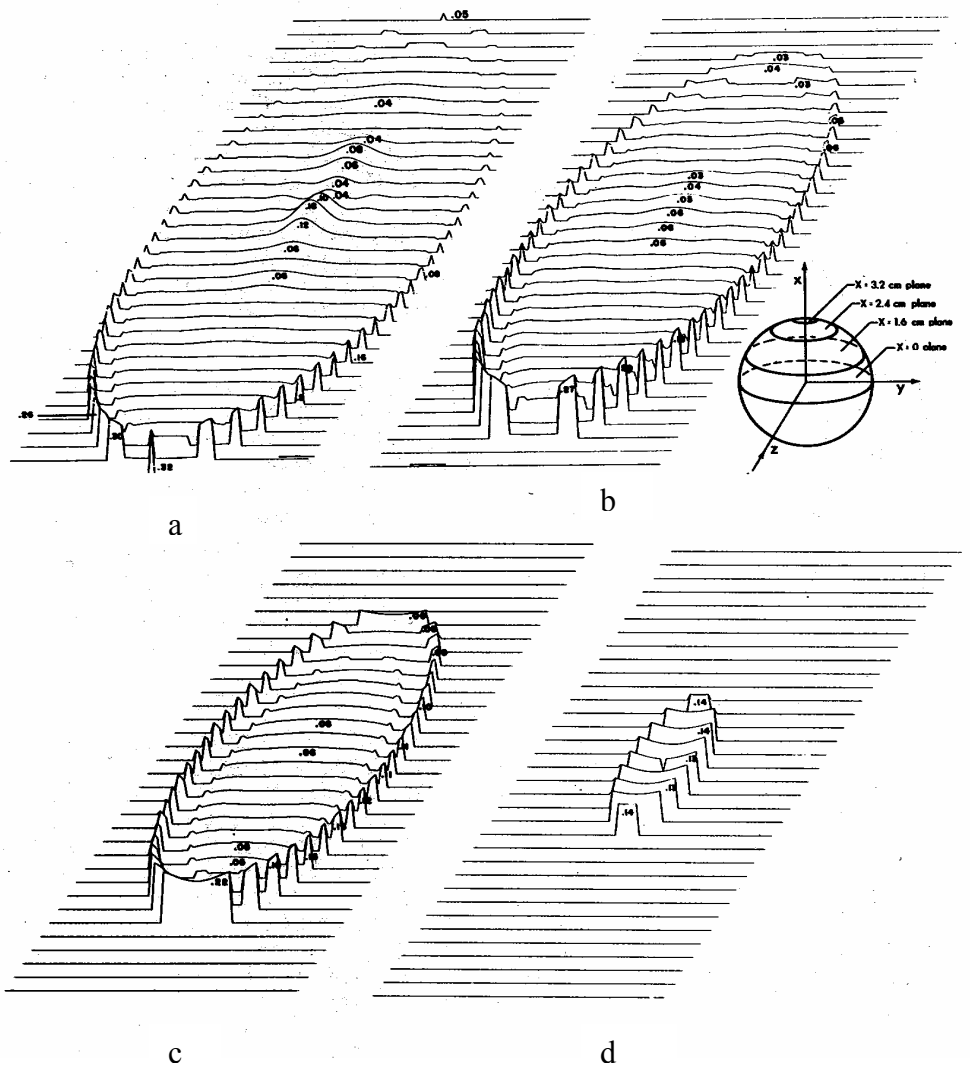

Figure 4.8: Absorption in different planes of the spheroid model shown in Fig. 4.6, [printed with permission from reference 10]. Normalized power density (NPD) for a sphere of radius 3.3 cm at different planes, (a) plane x = 0, maximum NPD in the core is 0.10, (b) plane x = 1.6 cm, maximum NPD in the core is 0.06, (c) plane x = 2.4 cm, maximum NPD in the core is 0.06, (d) plane x = 3.2 cm, maximum NPD in the core is 0.14.

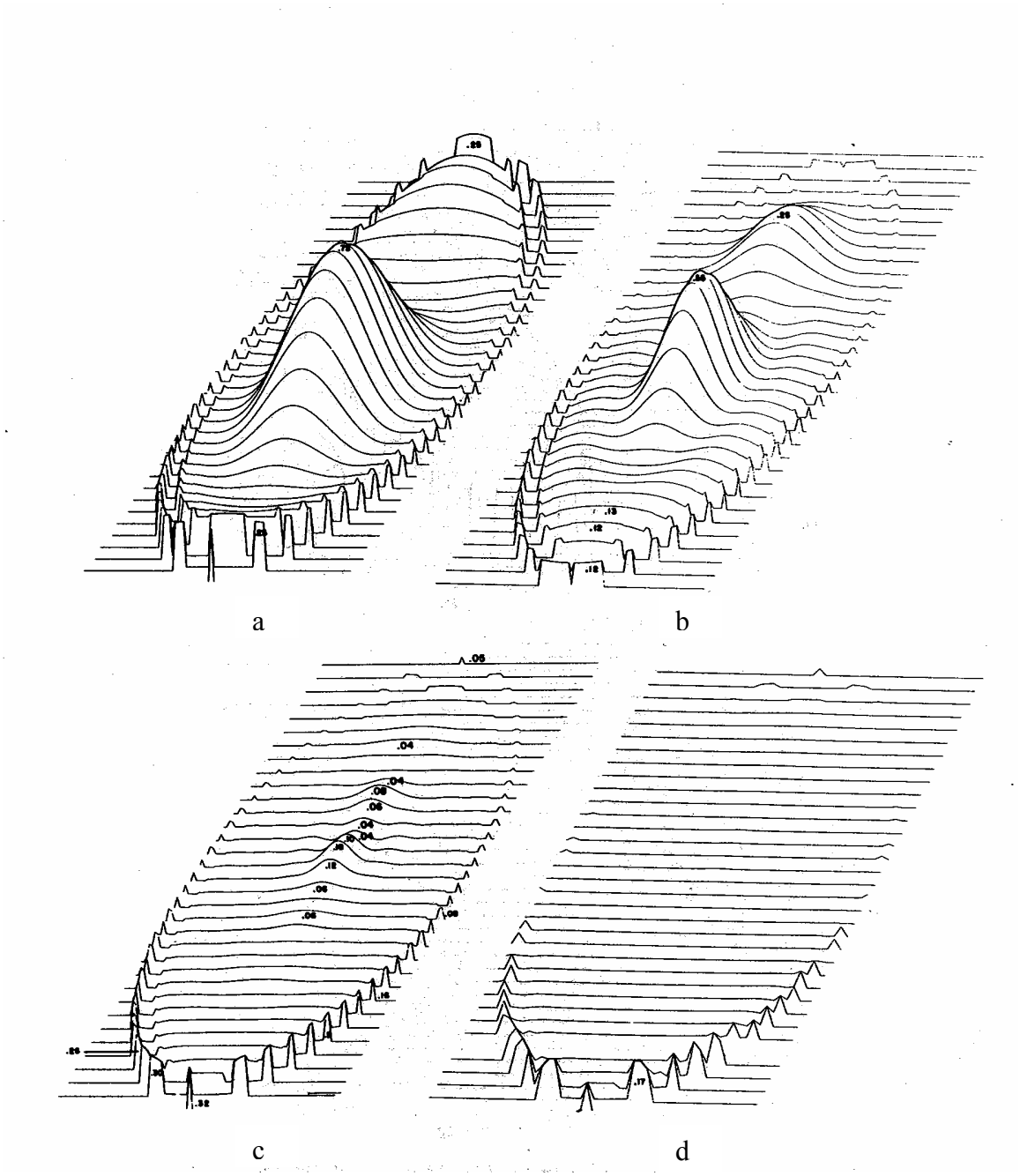

Figure 4.9: Absorption for different radii of the brain core for the spheroid model in Fig. 4.6, [printed with permission from reference 10]**.** It shows NPD for simulations at 3 GHz and different radii, (a) radius = 1.1 cm, peak NPD = 0.78, (b) radius = 1.65 cm, peak NPD = 0.55, (c) radius = 3.3 cm, peak NPD = 0.18, (5d) radius = 6.6 cm, peak NPD is almost zero.

It can be seen from the Figure 4.10 that when brain conductivity changes from 0.5 $mho.m^{-1}$ to 3 $mho.m^{-1}$ the two peaks for the values of electric field at the center of the sphere at 0.5 $mho.m^{-1}$ change to one peak with a diminished amplitude. But the energy value changes only from 0.42 to 0.39. From the observed conductivity values for different tissues in human body, it can be seen that range of conductivity variation is only from 0.05 to 10 $mho.m^{-1}$ [16] for biological tissues for any practical value of the frequency of EM waves. So it might be said that absorbed power densities do not critically depend on the conductivity values of biological tissues. But both electric field and energy deposition depends heavily on the dielectric constant values of different layers as can be seen from the Figure 4.11 also reprinted from reference [10]. It is obvious that normalized power density value increases with increase in the value of relative permittivity of the brain core, which agrees with the discussion in section 2.6, since brain core is a dielectric medium.

Summary of useful results from the simulation results in reference [10]:

(a) For incident field directed along the z axis, power deposition occurs in the other two perpendicular directions being high at the top and the bottom. There are also hot spots in the interior points and it depends on the frequency. (b) Power deposition in the outer shells reaches its maximum at higher frequencies than in the interior. (c) Absorbed power density does not critically depend on the conductivity values of biological tissues.

4.3 Non-Thermal Effects of EM Radiation on a Human Body

In all of the above discussion energy absorption due to conductive losses has been described, which eventually shows up as heating in the muscles and tissues. There are also a number of non-thermal effects that occur in a human body when the E or H field interacts with tissues and muscles.

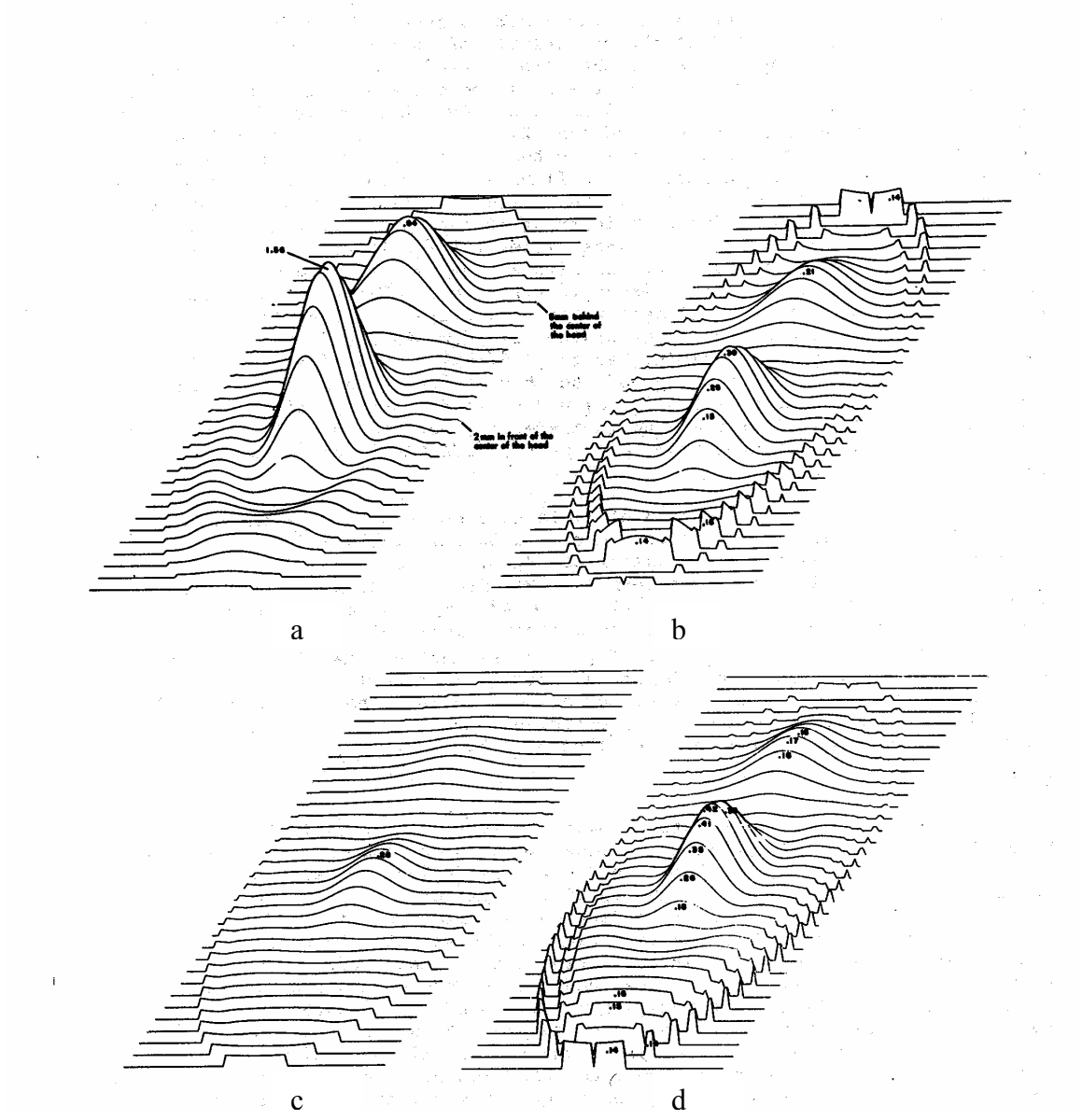

Figure 4.10: Absorption for different values of conductivities of the brain for the spheroid model in Fig. 4.6, [printed with permission from reference 10]. It shows E field and NPD for simulation at 3 GHz and different conductivity (σ) values of brain core. (a) Normalized E field peaks are 1.88, 0.64 for $\sigma = 0.5$ mho.m^{-1}, (b) NPD peaks are 0.39, 0.21 for $\sigma = 0.5$ mho.m^{-1}, (c) Normalized E field peak is 0.28 for $\sigma = 3.0$ mho.m^{-1} and (d) NPD peaks are 0.42, 0.18 for $\sigma = 3$ mho.m^{-1}.

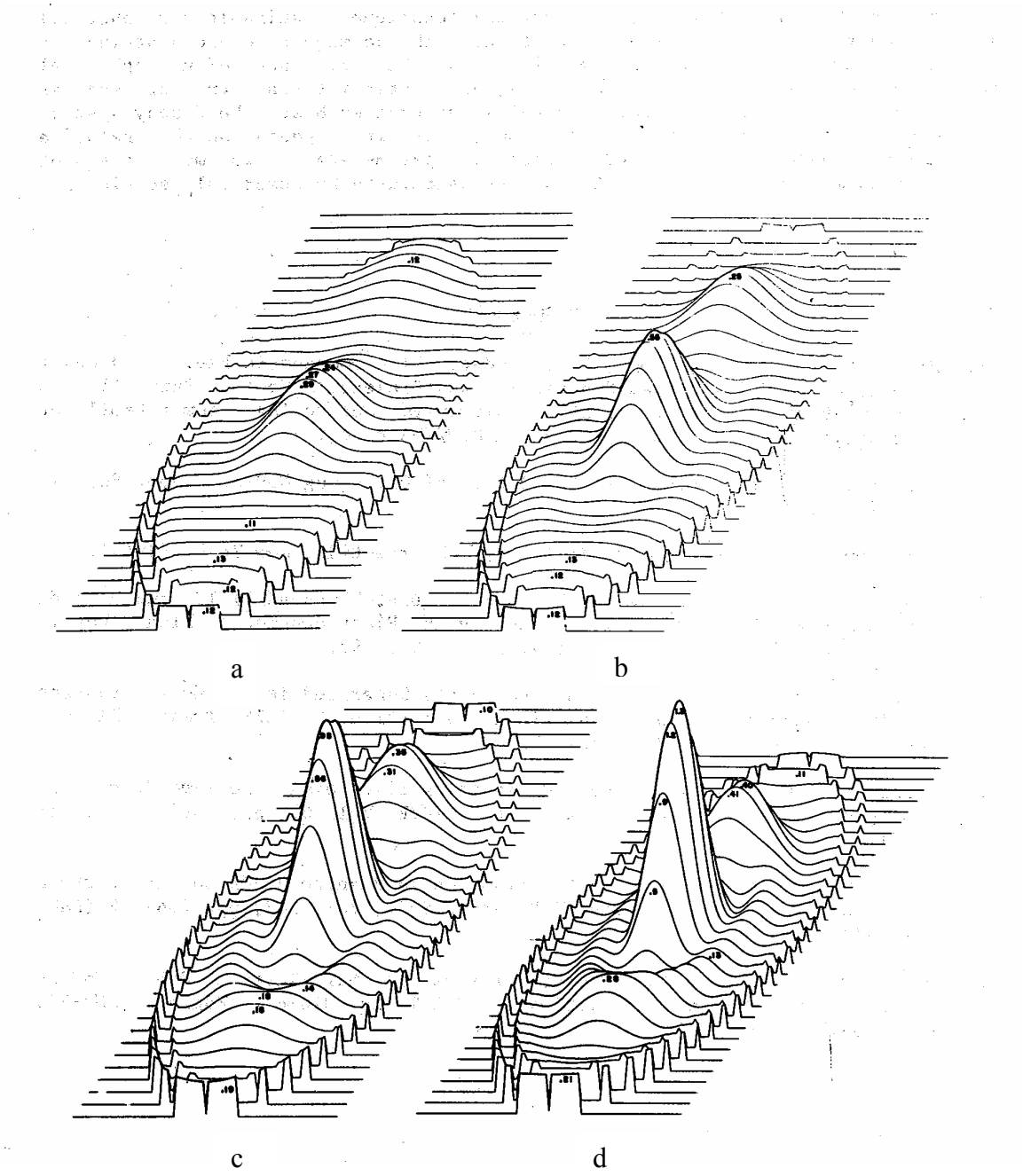

Figure 4.11: NPD for different values of relative permittivity for the brain core, [printed with permission from reference10]. It shows NPD for simulation at 3 GHz with different values of relative permittivity (ε_r) for brain, (a) $\varepsilon_r = 29$, peak NPD = 0.29, (b) $\varepsilon_r = 42$, peak NPD = 0.55, (c) $\varepsilon_r = 55$, peak NPD = 0.98, (d) $\varepsilon_r = 68$, peak NPD = 1.2.

4.3.1 Field-Force Effect

DC electric fields can evoke forces acting on particles. AC electric fields can also evoke forces while acting on biological body. Observation about orientation of unicellular animals in the direction of the applied electric field proves field-force effect [2]. But it has been found that magnitude of AC field required to evoke field force effect in biological cellular particles was of the order of 100 $V.cm^{-1}$ [2]. This magnitude is even higher for macro-molecules. At such high values of electric field, associated heating becomes very high. So thermally insignificant field-force effect is not possible in the presence of continuous EM waves. The time constant T (time by which the affected cells react) associated with field force effect is a function of the applied field magnitude. It has been shown that T varies inversely with square of the electric field magnitude (E^2), provided E is greater than E_{th}. The latter is defined as electric field required to overcome Brownian disturbance.

4.3.2 Excitation of Biological Membrane

Electric field in radiation causes a potential difference to be developed across the cell membranes and if it is greater than the existing rest potential across the cell membranes, it causes unwanted stimulation of the cell membranes. For a cell membrane with specific resistance at the inside membrane ρ_i, membrane capacitance C_M, specific resistance at the outside membrane ρ_o and resistance along the direction perpendicular to the membrane R, if an alternating electric field of magnitude (E) with a frequency ω is applied perpendicular to the cell membrane, magnitude of the alternating potential difference ΔV that is developed across the membrane can be determined with the following expression [2].

$$\Delta V = \frac{2RE}{\sqrt{1+[\omega C_M R(\rho_o - \rho_i)]^2}}.$$

Frequency dependence of the developed potential difference also can be shown with a bode diagram and the 3 db frequency f_o for biological tissues has been found as 1 MHz, from reference [1]. So for EM waves above 1 MHz, this effect starts becoming insignificant. Introducing the typical values of the cell membrane ρi, ρ_o , R, C_M and thermally insignificant value for E, the calculated value of ΔV is found to be about 10^6 times lower than the rest potential [2]. In other words, the electric field required to cause potential difference greater than the rest potential is found to be near 500 $kV.cm^{-1}$ [2] which is never encountered in normal radiation or which should be avoided for energy transmission through a biological medium.

CHAPTER 5

MODELING AND SIMULATION OF TRANSMITTER-RECEIVER COUPLING FOR BIO-IMPLANTABLE APPLICATIONS

5.1 Development of a Simplified Model for Simulation using Finite Element Technique

Geometry of a simplified model for the coupled transmitter-receiver system to be used in an implantable bio-sensor inside a human body is shown in Figure 5.1. This geometrical model has been used for simulation to evaluate the current density induced inside the body and in the implanted receiver by the EM waves excited at the transmitter input port, namely port 1 in Fig. 5.1. Fullwave 3D EM field solver [19] has been used for simulation. Different objects in the model shown in Figure 5.1 are:

1: A the solid annular Cu conductor with two ports at its ends through which an approximately circling time varying current is excited. It is in layer 2. Alternating E field is applied between port 1 and the ground plane and E field leaves the annular Cu conductor through port 2 to the ground plane.

2: A dielectric layer in layer 3 that acts as an insulator between the upper parts of the model from the ground plane below.

3: A solid dielectric put between ports 1 and 2 of the annular Cu conductor acting as an insulator between the ports.

4: The cylindrical model for a human body with three layers namely, skin, fat, stomach and the central core having characteristics of white material [16] in a human body. This cylindrical part comprising layer 1 extends through layer 2.

Dimensions of the different parts will be given later in this chapter. The receiver modeled as a cube is placed 1 cm front and 1 cm right to the center of the annular Cu conductor in layer 2. The annular Cu conductor is wrapped around the skin layer.

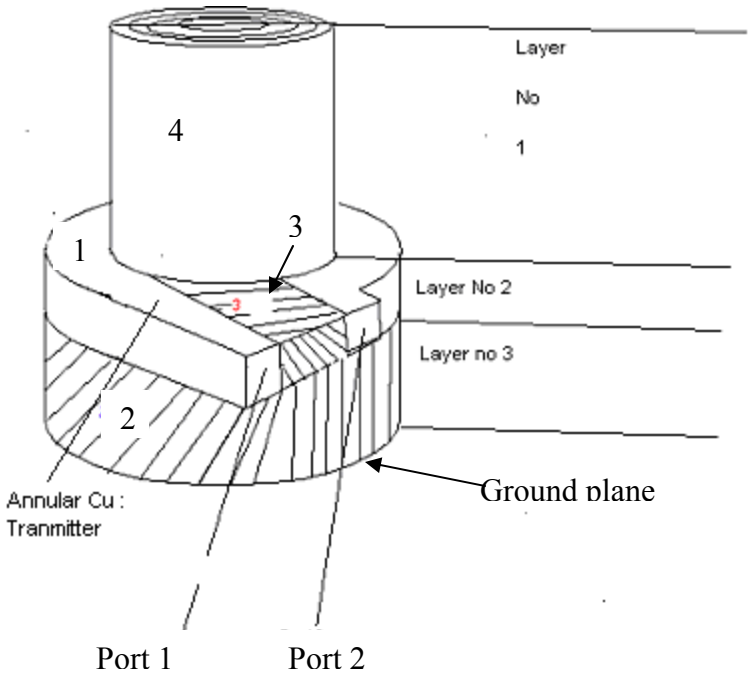

a) General view of the model

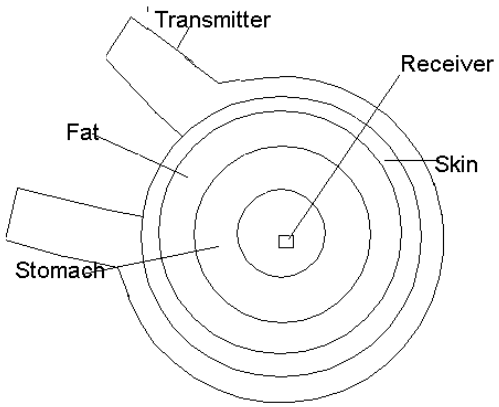

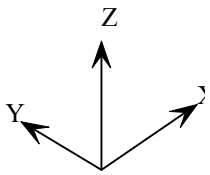

b) Cross-sectional view of layer 2, where transmitter and receiver are placed.

Figure 5.1: Geometry of a simplified model for simulation of human body with the implanted receiver. The implanted receiver is modeled as a cube as shown in (b), transmitter is modeled as an annular Cu conductor wrapped around the lower portion of the human body model and it is in layer 2. Layer 1 models the upper portion of a human body and layer 3 is an insulation between the ground plane and the upper portion of the model.

A cut diagram showing position of the cube is shown in Fig. 5.2

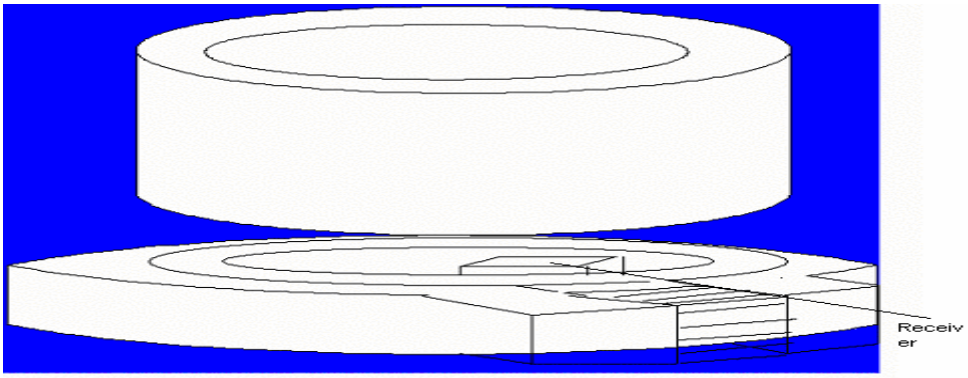

Figure 5.2: The receiver – transmitter position in the model. It shows position of the receiver in layer 2.

5.2 Goals for the Model

In the real biomedical system to be designed, a biocompatible sensor will be placed at the right bottom corner of a human stomach. For recharging the battery in the sensor, EM power will be transmitted with the help of a circular copper coil wound around a human waist and the transmitted power is received with a receiver coil in the implanted sensor circuitry. The transmitted EM power undergoes reflection and absorption by the intervening human body before part of it reaches the implanted receiver. Main objective here for this modeling is to do a simulation to find the energy coupling between the transmitter and the receiver, by taking into account both absorption and reflection of transmitted EM power by the human body which is modeled as a multilayered biological medium. Normal circuit simulation tool will not take into account the absorption and reflection of EM power by a biological medium and accurate electrical modeling of different layers in a human body also would be

complex. Therefore the above simplified model described in section 5.1 and shown in Fig. 5.1 has been developed so that electric and magnetic field distribution inside different layers namely skin, fat, stomach and central core can be solved with the Full-Wave 3D EM field solver [19]. Simulation will show relative magnitudes of E fields induced inside different layers in the model, for an EM wave with a specific E field excited in the annular Cu layer wrapped around the skin, fat and stomach annular layers as shown in (b) in Fig. 5.1. Relative current density distribution inside the model will also be found. Then energy coupling between the receiver modeled as a solid cube and the transmitter modeled as a solid annular Cu conductor will be calculated from the respective induced electric fields.

5.3 Software Package Used and Its Working Principle

Software package used here for simulation is called Full Wave 3D EM field solver [19]. This package [19] solves exact Maxwell's equations and finds E field distribution. It finds two dimensional field or current density distribution in any cross sectional plane of the problem geometry. It requires two input files namely *problem_efem* and *problem.g*. The *problem_efem* file is a text file as shown in Appendix A which gives input to the solver to build up the problem geometry assigning appropriate EM properties to appropriate parts. All the different shapes present in the problem model with different EM properties have to be described with properly connected points in the *problem_efem* file. Only triangular and quadrangular unit shapes can be used to generate different objects with different shapes in the model. This geometrical constraint is required by the software package. The unit triangular or the quadrangular shapes are generated by joining well defined points at appropriate places in the problem geometry.

Coordinate system to define the points and give each one of them a unique location is Cartesian and in our problem model, x axis passes parallel through the line joining port 1 and port 2. Coordinate system and location of the model shown in Fig. 5.1 will be clear in the mesh diagram shown in Fig. 5.3 that will be described later. For generating the annular shapes, for the model shown in Fig. 5.1 quadrangular shapes have been connected in the anti-clockwise direction. Each one of the unit shapes is assigned a layer. Thickness is given by the layer in which they belong. The conductor description *infoConductor0* to *infoConductor49* in Appendix A describes the Cu annular conductor for the above model. It belongs to layer 2 and so gets the thickness of layer 2. Similarly all the different shapes skin, fat, stomach regions are generated. Because of the restriction of using triangular or the quadrangular shapes for generating the annular layers, they are not perfectly circular or elliptical. For example for generating the annular Cu section, 50 small quadrangular shapes were joined together in the *problem_efem* file. More small quadrangular shapes can be defined, but that increases the simulation time because with increase in one more quadrangle, more points have to be defined which occupy more system memory.

The second file *problem.g* as shown in Appendix B is used to generate the triangular mesh over the problem geometry. All the lines that can be seen in the top view of the model in Fig. 5.1 have to be described by joining all the points in anticlockwise direction. Points defined in the *problem_efem* file have to match to the points defined in *problem.g* file. Size of the mesh that should be generated around a point can be specified at each of the point.

5.3.1 Problem Geometry and Property Setup for Simulation

The software [19] builds the problem geometry and assigns EM properties to different parts of the geometry from the input text file *problem_efem*. Two fold assignment of EM properties is done. In the first place different vertical layers, layer 1, layer 2 and layer 3 as shown in Fig. 5.1 are assigned different EM properties. Then for each of the shapes described in the *problem_efem* file, its particular volume in the layer where it belongs is overwritten with the EM properties that are specified with that shape. After it builds up the problem geometry and finishes assignment of EM properties to different parts, it then creates meshes in the cross-sectional plane of the layer 2 and then solves Maxwell's equations to give E field at each of the triangular meshes. Figure 5.3 shows mesh structure created for the simulation of the model shown in Fig. 5.1 for elliptical shapes. This is the mesh created in the cross sectional plane of the layer 2 where both the transmitter and receiver are placed as shown in Fig. 5.1. It also clearly shows orientation of the model in the Cartesian coordinate system. Clearly the X axis passes through the ports 1 and 2. Although it is difficult to identify the exact sizes of each and every annular section from Fig. 5.3, an approximate idea about the sizes of various sections can be readily obtained.

5.4 Dimensions for the Circular Model

As shown in Fig. 5.1, horizontal layer 2 contains both the Cu cube placed in the central core and the annular Cu conductor wrapped around the annular skin layer. Height of layer 2 is 2 cm. So all of the followings placed in layer 2 will have a height of 2 cm.

1. The outer annular Cu layer has a thickness of 1 cm. It is in layer 2 and diameter of the outer side of this annular region is 40 cm.

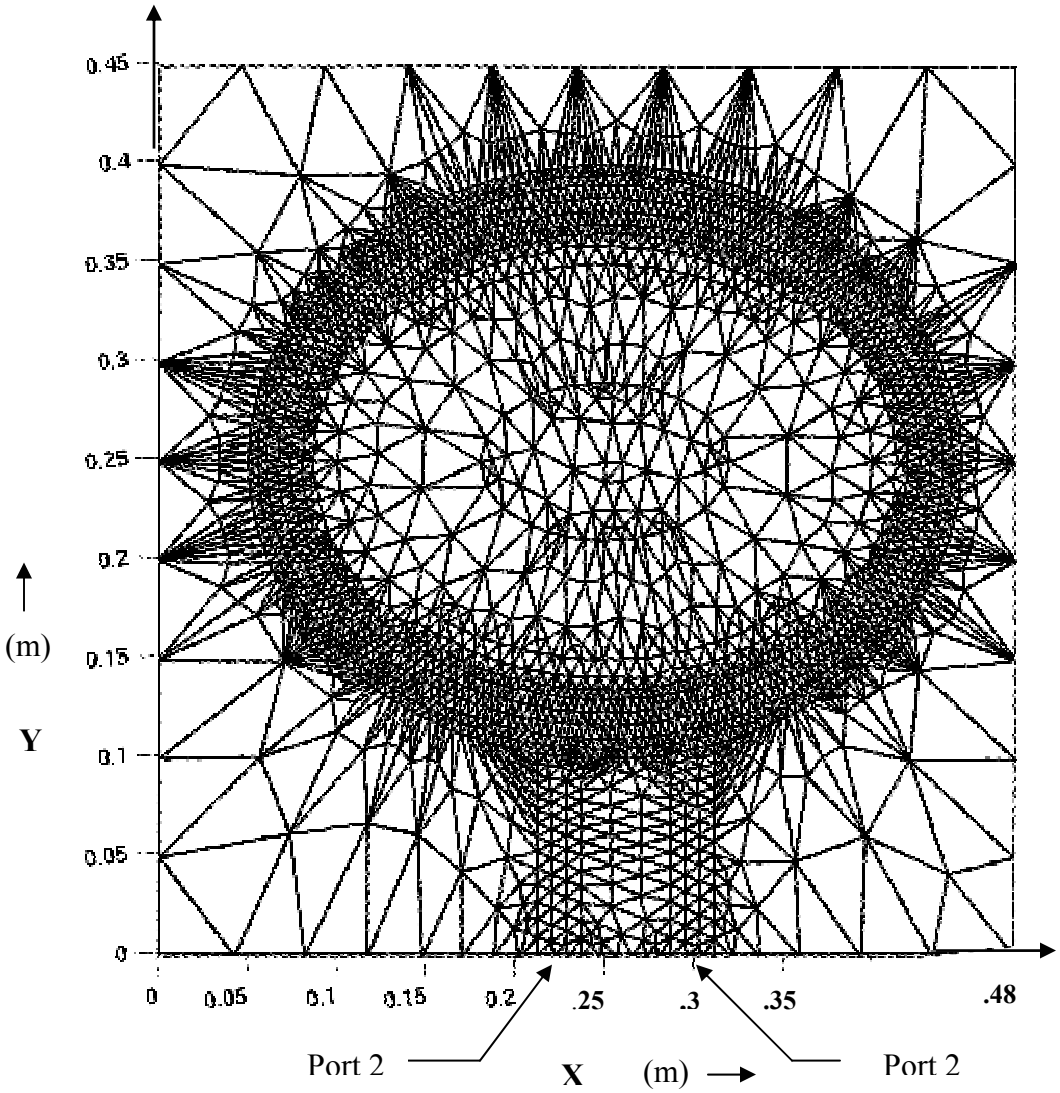

Figure 5.3: Triangular meshes in the layer 2 cross-sectional plane of the model in Fig. 5.1. It also shows dimension of different annular regions. It can be seen that x axis passes through port 1 and port 2. Orientation of the model and its position with respect to the coordinate system is also obvious in the above figure.

2. Next annular layer is skin which is also 1 cm thick and belongs to layer 2. It touches the outer annular Cu conductor. Its outer diameter is 39 cm.
3. Next to skin is the annular region with thickness 2 cm representing fat. This also belongs to layer 2 and has an outer diameter of 38 cm.
4. Next annular region has thickness equal to 8 cm and it is given the properties of stomach. This also belongs to layer 2 and has an outer diameter of 36 cm and inner diameter of 28 cm.
5. Rest of the central core region next to the stomach annular region is given properties of white material [16].
6. The Cu conductor cube, placed at center of the layer 2 representing the receiver has a height of 2 cm and area 4 cm^2.
7. Underneath layer 2, there is a dielectric insulating slab which is in the layer 3 and has a height of 8 cm.
8. The layer 1 has a height of 4 cm and it has all the annular layers namely skin, fat, stomach and central core with the same dimension as in Layer 2.

5.5 Model Justification

As mentioned in section 5.2, main objective is to take into account reflection and absorption of transmitted power by a multilayered biological medium in a bio-medical system described in section 5.2 and estimate power coupling. Finding the induced current density is also important to see if it crosses the safe limit. The above model has very simplistic shapes and dimensions for various parts of a human body and will only approximately represent different layers such as skin, fat and stomach in a human body. But an overall cylindrical symmetric structure for the human body has been maintained. As discussed in section 4.1 [18], as long as wavelengths of incident

EM waves are larger compared to cell sizes, shapes of the medium do not affect much in reflection or absorption. Even at 300 GHz frequency, corresponding wavelength is 1 mm. So EM field induced in the above model will be good for a qualitative understanding of the power coupling between the transmitter and the receiver in the real system. Relative current densities induced inside different layers in the model with properties of skin, fat, and stomach will also be useful in deciding the safe limit of excitation current. A drawback of the model is absence of any air gap between the annular cu layer representing the transmitter and the skin layer. But the results will not be characteristically very different, because skin has very small conductivity ~ 10^{-4} $s.m^{-1}$ to 10^{-1} $s.m^{-1}$[16]. In the above model shown in Figure 5.1, different layers of bio-tissues and fat are represented by the cylindrical layers of skin, fat and stomach respectively. The inner central core is also given characteristics of the white material [16] present in a human body and the receiver is represented by the conductor cube placed in the inner central core in the same layer as the transmitter. So E fields induced in the inner cube are expected to be similar to the E fields induced in the implanted coil receiver of a real bio-implantable system described in section 5.2. Therefore the energy density coupling calculated from the induced E fields in the inner solid cube conductor and the outer annular Cu layer will be much similar to those expected in a real bio-implantable system.

5.6 Excitation Method

Time varying E field of a given frequency to be specified in the *problem_efem* file is applied to the port 1 (see Figure 5.1) directed from ground plane to port 1. One cannot start the simulation by applying any current or voltage function as this software [19] is a field solver. But E field in the appropriately applied TEM wave will lead to

proper current flowing in desired parts. This E field applied at port 1 has components in all three directions. Due to the electric field, current flows around the annular conductor in the circular direction following its shape. Although there would be currents flowing in other directions, but those components will be very small compared to the current in the annular Cu conductor because of its very high conductivity. Current enters the annular Cu layer from the ground plane through port 1 and then it leaves the annular layer through port 2 into the ground plane. This excitation method will be producing currents in the annular Cu conductor similar to a situation where Cu coil is wound around the waist of a human body.

Figure 5.3 shows mesh structure created in the layer 2 cross-sectional plane of the model in Fig. 5.1 for elliptical shapes of the different layers. Obviously cross-section of layer 2 is in the x-y plane. It also shows dimension of different annular regions. It can be seen that x axis passes through port 1 and port 2. Orientation of the model and its position with respect to the coordinate system is also obvious from this figure. The outer rectangular boundary that is shown in the mesh diagram in Fig. 5.3 is the problem boundary. Actually all the layers namely layer 1, layer 2 and layer 3 will have this shape. Then in layer 2 and layer 1, extra annular shapes are overwritten with appropriate properties for appropriate region as specified in the *problem_efem* file.

5.7 Description of EM Fields Induced in the System

It has been mentioned already that this system is excited with a transverse EM wave applied at the port 1 in the annular Cu conductor. Part of this wave might get reflected and the rest of it is transmitted. The excited E field around port 1 for a particular simulation is shown in Figure 5.4. E field would have all three components, tangential

(E_φ), radial (E_r) and in the z direction (E_Z). Their magnitudes would depend on properties of the medium where they are induced. Figure 5.4 shows E field only in the X Y cross sectional plane of the port 1. As the ground plane has the same dimensions as the boundary of the problem model and excitation is applied from ground plane to port 1, it can be seen that E field exists all over the ground plane having highest magnitude at port 1. Arrow shows direction of electric fields and their lengths show magnitudes of electric fields. Magnitudes are relative to the field applied at the port 1. It can be seen in Fig. 5.4 that E fields with highest magnitudes are located around 0.25 m, which is approximately the location of the excitation port, namely port 1. These fields are applied from the ground plane to the port 1. Smaller arrows in the far left and right to the port 1 shows that port 1 is coupled to the entire ground plane, but excitation is mainly localized at port 1 since at port 1 E fields have maximum magnitudes. The oppositely directed arrowheads in Fig. 5.4 are the reflected components of the E fields excited. E fields due to port 2 are not shown in this Figure.

5.8 Edge Based Finite Element Technique (EBFET)

Full Wave 3D EM field solver [19] uses EBFET [11] for solving the Maxwell's equations. Different steps involved in simulating with edge based finite element techniques are given below [11].

5.8.1 Discretization or Subdivision of the Entire Domain

The problem should be well defined with physical geometrical boundaries. The outer rectangular boundary as shown in Figure 5.3 was selected for the model developed in this thesis work.

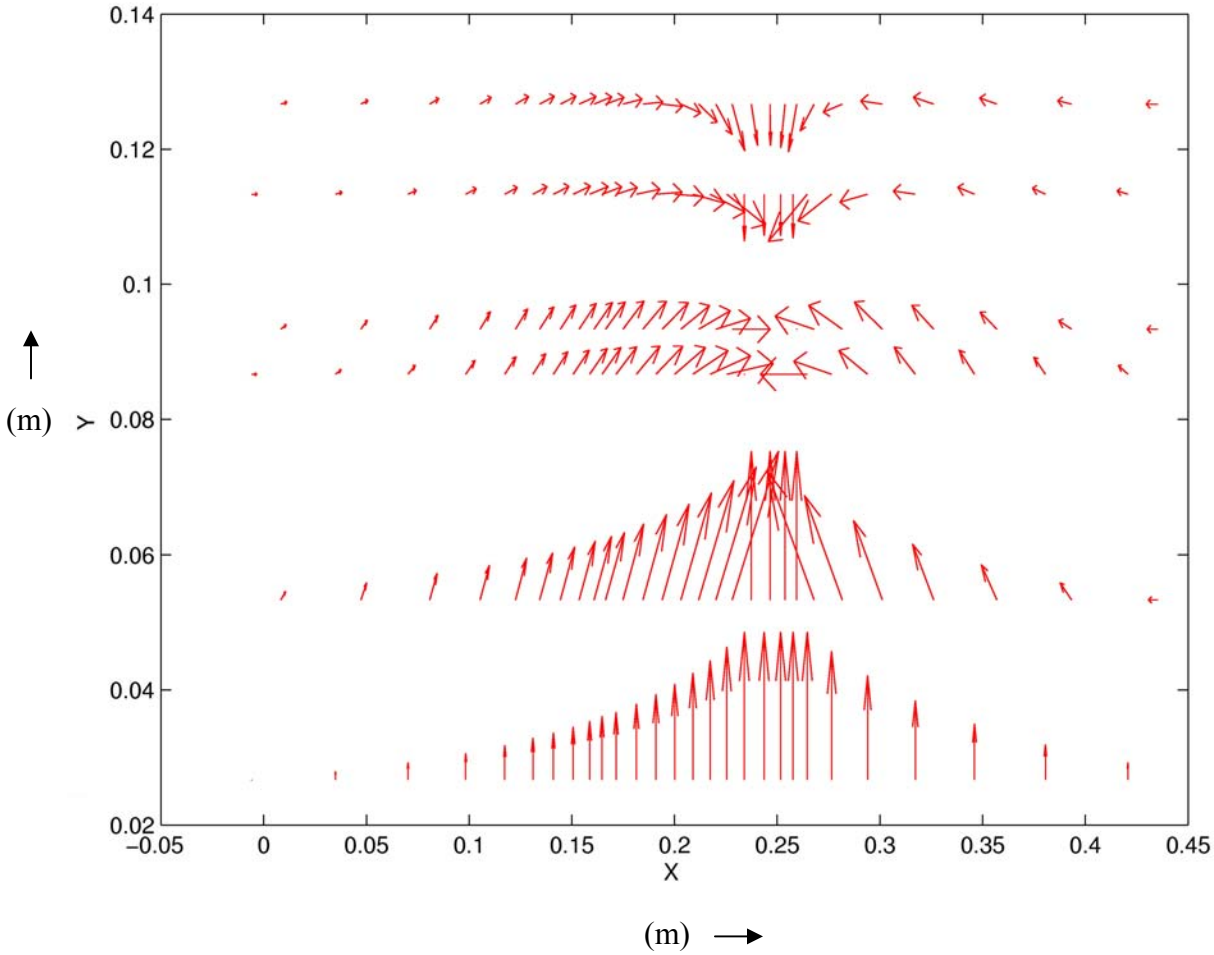

Figure 5.4: Simulated E field excited by port 1 in the X-Y cross sectional plane. Resulting E fields at port 2 are not included here. It shows vectors whose directions are along the E fields and lengths are proportional to magnitudes of E fields. All other E field magnitudes are shown relative to the E field magnitude around the port 1 located around 0.25 m.

The entire domain is divided into a number of triangular elements in the cross sectional area. Actual number of triangular elements depends on the mesh size. It can be seen from Fig. 5.3 that different parts have different mesh sizes. Critical regions have very small mesh sizes associated with them. Mesh sizes are assigned in the *problem.g* file and will be described in section 6.1. Each of these triangular elements is a sub domain, where Maxwell's vector equations are solved by using the minimization of variational functional technique [11] and E and H field values are solved at each of the three different edges of the triangle.

5.8.2 Selection of the Interpolation Function

After values of E and H fields are obtained at each of the three edges of a triangular element, values of E or H field for each of the triangular elements are calculated by interpolated values of the E or H fields at the three edges. Suitable interpolation functions are selected for each of the three edges and then E or H field at the respective edges is multiplied by the corresponding interpolation function and all three products are added to give the E or H field for the that triangular element as can be seen from equation (5.4) derived below. For the nth triangular element shown in Figure 5.5, interpolation functions along the edges 1, 2 and 3 are N_1^n, N_2^n and N_3^n respectively. First order derivation of these interpolation functions are given below [11].

$$N_1^n = (L_1^n \nabla L_2^n - L_2^n \nabla L_1^n) l_1^n \tag{5.1}$$

$$N_2^n = (L_2^n \nabla L_3^n - L_3^n \nabla L_2^n) l_2^n \tag{5.2}$$

$$N_3^n = (L_3^n \nabla L_1^n - L_1^n \nabla L_3^n) l_3^n \tag{5.3}$$

and $E^n = \sum_{i=1}^{3} N_i^n E_i^n$ (5.4)

Here l_1^n, l_2^n, and l_3^n are lengths of the edges 1, 2 and 3 respectively, L_1^n, L_2^n and L_3^n are the three area coordinates of the nth triangular element and they are defined as [11]: $L_1^n = \frac{\Delta_1}{\Delta}$, $L_2^n = \frac{\Delta_2}{\Delta}$ and $L_3^n = \frac{\Delta_3}{\Delta}$; where Δ = Area of the whole triangle and Δ_i = area of the ith triangle as shown in the Figure 5.6. P is a point which can be anywhere inside the triangle.

5.8.3 Derivation of Elemental Equations

Maxwell's equations are solved at each of the three edges of a triangular element using variational formulation of Maxwell's vector equations (5.5) and (5.6) which are valid for an inhomogeneous as well as an anisotropic medium.

$$\nabla \times \mathbf{E}(\mathbf{r},t) = -\frac{\partial}{\partial t}\boldsymbol{\mu}(\mathbf{r}) \cdot \mathbf{H}(\mathbf{r},t) \tag{5.5}$$

$$\nabla \times \mathbf{H}(\mathbf{r},t) = \frac{\partial}{\partial t}\boldsymbol{\varepsilon}(\mathbf{r}) \cdot \mathbf{E}(\mathbf{r},t) + \mathbf{J}(\mathbf{r},t) \tag{5.6}$$

As shown in the equations (5.5) and (5.6), permeability and permittivity constants are functions of position, **r**. Assumptions that are made on the properties of the medium are that in the multilayered structure as described above in Figure 5.1, each of the different layers is an isotropic medium. In that case, equations (5.5) and (5.6) can be reduced to equation (5.7) for sinusoidal time variation for both E and H field and μ being independent of position. Equation (5.7) is valid in each of the different layers.

Variational minimized functional form of this equation is written for each of three edges of each triangular element by the software [19]. Boundary conditions

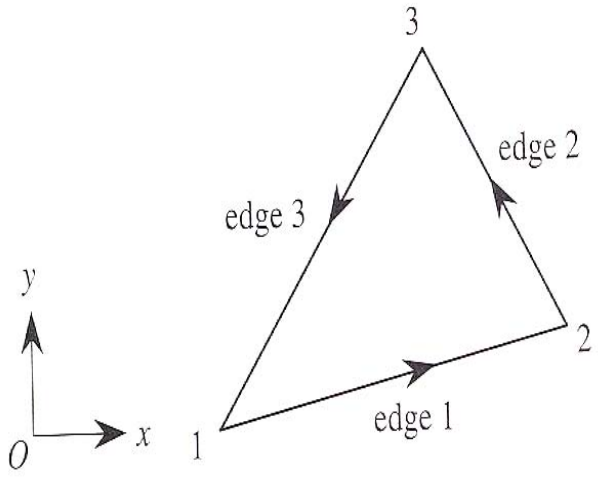

Figure 5.5: Triangular nth element in the mesh created in the cross sectional plane of a given problem geometry. N_1^n, N_2^n and N_3^n are the interpolation functions along the edges 1, 2 and 3 respectively.

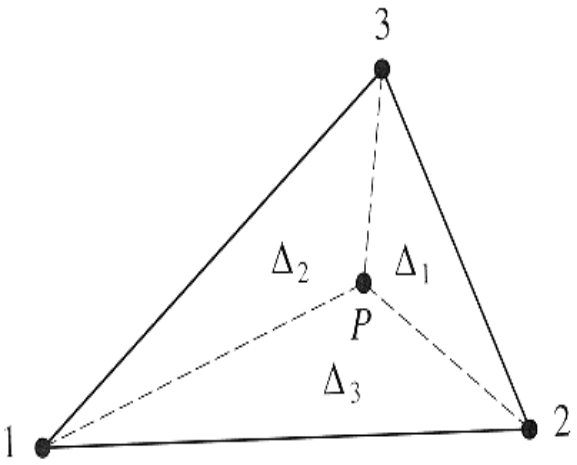

Figure 5.6: Definition of the area coordinates. P is a point which can be anywhere inside the triangle. Clearly maximum value of $L_1^n = \frac{\Delta_1}{\Delta}$ is 1 and it is obtained when P is at 1.

are used to merge the different equations into a single global matrix and then that matrix is solved to get E and H fields for each of the different edges by the software. Values of E and H for different elements are then obtained with equation (5.4).

$$\nabla \times (\frac{1}{\mu} \nabla \times \mathbf{E}(\mathbf{r})) - \omega^2 \varepsilon \mathbf{E}(\mathbf{r}) = j\omega \mathbf{J}(\mathbf{r}) \tag{5.7}$$

CHAPTER 6

SIMULATION AND RESULTS

6.1 Simulation Cases

Simulations were carried out to obtain current density distribution for a number of different frequencies between 1 kHz and 9 GHz for both circular and elliptical shapes for the different layers namely skin, fat, stomach and the outside annular Cu layer as described in section 5.1 for the model in Fig. 5.1. Motivation behind the choice of the above frequency range is to cover all the different frequency zones of absorption as mentioned in [5, 6] and as discussed in chapter 4. Frequencies as high as 9 GHz are used to see resonance and coupling value after resonance. For each of these simulations a different *problem_efem* file and a *problem.g* file as described in section 5.3 have been used and they completely characterize the model for that particular frequency of simulation. Software reads the *problem.g* and *problem_efem* file to build up problem geometry from the unit shapes as generated in the *problem_efem* file and assigns properties as described in section 5.3.1. Frequency dependent values of ε_r and σ used in the *problem_efem* file for each of the different simulation frequencies were taken from reference [16]. In some cases, simulations were carried out for a number of frequencies very close to the frequency for which the *problem_efem* file is valid for purpose explained later in this chapter. The *problem_efem* file generates the same problem geometry for each simulation frequency. Only the values of parameters such as relative permittivity and conductivity used in the *problem_efem* file for defining each of the unit quadrangular shapes as described in section 5.3 are different for different frequencies. For both dielectric and conductor, $\varepsilon = \varepsilon_r \varepsilon_0$ values are used for

their permittivity and σ values are used as their conductivity. This approach neglects losses due to displacement current.

In the *problem.g* file, proper mesh sizes associated with each one of the points are specified as can be seen from Appendix B. It can be seen from the mesh diagram in Fig. 5.3 that depending on associated mesh size, triangular meshes with different sizes are created all across the model cross section. Same mesh structure as shown in Fig. 5.3 was created for all the simulations and they involved the following considerations:

1. Very small mesh sizes have been used for the conductor – skin region to give high resolution and accuracy.
2. Mesh sizes in the inside layers are larger. This is because after the conductor – skin interface; skin, fat and stomach layers have smaller variation in terms of conductivity and dielectric properties and hence smaller variations in electric field is observed in those layers.
3. For reasonable accuracy, mesh dimensions should be less than $\frac{\lambda}{10}$ [19]. This has been maintained in mesh generation. Mesh sizes in the range of 0.5 cm to 1 cm were chosen.

Simulation results are obtained in the form of:

1) Current density plots: These show relative 2D current densities induced in the X-Y cross sectional plane of the model layer 2 which contains the transmitter and receiver regions along with other layers namely skin, fat and stomach as described in section 5.1. A color scale is given beside each plot which specifies relative magnitudes for different colors. The scale is given in db.

Different colors correspond to different magnitudes. These current density plots give only a qualitative description of the relative magnitudes of current density distribution in the different parts in layer 2 of the model shown in Fig. 5.1. They can also be used for observation about specific effects such as attenuation inside different layers.

2) Besides these current density plots, each simulation produces text files with numerical relative magnitude of current density in each triangular mesh. A program was written to pick up meshes in a specific region and find the corresponding current densities. These values are accurate numerical values of current density derived from the E field values as computed by the Full Wave 3D Field Solver [19] and all the plots other than the colored current density plots that will be presented here are based on these values.
3) E field distribution plot around the port of excitation namely port 1 is also given by simulation.

6.2 Results

In the following sections, different simulation results are described starting with the energy density coupling between the transmitter and the receiver regions. Then Electric field coupling and S parameter plots showing reflection are given. At the end current density plots for both circular and elliptical shapes for the model are given.

6.2.1 Variation in Energy Density Coupling with Frequency

As discussed in section 5.5 energy density coupling calculated from the induced E fields in the inner solid cube conductor and the outer annular Cu layer will give values that can be expected in the coupled transmitter-receiver coils in a bio-implantable system. Energy density couplings were calculated for a number of

frequencies between 1 kHz and 9 GHz using the E field values at the receiver and transmitter regions. As discussed in section 6.1, to avoid errors due to color misinterpretation, accurate values of current densities were found with the help of a program from the numerical text results produced by simulation. Since both the excitation port and the receiver port are Cu conductors we can write,

$$\text{Receiver to transmitter energy density ratio} = [\frac{J_R}{J_P}]^2 \text{ and} \tag{6.1}$$

$$\text{Receiver to transmitter E field ratio} = [\frac{J_R}{J_P}], \tag{6.2}$$

where J_R and J_P are the current densities at the receiver and the transmitter respectively. Variation of energy density coupling between the transmitter and the receiver with frequency is shown in the Fig. 6.1, and the induced E field coupling between the transmitter and the receiver is shown in Fig. 6.2. It should be noted that each of the points in Fig. 6.1 and Fig. 6.2 corresponds to a different simulation and each one of these simulations has been done utilizing values of σ and ε_r [16] appropriate for that particular frequency of simulation. The following points can be noted from the energy density coupling shown in Fig. 6.1:

Between 1 kHz and 500 MHz, extrapolated energy coupling values almost remain constant with a value near 0.01. It has been discussed in sections 3.5 and 4.1 that absorption increases with frequency till attenuation factor starts becoming significant. It was also shown that at 500 MHz, E and H fields attenuate to almost e^{-1} times their value at the surface approximately at a depth of 16 cm inside dry skin and this depth reduces to 7 cm approximately at 1 GHz [section 3.5]. For the simulated model, total thickness of skin, fat and stomach layer is 12 cm. For higher frequencies

(frequencies near 500 MHz) attenuation factors (α) for human skin, fat and stomach will be approximately the same as conductivity and dielectric constant values differ very little at frequencies higher than 500 MHz. So absorption is expected to start decreasing around 500 MHz. This is because the exponential term decreases more than the increase in frequency from 500 MHz to 1 GHz in equation (2.16). In Fig. 6.1, one of the reasons for the nearly constant value of energy density coupling between 1 kHz and 500 MHz may be because of the opposite effects of absorption and induced EMF. Till 500 MHz increase in absorption is proportional to f^2 [section 4.1]. So transmission is expected to decrease as f^{-2}. But as discussed in section 3.2, received power due to induced EMF increases proportional to f^2 and also reflection at the port of excitation decreases with frequency. Because of these two opposite effects, energy coupling almost remains the same till 500 MHz. One of the reasons it increases very fast after 500 MHz is that both reduction in absorption and increase in induced EMF help better coupling. But around 1 GHz the system shows a peak resonance. This response is attributed to resonance cavity formation by the outside annular Cu conductor and the inner Cu cube as shown in Fig. 6.3. The lowest frequency of resonance for this structure would correspond to the case when two nodes happen to occur at the two conductors. So λ/2 ~ 16.5 cm is the distance between the inner cube and the outer Cu conductor. This gives a resonance frequency of 0.9 GHz. It has been already discussed that E and H field attenuates to e^{-1} times their value at surface at a depth of ~ 7 cm inside biological tissues like dry-skin, fat and stomach. One of the reasons for decrease in coupling after resonance is because of E field penetration being very small at frequencies higher than 1 GHz.

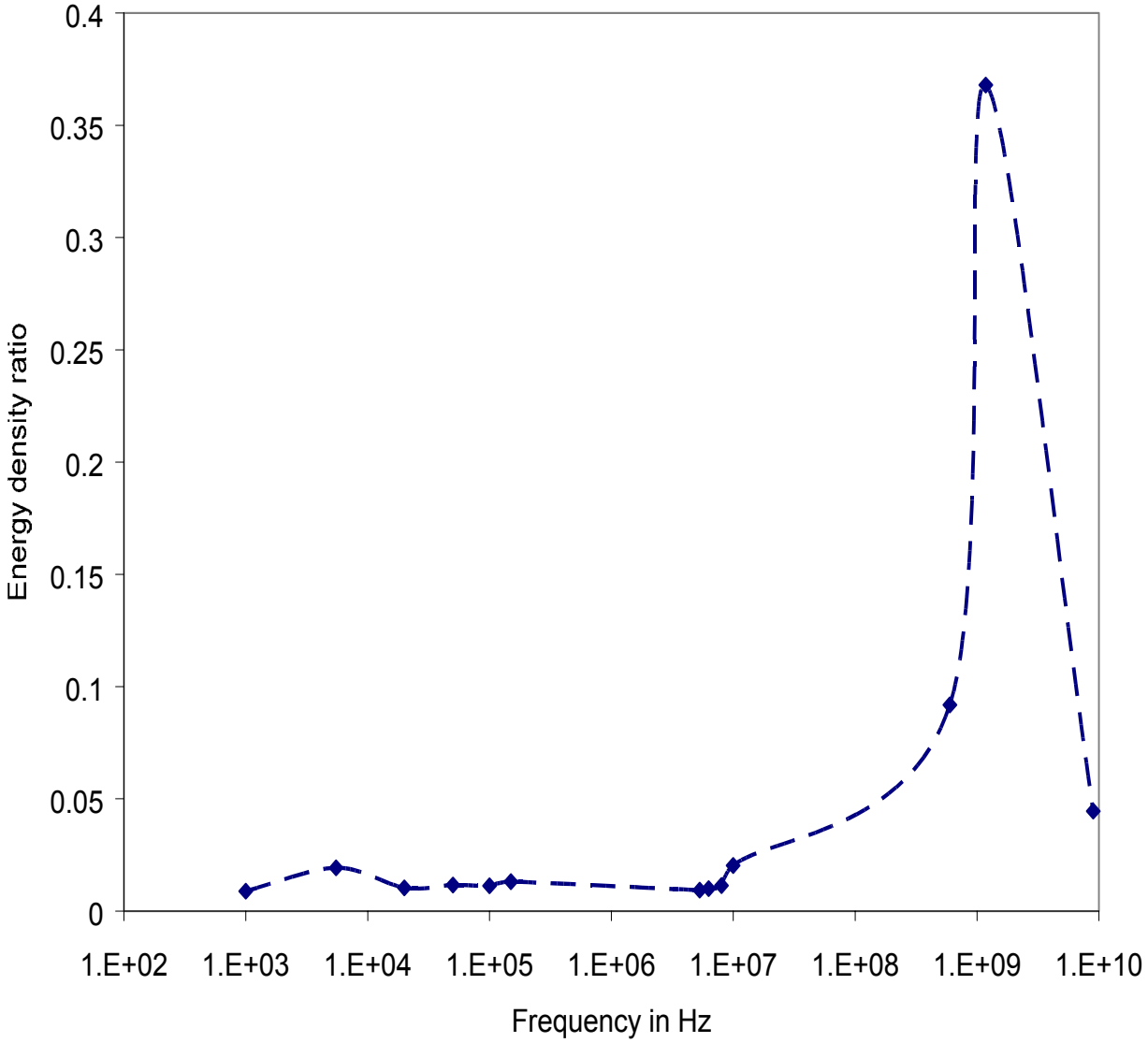

Figure 6.1: Receiver to transmitter region energy density ratio vs. frequency (1 kHz to 9 GHz). Each one of the points corresponds to a different simulation and each one of these simulations has been done utilizing values of σ and ε_r appropriate for that frequency of simulation.

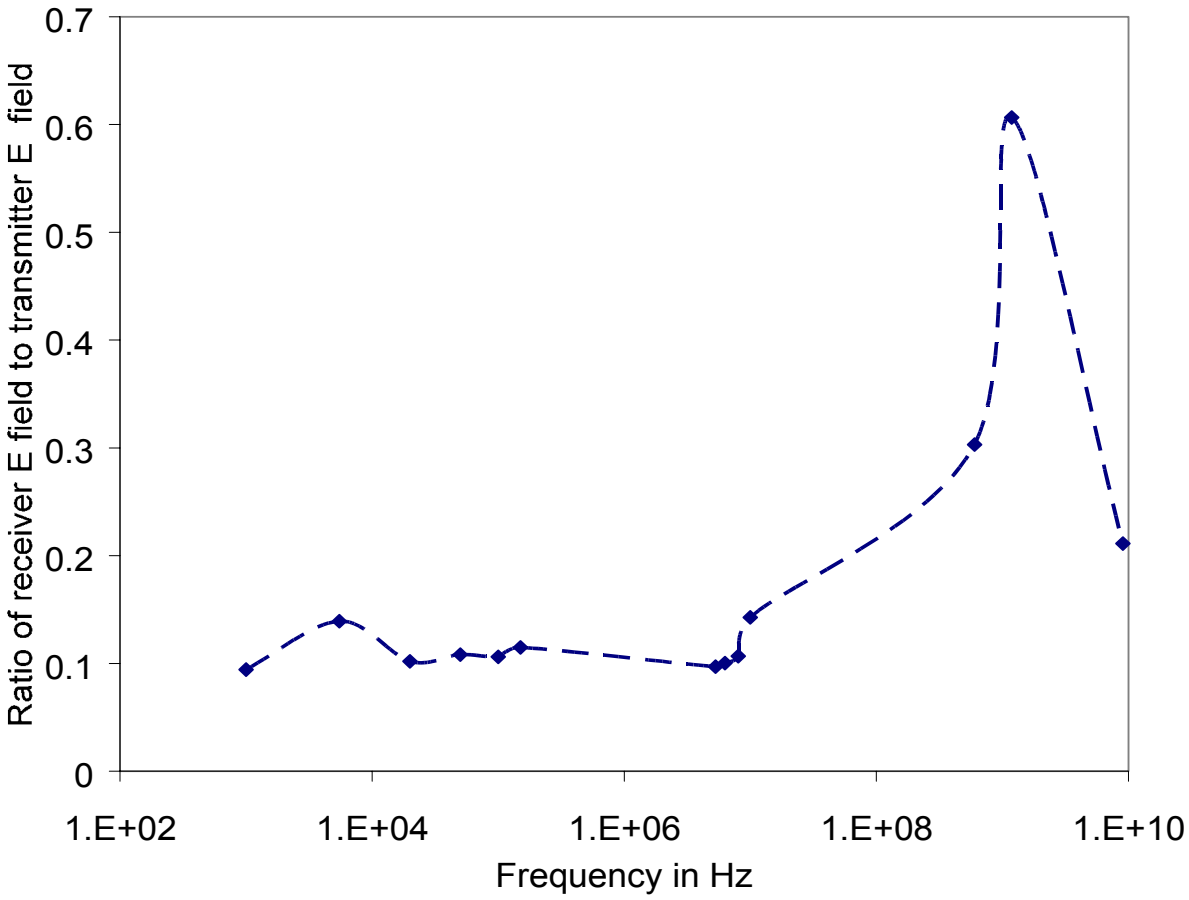

Figure 6.2: Receiver to transmitter region electric field ratio vs. frequency (1 kHz to 9 GHz). Each one of the points corresponds to a different simulation and each one of these simulations has been done utilizing values of σ and ε_r appropriate for that frequency of simulation.

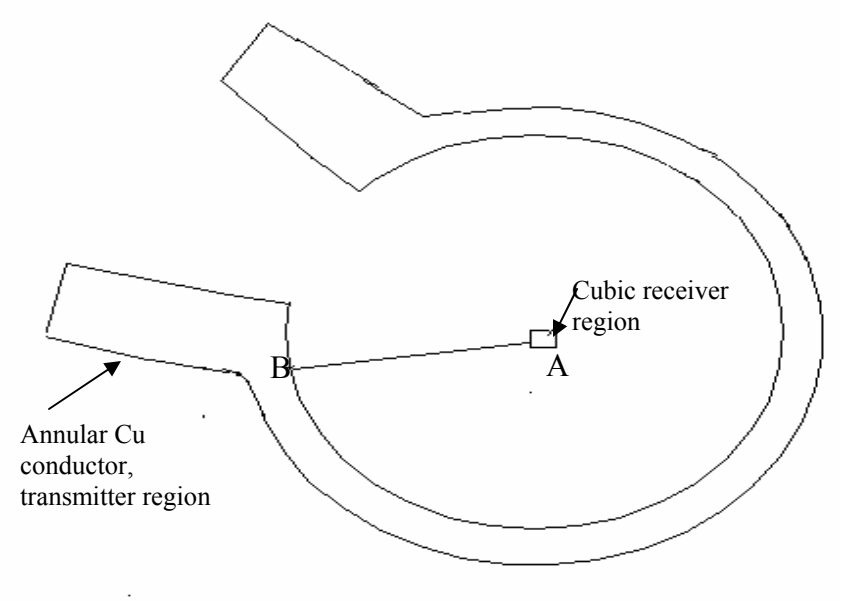

Figure 6.3: Resonance cavity formed by the transmitter and receiver regions, distance between A and B is 16.5 cm. The lowest frequency corresponding to resonance would be when half-wavelength is equal to 16.5 cm.

Lower reflection at the excitation port also plays an important role in giving better coupling at a higher frequency. Figure 6.4 shows variation of S_{11} which gives input reflection coefficient with frequency. It can be seen that reflection at the annular Cu transmitter excitation port decreases with frequency till ~ 30 MHz. At resonance reflection is nearly 1.

6.2.2 S Parameter vs. Frequency Simulation Results

As discussed in section 2.10, values of S_{11} for a two port system gives amount of reflection that occurs at the port of excitation. For our model in Fig. 5.1, simulations were carried out for a number of frequencies between 1 kHz and 9 GHz to give the S_{11} values that essentially give reflection at the port of excitation namely port 1 of the two-port Cu transmitter with a termination load of 50 ohms at port 2. Figure 6.4 shows values for input reflection coefficient (S_{11}) for the frequency range of 1 kHz and 9 GHz. Here also each one of the points corresponds to a different simulation and each one these simulations has been done utilizing values of σ and ε_r appropriate for that particular frequency of simulation.

From the discussion in sections 2.8 and 2.9, the transmitter-receiver to be used in a bio-implantable microsystem, modeled as shown in Fig. 5.1 can be characterized for reflection in the following manner.

1. At the air-Cu conductor interface, reflection decreases with increase in frequency. But at the annular Cu conductor – skin interface reflection would increase with increase in frequency [sections 2.8.2 and 2.8.3].
2. For the intermediate dielectric-dielectric interfaces, it can be seen from equation (2.24) that reflection is low for EM wave incidence from a medium with low permittivity to a medium with high permittivity value and reflection

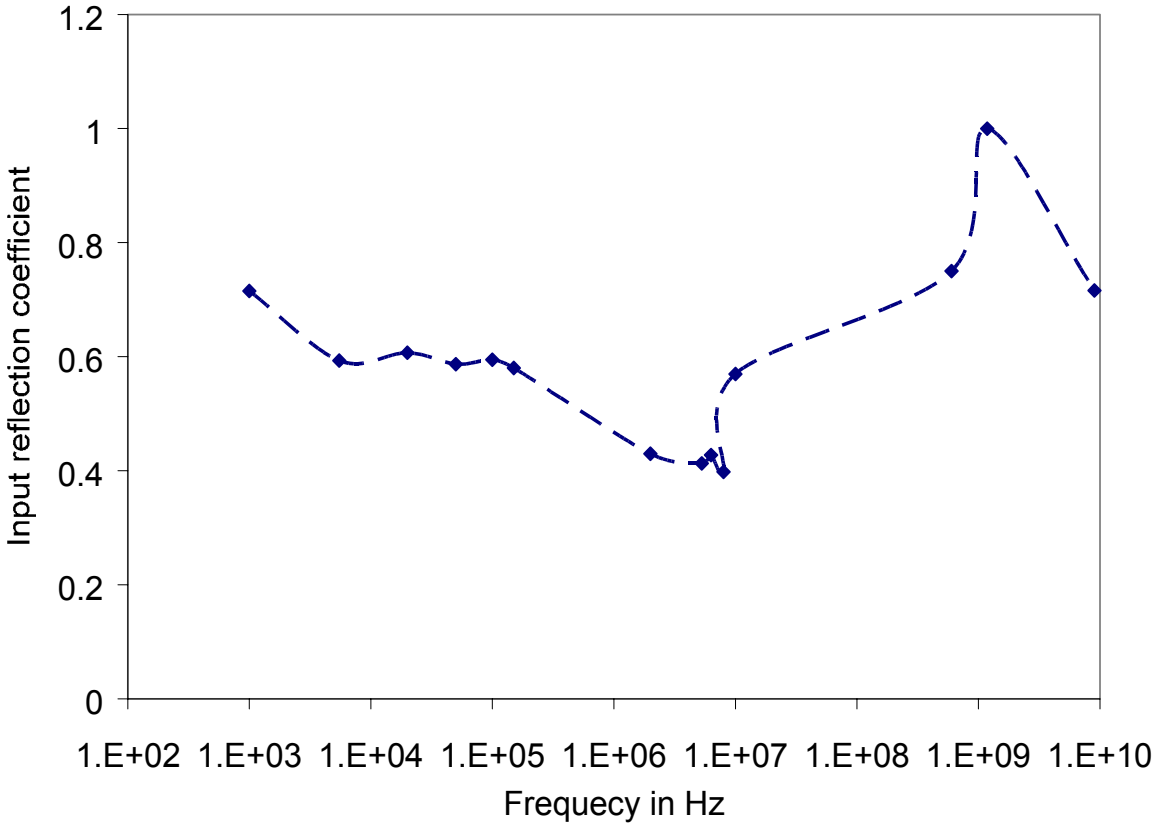

Figure 6.4: Input reflection coefficient (S_{11}) vs. frequency (1 kHz to 9 GHz), shows that reflection decreases steadily till approx. 30 MHz. Reflection is nearly unity around 1 GHz. Here each one of the points corresponds to a different simulation and each one these simulations has been done utilizing values of σ and ε_r appropriate for that frequency of simulation.

is high if the medium of incidence has higher permittivity value than the medium of transmission. At lower frequencies (f less than 1 MHz) fat has higher permittivity value compared to skin and stomach. So skin-fat interface will have smaller reflection compared to fat-stomach interface at lower frequencies. At higher frequencies permittivity difference between different layers decreases. Reflection is expected to decrease at high frequencies, but they still would follow the same low frequency trend.

3. At the stomach-receiver interface which is a dielectric-conductor interface, reflection is expected to decrease with increase in frequency. This can be seen from the results shown in equation (2.25) and the related discussions.

It can be seen from Fig. 6.4 that reflection decreases steadily till approximately 30 MHz. One of reasons for this may be decrease in reflection at the stomach-receiver interface and the intermediate dielectric layers with increase in frequency. Reflection is nearly 1 around 1 GHz which is due to resonance.

A few other simulations were carried out by varying the frequency of simulation on the same *problem_efem* file. So values of σ and ε_r used are same for that frequency range. Fig. 6.5 shows values of input reflection coefficient for the frequency range 50 kHz to 100 kHz. Although simulation frequency is varied from 50 kHz to 100 kHz, the values of σ and ε_r used in the input file are valid only for 50 kHz. This simulation partly shows that a little variation in the values of σ and ε_r does not affect reflection that much. If results of Fig.6.5 are compared to results of Fig. 6.4, we see that values of S_{11} are approximately the same in both the simulations for the same frequency range. These results may also imply that S_{11} may be dominated by the reflection at port 1 and not by internal reflections between the multilayers.

One more simulation was done to verify this trend. Figure 6.6 shows values of input reflection coefficient for the frequency range from 6.3 MHz to 63 MHz and here simulation was done with the input file having values of σ and ε_r for 10 MHz. Here also S_{11} values are almost the same as shown in Fig. 6.4 in the same frequency zone. This again implies that S_{11} may be dominant by reflection at port 1 and not by the multilayers inside.

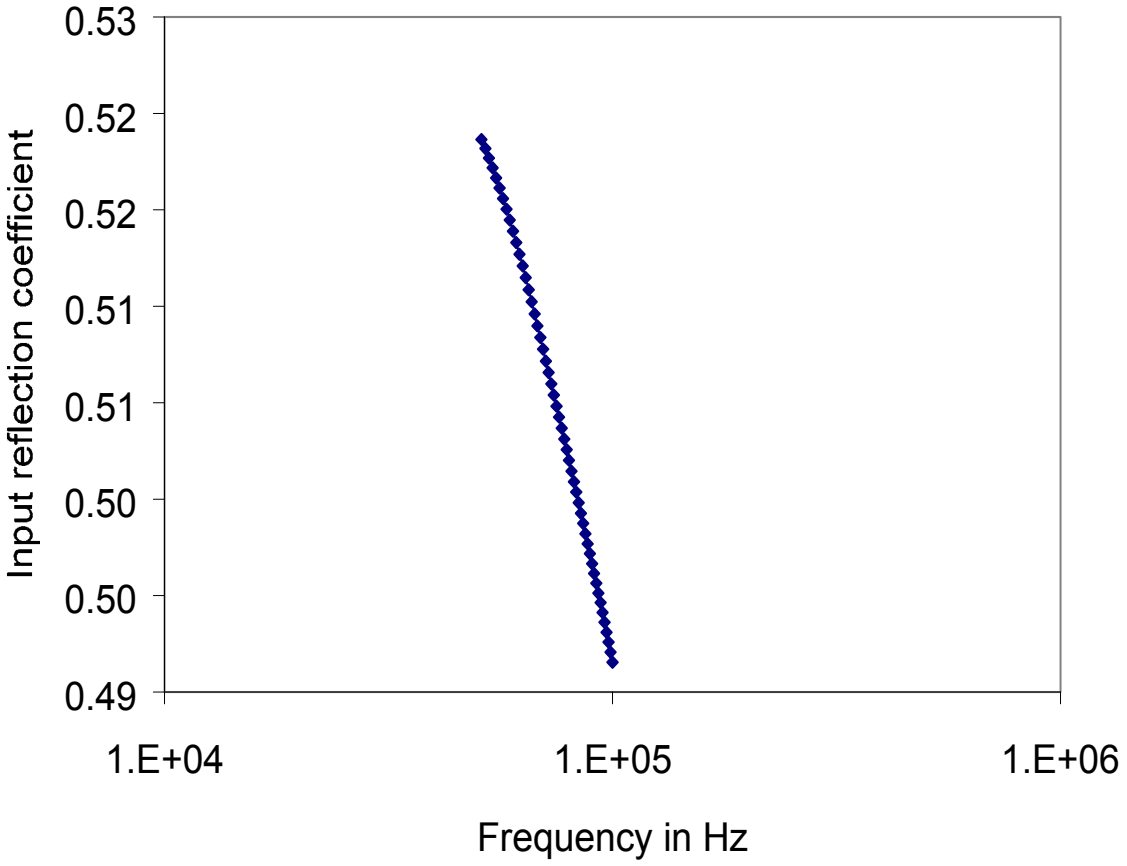

Figure 6.5: Input reflection coefficient (S_{11}) vs. frequency (50 kHz to 100 kHz), shows steady decrease in S_{11} in this frequency zone as found in Fig. 6.4. Simulation has been done on the input file with values of σ and ε_r valid for 50 kHz.

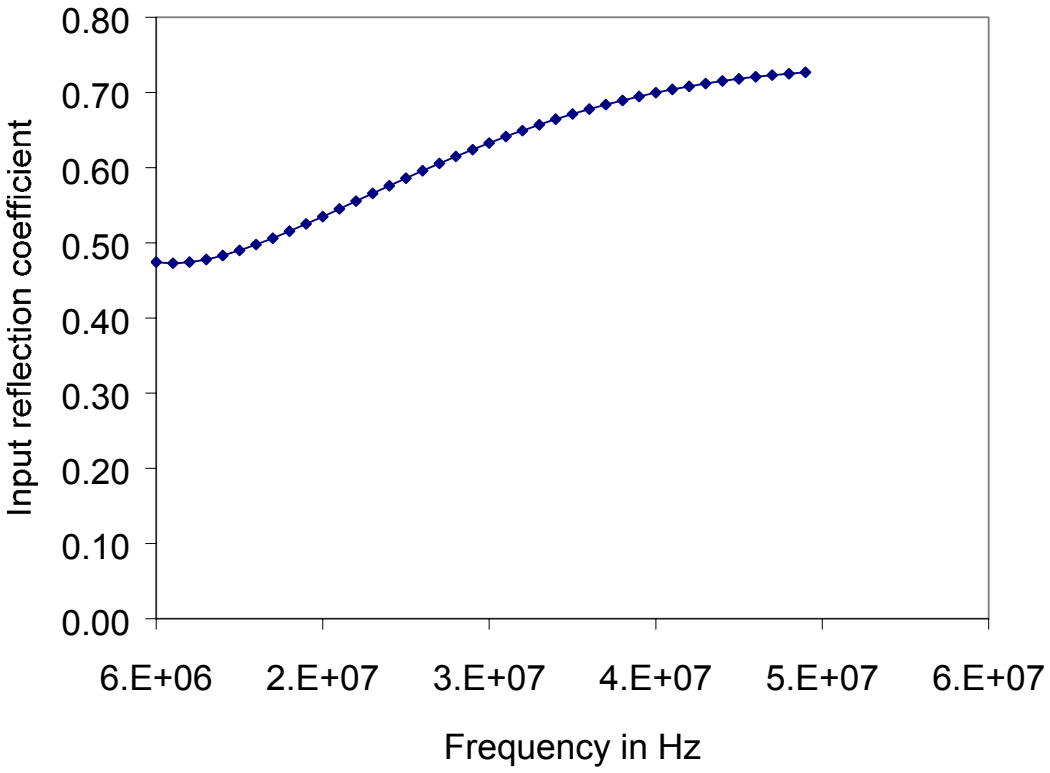

Figure 6.6: Input reflection coefficient (S_{11}) vs. frequency (6.3 MHz to 63 MHz), shows steady increase in S_{11} in this frequency zone as found in Fig. 6.4. Simulation has been done on the input file with values of σ and ε_r valid for 10 MHz.

In order to see the high frequency variation of S_{11}, another simulation was carried out for the frequency range of 1.18 GHz to 10 GHz on the input file having correct values of σ and ε_r corresponding to 2 GHz.

As has been found in the above two simulations in Figs. 6.5 and 6.6, reflection would not be affected much due to use of 2 GHz values of σ and ε_r for this frequency range. Figure 6.7 shows these results. It is obvious that these peaks are due to resonances.

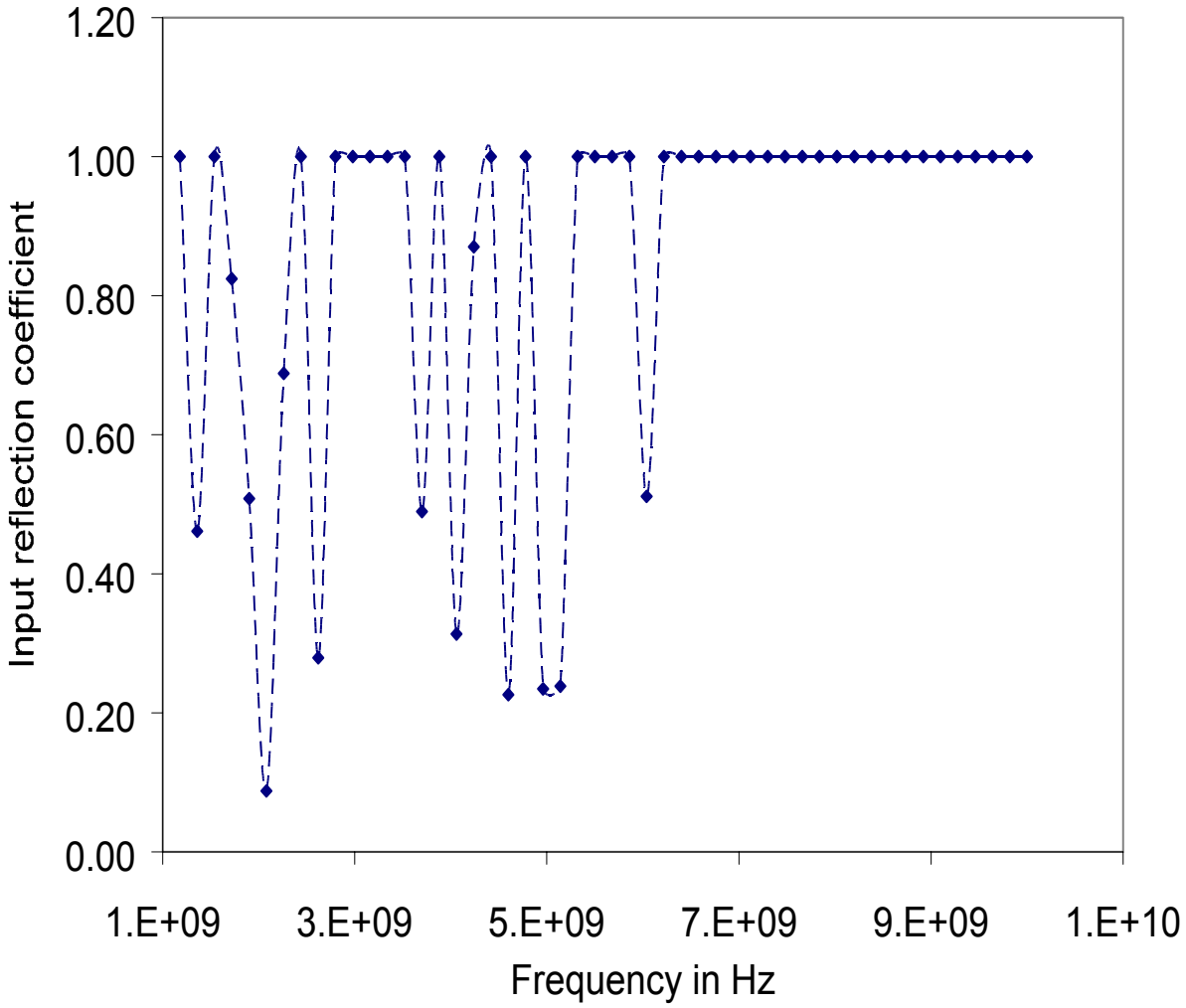

Figure 6.7: Input reflection coefficient (S_{11}) vs. frequency (1 GHz to 10 GHz), shows numerous resonances between these frequencies. Simulation has been done on the input file with values of σ and ε_r valid for 2 GHz.

6.2.3 Relative Current Densities Inside Different Layers

As discussed in section 2.1, safe limit for induced current density in a human body without causing any significant destructive damage is 3 $mA.cm^{-2}$ or 30 $A.m^{-2}$. This safe current density limit is to avoid heating inside human tissues. It may be noted that this safe limit does not include the damage that can be caused by ventricular fibrillation or disruption of heart beats which can be fatal at a current as low as 0.1 - 0.2 A [20]. Care should be taken to avoid induced current density greater than the safe current density limit of 30 $A.m^{-2}$ for thermal damage. Also it was discussed in section 2.4 that standing wave formation might result in substantial relative heating at different interfaces. Simulations were carried out at different frequencies to find the relative current densities in different layers namely transmitter, skin, fat and stomach in the simplified human body model described in section 5.1 and shown in Fig. 5.1.

As an example, for a secondary coil current requirement of 100 mA and secondary coil Cu wire diameter of 0.0815 cm, assuming that current would flow only through part of the cross section of the wire (due to skin effect, skin depth of Cu being 0.015 cm at 1 MHz from Table 3.1), the effective cross section of the wire is given by: $\pi \times \left[0.04075^2 - \left(0.04075 - 0.015\right)^2\right] = 3.133 \times 10^{-3}$ cm^2. So current density at the secondary coil is 3.2×10^5 $A.m^{-2}$. For values of E field coupling as shown Fig. 6.2 and using equation (6.2), for 0.1 coupling, current density requirement for the transmitter would be 3.2×10^6 $A.m^{-2}$. Coupling value of 0.1 has been used as it is the most representative of all the values present in the frequency range of 1 kHz to 10 MHz and skin-depth value at 1 MHz is also used for the same reason.

In Fig. 6.8, current densities in different layers namely skin, fat, and stomach are shown for a current density of 3.2×10^6 $A.m^{-2}$ in the transmitter. Safe limit current

density, 30 A.m^{-2} is also shown in Fig. 6.8. Figure 6.8 shows that stomach and skin layers are the ones where maximum current densities may cross the safe limit for a higher value of current density than the one considered here at the transmitter coil. Those values can be easily found with data given in Fig. 6.8. Transmitter coil current density in amperes required to make a particular layer current density cross the safe limit at a particular frequency f is given by, $\frac{J_{Cu}(f)}{J_{layer}(f)} \times 30$, where $J_{layer}(f)$ and $J_{Cu}(f)$ are values of current densities of that particular layer and Cu transmitter at frequency f as given in Fig. 6.8. Power densities induced inside different layers are also calculated with the formula $\frac{J^2}{\sigma}$. Values of σ used are taken from the *problem_efem* files for those particular simulations. Figure 6.9 shows the power density plot vs. frequency and here also it can be seen that for the transmitter current density requirement of 3.2x10^6 A.m^{-2}, power densities induced inside different layers in our model in Fig. 5.1 are considerably below the safe limit power density of 100 W.m^{-3} [2]. It may be noted that power densities of the order of 10^5 W.m^{-3} would result in severe heating of the annular Cu conductor for the given dimension of the model. Such a high value has been taken as an example to simulate transmitter wire current density of 3.2x10^6 A.m^{-2}.

6.2.4 Current Density Plots

Current density plots were obtained for a number of frequencies between 1 kHz and 1.18 GHz for both circular and elliptical shapes for the different layers namely skin, fat, stomach and the outside annular Cu conductor. As mentioned in section 6.1, these current density plots show relative 2D current densities induced in the X-Y cross

sectional plane of the layer 2, which has all these above layers of skin, fat, stomach and the annular Cu conductor as described in section 5.1.

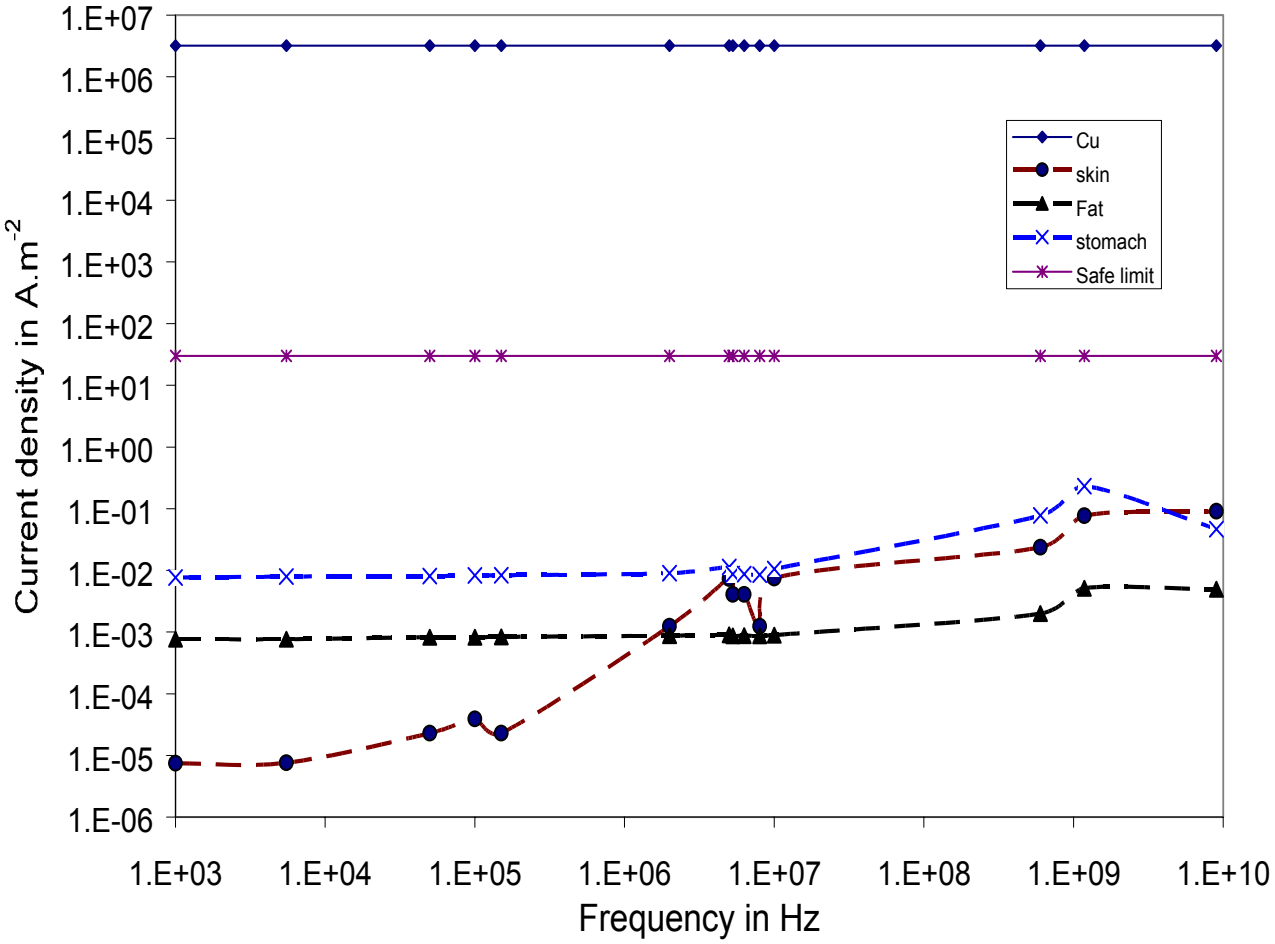

Figure 6.8: Current density vs. frequency for the frequency range 1 kHz to 9 GHz, for a transmitter current density of 3.2×10^6 A.m^{-2}. It shows that for the receiver current of 100 mA, induced current densities in the intermediary layers are far below the safe limit.

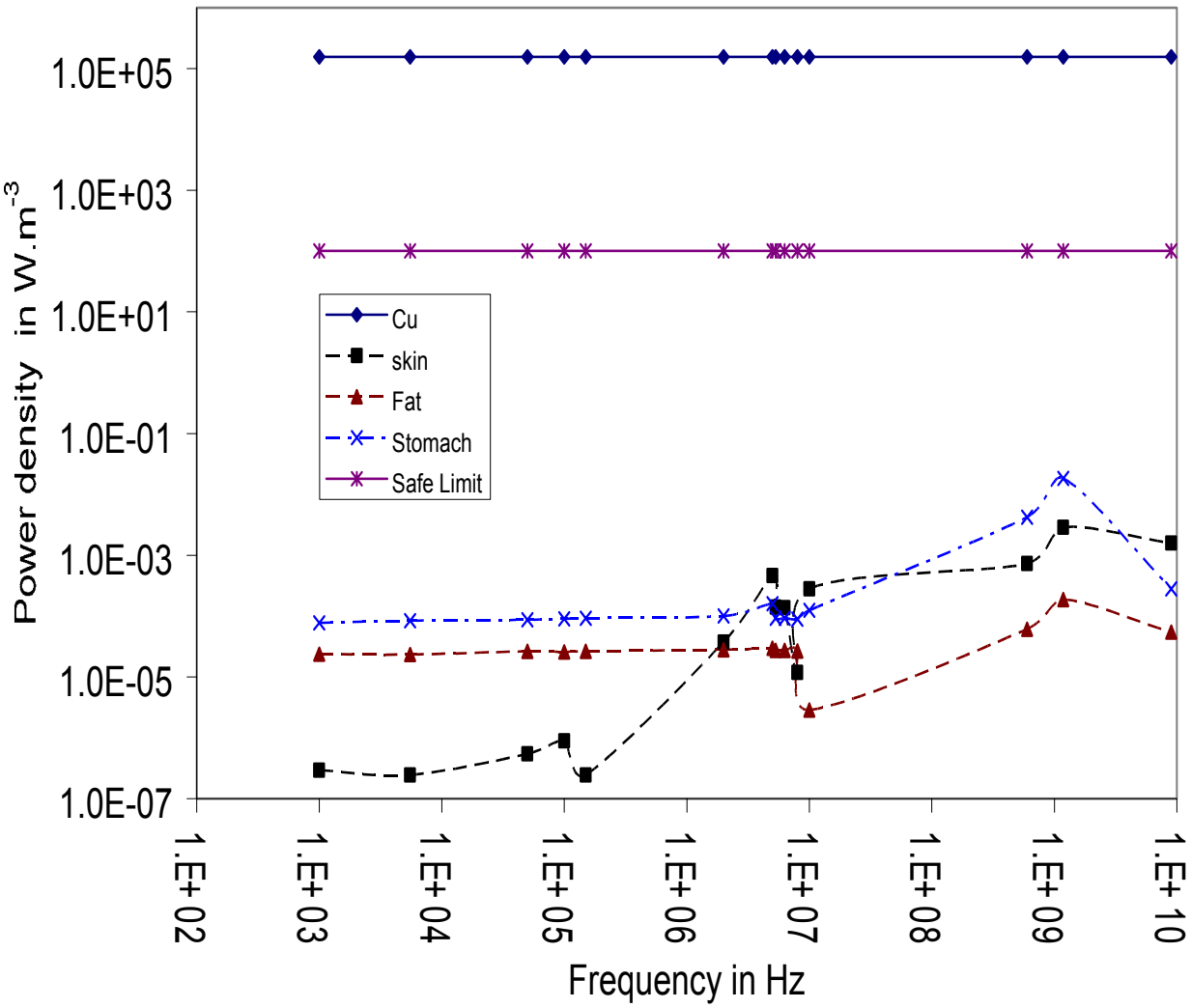

Figure 6.9: Induced power density in different layers vs. frequency (1 kHz to 9 GHz), for a transmitter current density of 3.2×10^6 A.m^{-2}. It shows that induced power densities are well below the safe limit, even for this high power density in the transmitter.

These plots give current densities of different layers relative to the current density in the outside annular Cu conductor where the excitation port is located. These plots are useful in obtaining a qualitative interpretation regarding the current density distribution inside the model shown in Fig. 5.1. These are also helpful in identifying absorption with distance and in getting a visual estimate of the current density coupling or the E field coupling between the transmitter and the receiver. Table 6.1 shows values of σ and ε_r used for the simulations at different frequencies. A different *problem_efem* file was written for each of one the different frequency simulations using the appropriate values for σ and ε_r as indicated in Table 6.1.

For each current density plot, a color scale is given beside each plot which specifies relative magnitudes associated with different colors. The scale is given in db. Color corresponding to the current density in the excitation port namely port 1 is marked as Cu in the color scale, which corresponds to a current density of 1 $A.m^{-2}$. All the other current densities are relative to the current density in the annular Cu layer. So magnitude of current density in any other region can be found as described below.

Let us assume that color corresponding to the region of interest is A. Let us say that A corresponds to value of C in the db scale. Let us also say that value of color corresponding to the color of the transmitter excitation port is T marked as Cu beside the scale. Then current density of the region is given by,

$$\text{Current density of the region} = 1 \times 10^{\left\lfloor \frac{C-T}{20} \right\rfloor} \text{ A.m}^{-2}. \qquad (6.3)$$

Table 6.1: Values of parameters used for simulation at different frequencies for the current density plots taken from reference [16].

Parameter → Frequency ↓	Skin conductivity in $s.m^{-1}$	Skin relative permittivity value (ε_r)	Fat conductivity in $s.m^{-1}$ (σ)	Fat relative permittivity value (ε_r)	Stomach conductivity in $s.m^{-1}$ (σ)	Stomach relative permittivity value (ε_r)	Central core conductivity in $s.m^{-1}$ (σ)	Central core relative permittivity value (ε_r)	Figures using these parameters
1 kHz	$1.8x10^{-4}$	1170	0.0246	2080	0.753	655	0.0002	10.5	Fig. 6.10& Fig. 6.14
10 kHz	$2.49x10^{-4}$	1040	0.0256	1150	0.753	655	0.0002	1	
50 kHz	$5.34x10^{-4}$	967	0.026	187	0.753	655	0.0002	1	Fig. 6.11 & Fig. 6.12
100 kHz	$8.93x10^{-4}$	934	0.0262	94	0.753	655	0.0009	1	Fig. 6.15
2 MHz	$2.89x10^{-2}$	701	0.0269	20.1	0.8	150	0.001	1	Fig. 6.13 & Fig. 6.16
5 MHz	$9.5x10^{-2}$	494	0.027	16.6	0.8	150	0.0019	1	Fig. 6.17
2 GHz	1.56	45.1	0.095	4.43	2.25	68.4	0.09	1	

6.2.4.1 Current Density Plot for Circular Model

Figure 6.10 shows current density plot for simulation frequency 1 kHz. Values of σ and ε_r used in the *problem_efem* file are appropriate for 1 kHz. This shows that induced current densities in the skin, fat and stomach regions are about 8 to 11 orders smaller than current density in Cu. The inside cubic Cu region which models the receiver has almost the same color as that in the transmitter region. The current density in the receiver in this case is approximately 0.1 $A.m^{-2}$.

Current density plot shown in Figure 6.11 is for simulation frequency 50 kHz and values of σ and ε_r used are also appropriate for 50 kHz. But central core conductivity was overwritten with a value of 0 $s.m^{-1}$. This was done to see the effect of insulating enclosures around the receiver. As can be seen from Fig. 6.11, no current is induced in the core. Color white corresponds to zero current. Displacement current is too small for a value of 1 for ε_r in the core at 50 kHz. If coupling in Fig. 6.10 and Fig. 6.11 are compared, it can be seen that coupling in Fig. 6.11 is higher compared to that in Fig. 6.10. This is partly because of the higher frequency of simulation and less loss due to no conductivity of the central core.

Another current density plot was obtained at 50 kHz frequency as shown in Fig. 6.12, but in this simulation central core conductivity of 0.0002 $s.m^{-1}$ has been retained as given in Table 6.1. Comparison of Fig. 6.12 to Fig. 6.11 shows that conductive enclosures decreases current density coupling as coupling in Fig. 6.12 is less than that in Fig. 6.11, because of higher loss due to the loss in central core, other conditions remaining same for both of these simulations. That coupling remains almost the same between 1 kHz and 50 kHz also can be verified by comparing

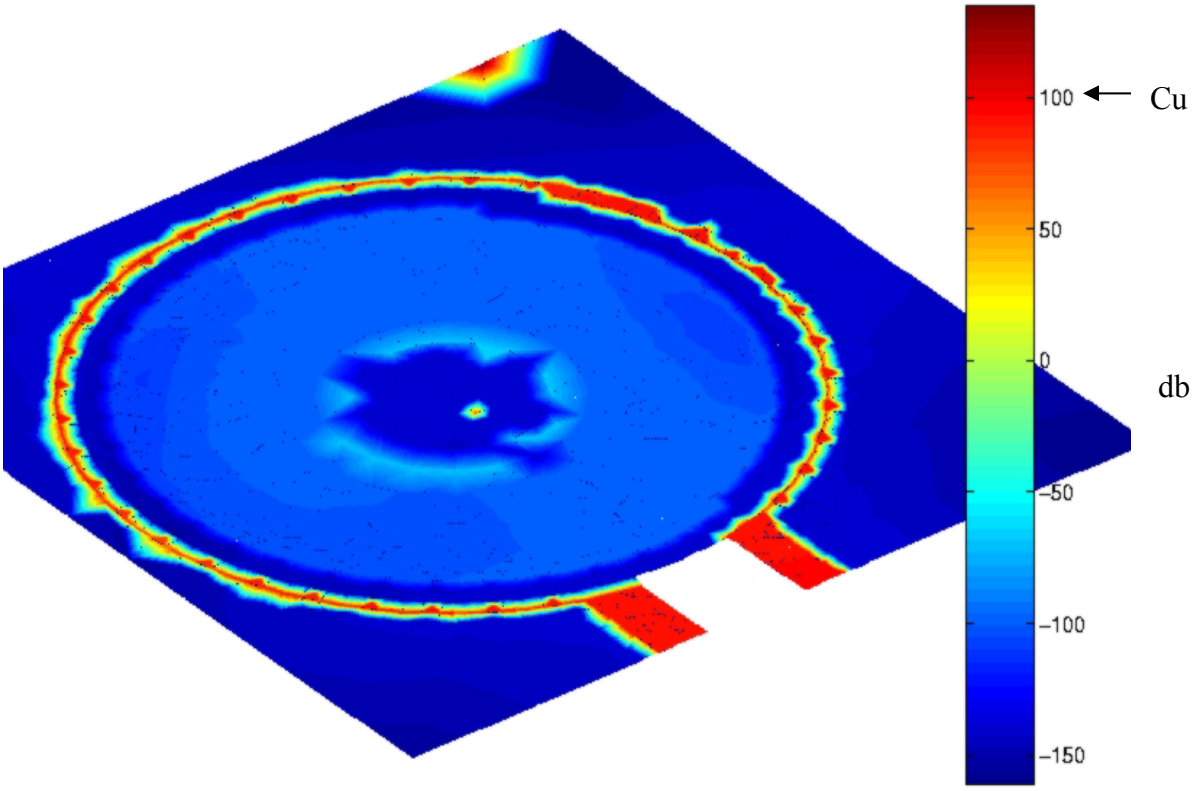

Figure 6.10: 2D current density plot in the layer 2 of the model in Fig. 5.1. Simulation frequency is 1 kHz and parameters used are also for 1 kHz. This plot is in conformity with the relative current densities shown in Fig. 6.8. Values for current density in different areas can be found using equation (6.3). Cu marks Current density at the transmitter port 1.

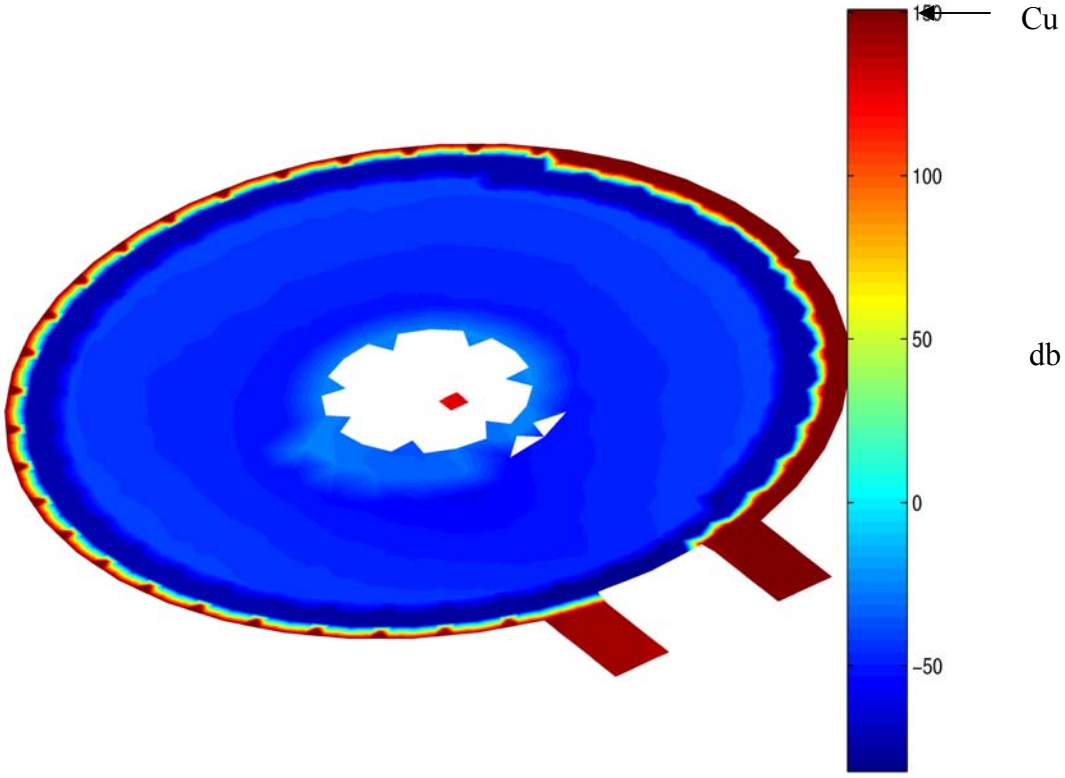

Figure 6.11: 2D current density plot in the layer 2 of the model in Fig. 5.1. Simulation frequency is 50 kHz and parameters used are also for 50 kHz. Central core conductivity is overwritten with value 0 $s.m^{-1}$. Values for current density in different areas can be found using equation (6.3). Cu marks current density at the transmitter port 1.

Fig. 6.12 with the current density plot at 1 kHz as shown in Fig. 6.10. Both of these plots show approximately same current density coupling.

Losses increases at 2 MHz because of higher conductive as well as dielectric loss, but coupling almost remains the same as 50 kHz as shown in Fig. 6.2. Fig. 6.13 shows current density plot at 2 MHz.

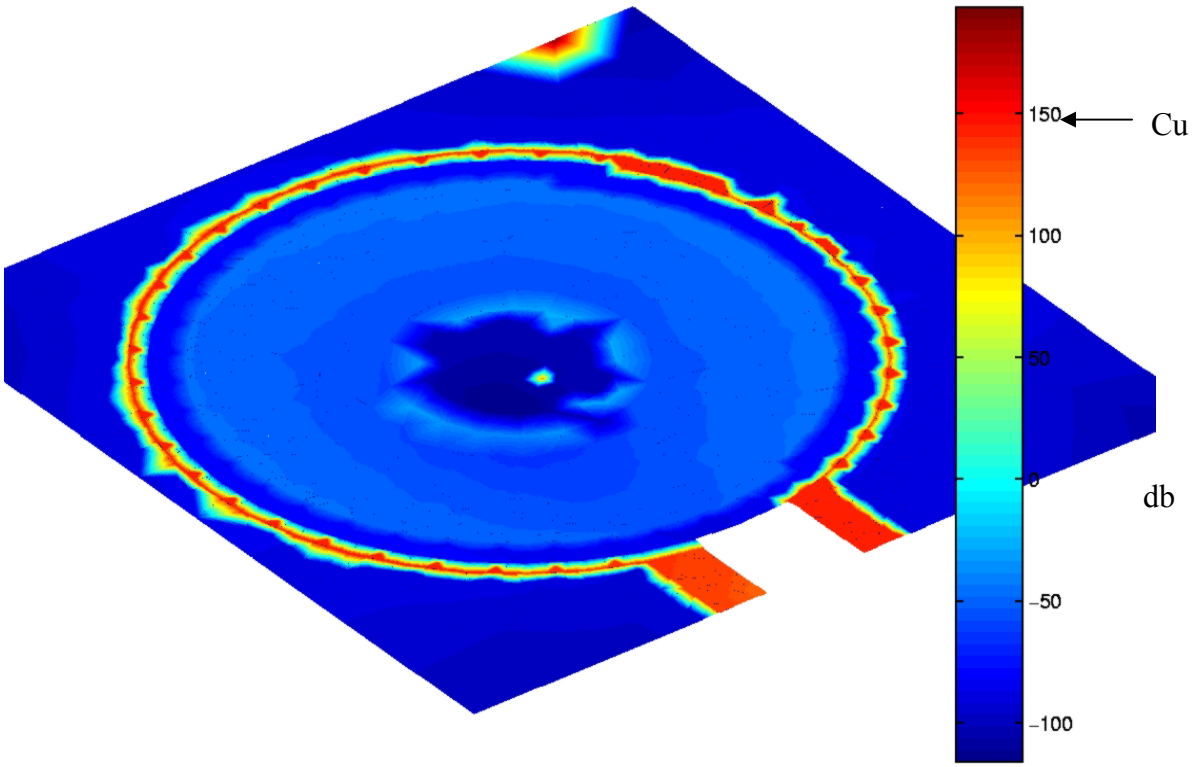

Figure 6.12: 2D current density plot in the layer 2 of the model in Fig. 5.1. Simulation frequency is 50 kHz and parameters used are also for 50 kHz. Central core conductivity is 0.0002 $s.m^{-1}$ as mentioned in Table 6.1. Values for current density in different areas can be found using equation (6.3). Cu marks current density at the transmitter port 1.

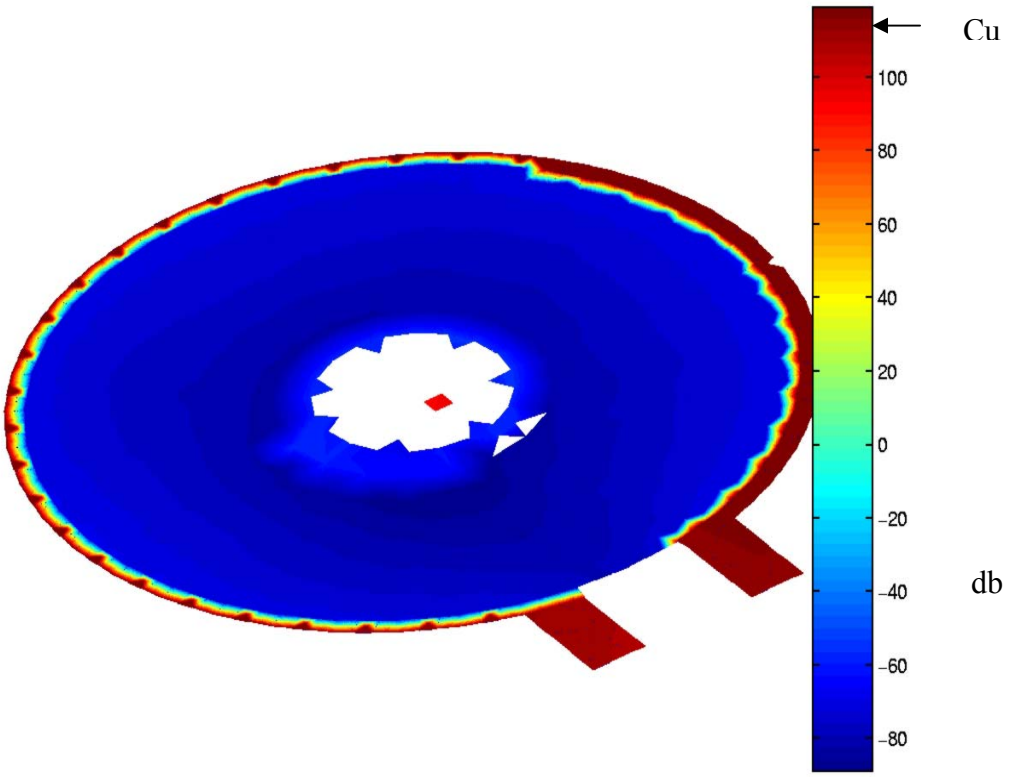

Figure 6.13: 2D current density plot in the layer 2 of the model in Fig. 5.1. Simulation frequency is 2 MHz and parameters used are also for 2 MHz. But central core conductivity is overwritten with 0 $s.m^{-1}$. Values for current density in different areas can be found using equation (6.3). Cu marks current density at the transmitter port 1.

Here also central core was given conductivity of 0 $s.m^{-1}$ which makes the coupling better than shown in E field coupling plot in section 6.2.1. Another observation on this simulation is that current density in the skin layer is much higher here compared to the other low frequency plots shown in Figs. 6.10 to 6.12. One of the reasons for this is the increase in skin conductivity with increase in frequency.

6.2.4.2 Current Density Plots for Elliptical Model

Current density plots shown in Figs. 6.10 to 6.13 are all for circular cross sections. Elliptical shapes for these layers would better represent the actual shapes in a human body, than the circular ones. Different *problem_efem* file and *problem.g* file were written to build up elliptical shapes for the different layers in the model shown in Fig. 5.1. Here also because of the restriction of the software, [19] only quadrangular or triangular unit shapes are used to define the elliptical annular shapes for different layers namely skin, fat, stomach and outside Cu conductor. The edges are hence not perfectly smooth. Dimensions used for different regions are shown in Table 6.2.

Fig. 6.14 shows the current density plot for the elliptical model for simulation frequency 1 kHz. Values of σ and ε_r used in the *problem_efem* file are also appropriate for 1 kHz as shown in Table 6.1. But central core conductivity is changed to 0.00059 which is a more conservative number. If the 1 kHz plots for circular shape shown in Fig. 6.10 and for the elliptical shape shown in Fig. 6.14 are compared, it can be seen that same order of magnitude difference exists between the current densities of stomach and the outside annular Cu layer in both the cases. So it can be concluded that at least for this simulation, shape does not affect current density coupling. But coupling is less in Fig. 6.14, due to more losses in the central core.

Table 6.2: Dimension of the elliptical model

Major axis of outer boundary of annular Cu layer	40 cm
Minor axis of outer boundary of annular Cu layer	25 cm
Major axis of outer boundary of annular skin layer	39 cm
Minor axis of outer boundary of annular skin layer	24 cm
Major axis of outer boundary of annular fat layer	38 cm
Minor axis of outer boundary of annular fat layer	23 cm
Major axis of outer boundary of annular stomach layer	36 cm
Minor axis of outer boundary of annular stomach layer	21 cm
Major axis of inner boundary of annular stomach layer	28 cm
Minor axis of inner boundary of annular stomach layer	16 cm
Length of the inner cube	2 cm

Current density plots for simulations carried out at 100 kHz, 2 MHz and 5.3 MHz are shown in Figs. 6.15, 6.16 and 6.17 respectively. These figures show that current density coupling remains approximately the same between the frequency ranges of 100 kHz to 5.3 MHz as shown in Fig. 6.2. In all of these plots, 6 to 10 order magnitude difference between the current densities in the dielectric regions and that in the Cu conductor is obtained.

Values of σ and ε_r for stomach change substantially around 5 MHz [16]. From the Fig. 6.17 it can be seen that corresponding current densities have also increased and thus there will be more heating. This is due to increase in conductivity.

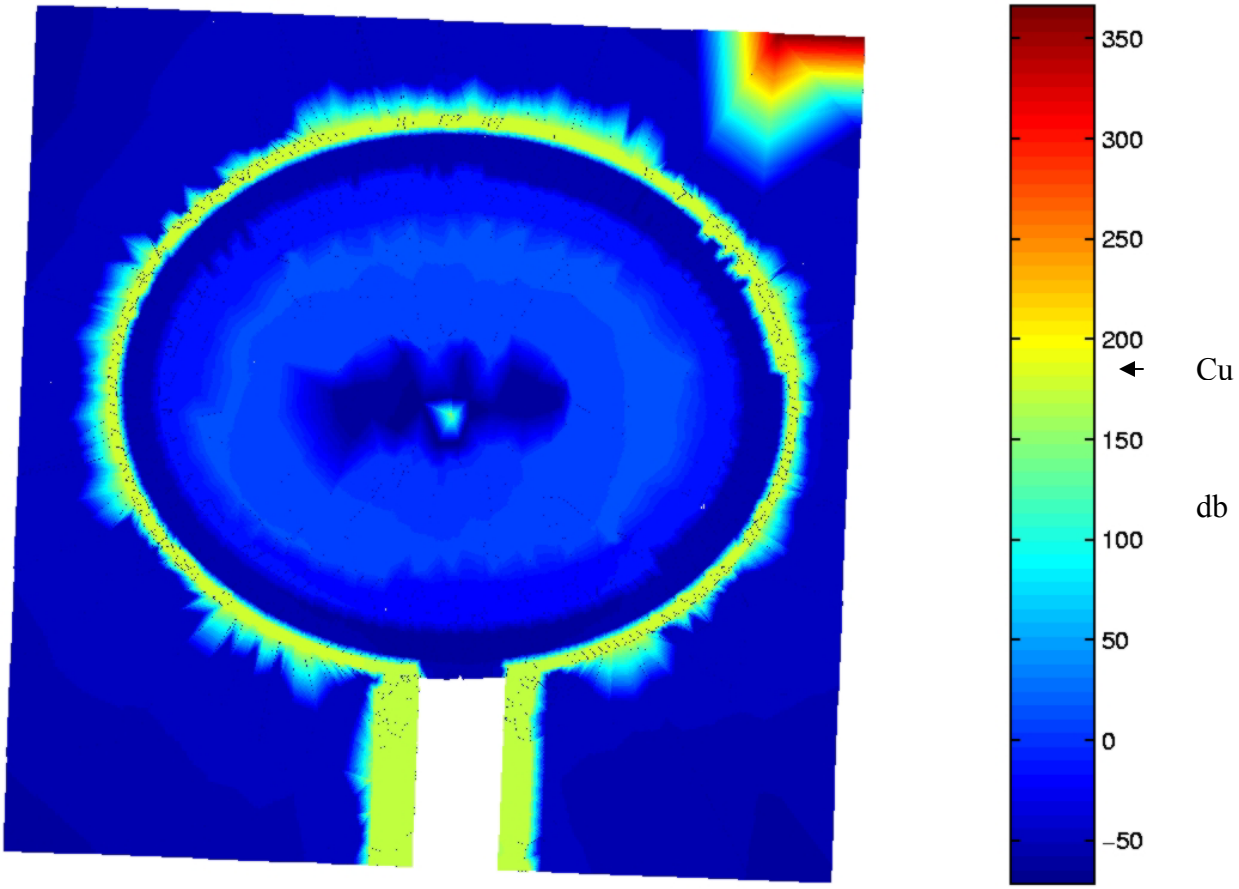

Figure 6.14: 2D current density plot in the layer 2 of the model in Fig. 5.1 for elliptical dimension. Simulation frequency is 1 kHz and parameters used are also for 1 kHz. But the inner core conductivity of 0.00059 $s.m^{-1}$ has been used. Cu marks current density at the transmitter port 1. Values for current density in different areas can be found using equation (6.3).

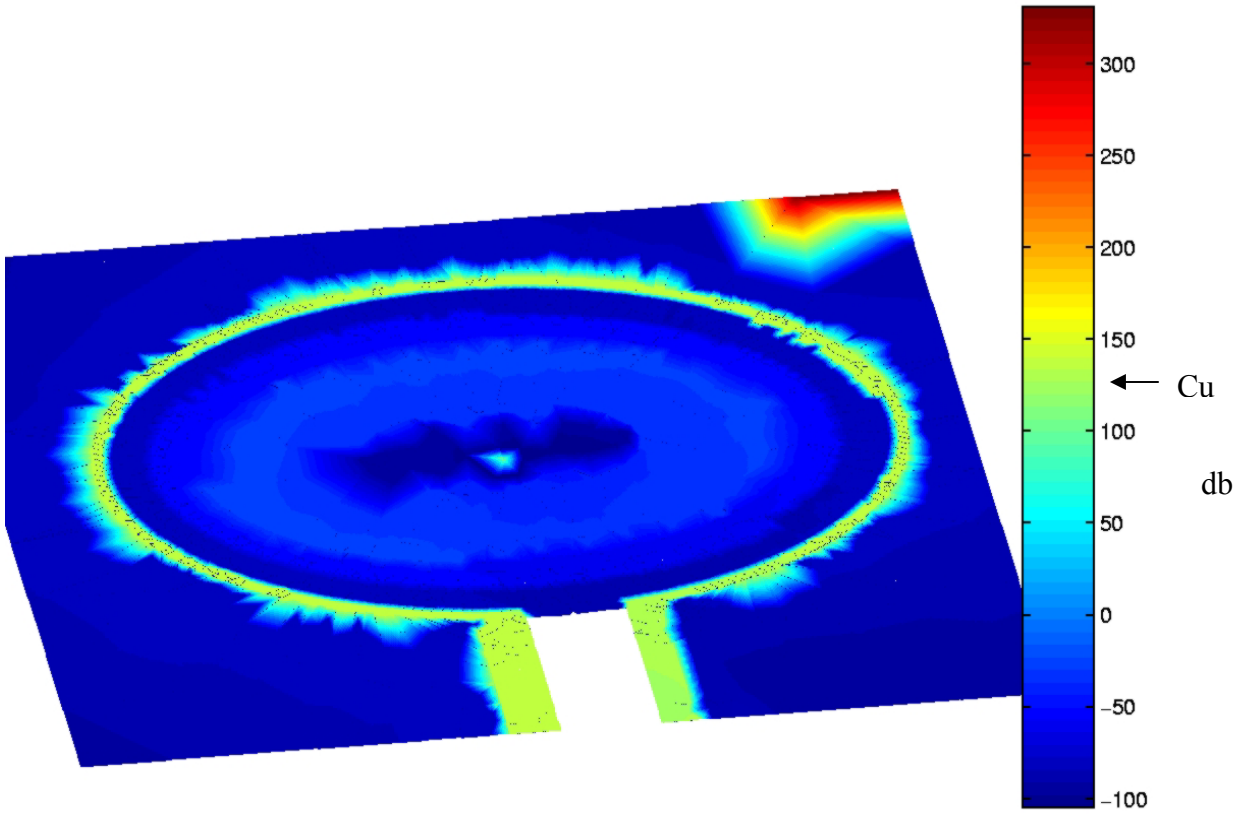

Figure 6.15: 2D current density plot in the layer 2 of the model in Fig. 5.1 for elliptical dimension. Simulation frequency is 100 kHz and parameters used are also for 100 kHz as shown in Table 6.1. Cu marks current density at the transmitter port 1. Values for current density in different areas can be found using equation (6.3).

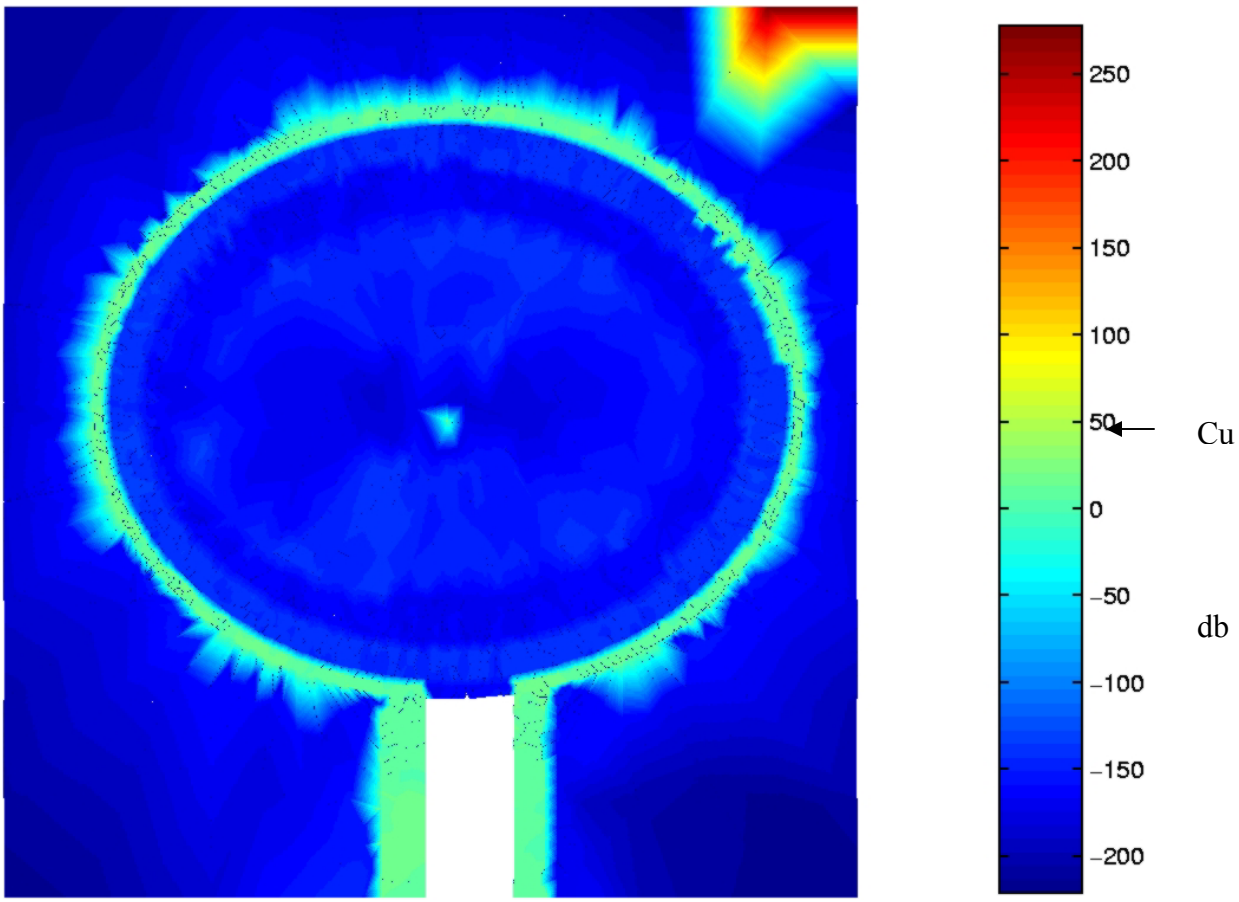

Figure 6.16: 2D current density plot in the layer 2 of the model in Fig. 5.1 for elliptical dimensions. Simulation frequency is 2 MHz and parameters used are also for 2 MHz as shown in Table 6.1. Cu marks current density at the transmitter port 1. Values for current density in different areas can be found using equation (6.3).

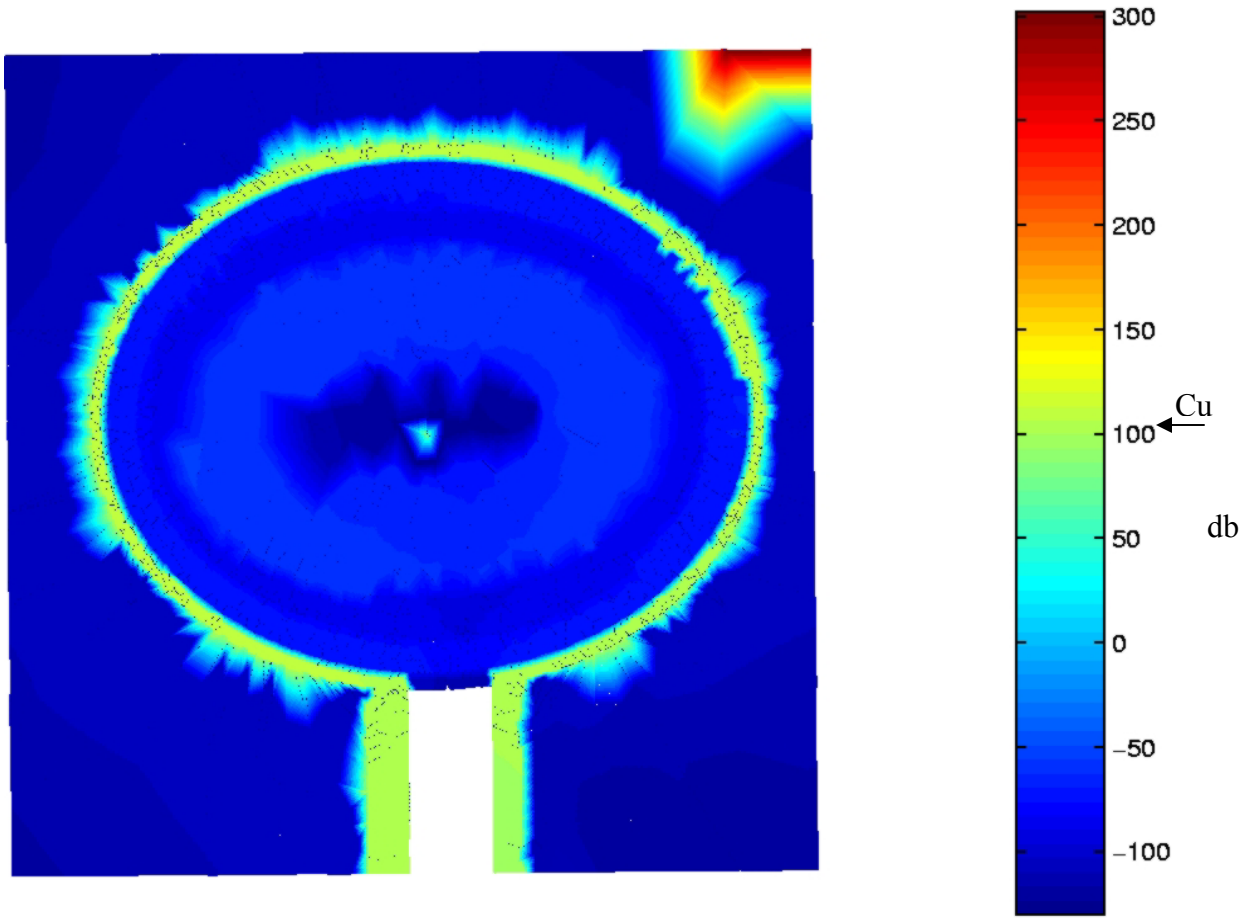

Figure 6.17: 2D current density plot in the layer 2 of the model in Fig. 5.1 for elliptical dimension. Simulation frequency is 5.3 MHz and parameters used are for 5 MHz as shown in Table 6.1. Cu marks current density at the transmitter port 1. Values for current density in different areas can be found using equation (6.3).

6.3 Summary and Conclusion of Chapter 6

Simulated electric field and energy density couplings between the receiver and the transmitter regions for a number of frequencies between 1 kHz and 9 GHz are obtained in this chapter. Simulated input reflection coefficient (S_{11}) is shown for frequencies between 1 kHz and 9 GHz. It was observed that values for S_{11} were insensitive to small variations in the values for σ and ε_r. Perhaps a significant contribution to S_{11} may arise from reflection at port 1 and port 2 and not due to reflections in the multilayered media at frequencies upto 30 MHz. At resonance due to the transmitter-receiver geometry, S_{11} increases to unity approximately at 1 GHz.

For a transmitter current density of 3.2×10^6 $A.m^{-2}$, induced current densities and power densities values in different layers are obtained. Relative current density plots were obtained for both circular and elliptical shaped cross-sections for the model. Different colors in different regions in the current density plot correspond to different magnitudes. These current density plots provide a qualitative interpretation of induced current densities in different layers of the simplified model.

CHAPTER 7

CONCLUSION AND SUGGESTIONS FOR FURTHER RESEARCH

7.1 Summary and Conclusions

Discussion on the different aspects of effects of EM radiation incident on a biological medium has been given in chapters 2, 3 and 4. Different EM phenomena such as absorption and reflection related to interaction of EM waves with a biological medium have been discussed and analytical expressions to measure them quantitatively are mentioned. Some of the existing works on similar topics in the literature are visited and their important results highlighted. Analytical discussions are substantiated with simulated results. A simplified model for the implanted receiver coupled to an external transmitter is presented in section 5.1 and goal for that model is explained in section 5.2. Main motivation here is to estimate the losses associated with transmission of EM power through a biological medium by solving Maxwell's equations directly which will ensure all related EM phenomena being accounted for. A Full Wave 3D field solver [19] is used to simulate E field distribution in a simplified model. The results will be useful to estimate losses encountered in transmitting EM power through a multilayered biological medium with different cross-sections.

One of the contributions of this work is that it shows how frequency affects transmission of EM energy to a coupled receiver implanted in a multilayered biological medium approximating a human body. Coupling between a receiver and a transmitter should increase with frequency. Simulation results for the simplified model show that energy coupling remains almost the same with a value near 0.01 in the frequency range

between 1 kHz and 500 MHz. One of the reasons for this may be increase in absorption of EM energy by the different layers in the model till the frequency is high enough to cause substantial attenuation. With increase in frequency, E or H field magnitude available at a depth inside a biological medium goes on decreasing due to attenuation. At the resonance frequency of approximately 1 GHz due to the receiver–transmitter geometry, coupling is nearly one and after that it starts decreasing. One of the reasons for decrease in coupling at frequencies higher than 1 GHz is possibly due to the fact that E or H field gets highly attenuated for frequencies approximately above 1 GHz. The coupling results indicate no preferential frequency for the simplified model for an implanted receiver coupled to an external transmitter. Any frequency in the range between 1 kHz and 100 MHz can be taken, as coupling is nearly the same in this frequency range. Factors which may affect selection of a particular frequency include resonances of both the receiver and the transmitter which would result in minimum loss. Resonance due to receiver and transmitter geometry should however be avoided as it would result in practically no energy reception by the receiver. Any frequency may be selected between the range 1 kHz and 100 MHz with proper consideration of the factors mentioned above.

A second contribution of this work is that it describes different radiation related effects such as absorption and reflection of radiation by biological tissues. It discusses these effects in different mediums with different interfaces such as conductor – dielectric interface and dielectric – dielectric interface. Quantitative results are summarized. Similar technique can be applied to other biological mediums with different shapes.

A third contribution of this work is to find out the limiting current density in the transmitter coil which can cause EM radiation related hazards to a human body due to

thermal effects. Simulated results show that for a secondary coil current of 100 mA, induced currents in different layers of the simplified model are 2 to 3 orders of magnitude lower than the safe limit current density of 30 $A.m^{-2}$ from heating consideration. It can be shown from the data shown in Fig. 6.8 and the formula presented in section 6.2.3 that only for a current density of 10^{+9} $A.m^{-2}$ in the Cu transmitter if frequency of operation is above 100 MHz, current density in the stomach region crosses over the safe limit Such high current densities in Cu transmitter are not practical implying damage due to heating will be small or negligible in the biological medium for realistic cases. Lowering frequency of transmission or current density of the transmitter results in lower values of induced current densities.

7.2 Suggestions for Future Research

Model used for the human body in this thesis is overly simplified. A very high value for skin thickness of 1 cm was used. Because of this, above 10 GHz no coupling between the transmitter and the receiver could be obtained as E or H field gets almost totally attenuated above 10 GHz inside the tissue layers. Skin layer of realistic dimension must be used in future work. Annular regular shapes are assumed for all three layers namely skin, fat and stomach in the human body model. Realistic shapes for these layers more appropriate for a human body should be defined to yield more realistic simulation results. The model dimensions in the z direction should be modified for more accurate modeling of a human body. One of the drawbacks of the simplified model is that there is no air layer defined between the Cu transmitter and the skin. A very thin air gap can be defined between the transmitter and the skin layer to make the model more realistic. Also for a more realistic modeling of the receiver described in section 5.1, receiver is needed to be

placed outside the stomach region. Some other EM 3D field solver where a current can be applied between the two ports of the transmitter Cu conductor should be used, as that kind of excitation would be more applicable for finding power coupling from a transmitter coil outside the body to a receiver coil implanted within the body. This work can also be used as a verification of the excitation method applied here. Instead of a solid cube receiver, a single turn of a receiver coil can be defined and H field should be obtained at the receiver to get the current or voltage coupling. One of the other areas where substantial amount of research is required is in finding a safe limit of induced currents for a human body. For verification of the simulation results, experiments can be conducted on a human body model with the implanted receiver coupled to an external transmitter. For improving accuracy of simulation, smaller mesh sizes can be defined.

REFERENCES

[1] J. A. Von Arx, "A Fully Integrated Neuromuscular Stimulation System-FINESS," Doctoral dissertation submitted to University of Michigan, Ann Arbor, 1998.

[2] H. P. Schwan, "Interaction of Microwave and Radio Frequency Radiation with Biological Systems," IEEE Trans. Microwave Theory Tech., vol. MTT-19, March 1971, pp.146-152.

[3] Arthur W. Guy, "Electromagnetic Fields and Relative Heating Patterns Due to a Rectangular Aperture Source in Direct Contact with Bilayered Biological Tissue," IEEE Trans. Microwave Theory Tech., vol. MTT-19, March 1971, pp. 214-223.

[4] H. P. Schawn and Geo. Morris Piersol, "The Absorption of Electromagnetic Energy in Body Tissues," in Biological Effects of Electromagnetic Radiation, IEEE Press , 1983, pp. 6-21

[5] Curtis C. Johnson and Arthur W. guy, "Nonionizing Electromagnetic Wave Effects in Biological Materials and systems," in Biological Effects of Electromagnetic Radiation, IEEE Press, 1983, pp. 47-73.

[6] O. P. Gandhi, "State of the Knowledge for Electromagnetic Absorbed Dose in Man and Animals," in Biological Effects of Electromagnetic Radiation, IEEE Press , 1983, pp. 91-99.

[7] A. von Hippel, "Dielectrics and Waves," John Wiley & Sons, Inc., New York, 1954, pp. 19-40.

[8] S. J. Allen, W. D. Hurt, J. H. Krupp, and J. A. Ratliff, "Measurement of radio frequency power absorption in monkeys, monkey phantoms, and human phantoms exposed to 10-50 MHz fields," in Biological Effects of Electromagnetic Waves , selected papers of the USNC/URSI annual meeting, 1975, vol. 2 , pp. 83-95.

[9] H. Massoudi, Carl H. Durney, and Curtis C. Johnson, "Theoretical calculations of power absorbed by monkey and human prolate spheroidal phantoms in an irradiation chamber," in Biological Effects of Electromagnetic Waves , selected papers of the USNC/URSI annual meeting, 1975, vol. 2 , pp. 135 – 157.

[10] S. M. Neuder, R. B. Kellog and D. H. Hill, "Microwave power density absorption in a spherical multilayered model of the head," in Biological Effects of Electromagnetic Waves , selected papers of the USNC/URSI annual meeting, 1975, vol. 2 , pp.199-210.

[11] J. Jianming, "Finite element method in electromagnetics," John Wiley & Sons, Inc., New York, 2002.

[12] W. W. Mumford, "Some technical aspects of microwave radiation hazards," in Biological Effects of Electromagnetic Radiation, IEEE Press, 1983, pp. 455-475.

[13] J. A. Stratton, "Electromagnetic theory," Mcgraw-Hill book company, New York, 1941.

[14] T. H. Lee, "Design of CMOS Radio-Frequency Integrated Circuits," Cambridge University Press, 1998.

[15] P. Lacomme, J.C. Marchais, J.P, "Air and Spaceborne Radar Systems," Institution of Electrical Engineers, U.K., 2001.

[16] C. Gabriel and S. Gabriel, "Compilation of the Dielectric Properties of Body Tissues at RF and Microwave Frequencies," Physics Dept., King's College London.

[17] A. F. Emrey, R. E. Short, A. W. guy, K. K. Kraning, " The numerical thermal simulation of the human body when absorbing non-ionizing microwave irradiation with emphasis on the effect of different sweat models," in Biological Effects of Electromagnetic Waves , selected papers of the USNC/URSI annual meeting, 1975, vol. 2 , pp. 96-117.

[18] P. W. Barber, O. P. Gandhi, M. J. Hagmann, and I. Chatterjee, "Electromagnetic absorption in a multilayered model for man," IEEE Trans. Biomed. Engg. vol. BME-26, pp. 400-405, 1979.

[19] Full-Wave 3D EM field solver, proprietary software.

[20] J. D. Irwin, "Basic Engineering Circuit Analysis," MacMillan, NY, 3rd edition, 1989, pp. 475.

APPENDIX A

A SAMPLE *PROBLEM_EFEM* FILE

```
GENERAL

lengthUnit = 1.e-2
problem = 1

FREQUENCY

freqUnit = 1.e+6
freqStart = 8
freqEnd = 8
nfreq = 1
fastFreqSweep = 0

DIELECTRIC_STACK    // Here different propertied of the three different

numStacks = 3         // layers are specified
thickStacks = 4 2 8
epsilonStacks = 2 2 2
dielLossInput = 1        //  When this is selected as one , then loss
dielLossStacks = 0.0 0.001  0.0  // is given as  conductivity.


In the following section all describes conductors and ports and  are
defined as quadrilateral with the four points described in
anticlockwise order. Each one of them is described as:
No of points   all the points ( x,y)   conductivity   relative
permittivity  layer_no


PORT

numPorts = 2
infoPort1 = 21.2073276361216 23.697143620441 0 5   6.66e+7 2 0 1
infoPort2 = 28.6988041435457 31.131849359382 0 5  6.66e+7 2 1 2
excitPort = 1

BOUNDARY CONDITION

boundConditionTrans = 0 0 0 1
boundConditionBox = 1 0 1 1 1 1

NON-UNIFORM CONDUCTOR AND DIELECTRIC

//CONDUCTOR 0  TO 49 DESCRIBES THE OUTER ANNULAR CU CONDUCTOR


//CONDUCTOR 50 TO 99 DESCRIBES THE NEXT ANNULAR LAYER WHICH IS SKIN.
```

////CONDUCTOR 100 TO 149 DESCRIBES NEXT ANNULAR LAYER WHICH IS FAT

////CONDUCTOR 150 TO 199 DESCRIBES THE NEXT ANNULAR REGION WITH WIDTH 8 CM WHICH IS GEVEN THE PROPERTIES OF STOMACH .

// CONDUCTOR 200 AND 201 DEFINES THE TWO RECTANGULAR CU CONDUCTORS WHERE THE PORTS ARE BENG DEFINED . CONDUCTOR 202 DESCRIBES THE DIELECTRIC REGION BETWEEN THE PORTS AND CONDUCTOR 203 DEFINES THE INNER CUBIC RECEIVER.

```
numConductor = 202
infoConductor0  =  4  44  25  45  25  44.8424536759642  26.8790504426259
43.850330992166 26.7537804131175 6.66e+7 1  2
infoConductor1  =  4  43.850330992166  26.7537804131175  44.8424536759642
26.8790504426259   44.3722967882786   28.7284971362605   43.4036819488647
28.4799306605098 6.66e+7 1  2
infoConductor2  =  4  43.4036819488647  28.4799306605098  44.3722967882786
28.7284971362605   43.5969364858807   30.5192027280955   42.6670896615867
30.1512558795558 6.66e+7 1  2
infoConductor3  =  4  42.6670896615867  30.1512558795558  43.5969364858807
30.5192027280955   42.5285882853151   32.2229553097885   41.6521588710493
31.7414249558026 6.66e+7 1  2
infoConductor4  =  4  41.6521588710493  31.7414249558026  42.5285882853151
32.2229553097885   41.1840836197606   33.8129128857084   40.3748794387726
33.2253853599945 6.66e+7 1  2
infoConductor5  =  4  40.3748794387726  33.2253853599945  41.1840836197606
33.8129128857084   39.5846046659881   35.2640262587091   38.8553744326887
34.5797578414619 6.66e+7 1  2
infoConductor6  =  4  38.8553744326887  34.5797578414619  39.5846046659881
35.2640262587091   37.7553506269515   36.5534336710233   37.1175830956039
35.7832047596217 6.66e+7 1  2
infoConductor7  =  4  37.1175830956039  35.7832047596217  37.7553506269515
36.5534336710233   35.7251407276085   37.6608209828513   35.1888836912281
36.8167662506613 6.66e+7 1  2
infoConductor8  =  4  35.1888836912281  36.8167662506613  35.7251407276085
37.6608209828513   33.5259601786254   38.5687417141671   33.0996621696941
37.6641589332226 6.66e+7 1  2
infoConductor9  =  4  33.0996621696941  37.6641589332226  33.5259601786254
38.5687417141671   31.1924562611405   39.2628919075971   30.8828334480835
38.3120324470906 6.66e+7 1  2
infoConductor10  =  4  30.8828334480835  38.3120324470906  31.1924562611405
39.2628919075971   28.7613924715861   39.7323354820109   28.5733228480068
38.7501797832101 6.66e+7 1  2
infoConductor11  =  4  28.5733228480068  38.7501797832101  28.7613924715861
39.7323354820109   26.2710693263163   39.9696765264594   26.2075158600005
38.9716980913621 6.66e+7 1  2
infoConductor12  =  4  26.2075158600005  38.9716980913621  26.2710693263163
39.9696765264594   23.7607209510509   39.9711758200331   23.8226849034984
38.9730974320309 6.66e+7 1  2
infoConductor13  =  4  23.8226849034984  38.9730974320309  23.7607209510509
39.9711758200331   21.2698969616472   39.7368097419129   21.4564021135648
38.7543557591187 6.66e+7 1  2
infoConductor14  =  4  21.4564021135648  38.7543557591187  21.2698969616472
39.7368097419129   18.8378393744401   39.2702706435074   19.1459474057181
38.3189192672736 6.66e+7 1  2
```

```
infoConductor15 = 4 19.1459474057181 38.3189192672736 18.8378393744401
39.2702706435074 16.5028643627006 38.5789086768139 16.9277211445656
37.6736480983596 6.66e+7 1 2
infoConductor16 = 4 16.9277211445656 37.6736480983596 16.5028643627006
38.5789086768139 14.3017585994101 37.6736159954754 14.8366706694396
36.8287082624437 6.66e+7 1 2
infoConductor17 = 4 14.8366706694396 36.8287082624437 14.3017585994101
37.6736159954754 12.2691996967506 36.5686551529042 12.905739711913
35.7974114760439 6.66e+7 1 2
infoConductor18 = 4 12.905739711913 35.7974114760439 12.2691996967506
36.5686551529042 10.4372098730721 35.2814344009951 11.1653493794185
34.5960054409288 6.66e+7 1 2
infoConductor19 = 4 11.1653493794185 34.5960054409288 10.4372098730721
35.2814344009951 8.83465145461379 33.8322334295169 9.6429188818831
33.2434178675491 6.66e+7 1 2
infoConductor20 = 4 9.6429188818831 33.2434178675491 8.83465145461379
33.8322334295169 7.48677216016377 32.2438838670541 8.36243355215558
31.7609582759172 6.66e+7 1 2
infoConductor21 = 4 8.36243355215558 31.7609582759172 7.48677216016377
32.2438838670541 6.41480733253045 30.5414095770916 7.34406696590393
30.1719822719522 6.66e+7 1 2
infoConductor22 = 4 7.34406696590393 30.1719822719522 6.41480733253045
30.5414095770916 5.63564538352278 28.7516324162444 6.60386311434664
28.5015235884948 6.66e+7 1 2
infoConductor23 = 4 6.60386311434664 28.5015235884948 5.63564538352278
28.7516324162444 5.16156172323021 26.902749665766 6.1534836370687
26.7758996880482 6.66e+7 1 2
infoConductor24 = 4 6.1534836370687 26.7758996880482 5.16156172323021
26.902749665766 5.00002536544921 25.0238897937473 6.00002409717675
25.0222971408308 6.66e+7 1 2
infoConductor25 = 4 6.00002409717675 25.0222971408308 5.00002536544921
25.0238897937473 5.15358125611642 23.14465354681 6.1459021933106
23.268343310356 6.66e+7 1 2
infoConductor26 = 4 6.1459021933106 23.268343310356 5.15358125611642
23.14465354681 5.61981017862097 21.2946476012239 6.58881966968993
21.5416710944757 6.66e+7 1 2
infoConductor27 = 4 6.58881966968993 21.5416710944757 5.61981017862097
21.2946476012239 6.3913668676729 19.5030181206063 7.32179852428926
19.8694835792325 6.66e+7 1 2
infoConductor28 = 4 7.32179852428926 19.8694835792325 6.3913668676729
19.5030181206063 7.45609573125767 17.7979915688277 8.33329094469479
18.2781254642391 6.66e+7 1 2
infoConductor29 = 4 8.33329094469479 18.2781254642391 7.45609573125767
17.7979915688277 8.79722235752002 16.2064300124496 9.60736123964402
16.7926680116196 6.66e+7 1 2
infoConductor30 = 4 9.60736123964402 16.7926680116196 8.79722235752002
16.2064300124496 10.3936177894565 14.7534079187405 11.1239368999837
15.4365140574911 6.66e+7 1 2
infoConductor31 = 4 11.1239368999837 15.4365140574911 10.3936177894565
14.7534079187405 12.2201314038663 13.4618171166611 12.859124833673
14.2310293088837 6.66e+7 1 2
infoConductor32 = 4 12.859124833673 14.2310293088837 12.2201314038663
13.4618171166611 14.2479871501742 12.3520061445139 14.7855877926655
13.1952057348796 6.66e+7 1 2
infoConductor33 = 4 14.7855877926655 13.1952057348796 14.2479871501742
12.3520061445139 16.4452369065296 11.4414596662026 16.8729750612031
12.3453623551224 6.66e+7 1 2
```

```
infoConductor34 = 4 16.8729750612031 12.3453623551224 16.4452369065296
11.4414596662026 18.7772638107224 10.7445230067794 19.0884006201863
11.6948881396607 6.66e+7 1 2
infoConductor35 = 4 19.0884006201863 11.6948881396607 18.7772638107224
10.7445230067794 21.2073276361216 10.272176147122 21.3969612543155
11.2540310706472 6.66e+7 1 2
infoConductor36 = 4 21.3969612543155 11.2540310706472 21.2073276361216
10.272176147122 23.697143620441 10.0318607383713 23.7622864394189
11.0297366891465 6.66e+7 1 2
infoConductor39 = 4 28.5138639363684 11.2415031535139 28.6988041435457
10.2587533787649 31.131849359382 10.7223868177647 30.8252568914129
11.6742276965804 6.66e+7 1 2


infoConductor40 = 4 30.8252568914129 11.6742276965804 31.131849359382
10.7223868177647 33.4682895426071 11.4109588040511 33.0448750654768
12.316894883781 6.66e+7 1 2
infoConductor41 = 4 33.0448750654768 12.316894883781 33.4682895426071
11.4109588040511 35.6713149370015 12.3136211390968 35.1377491901514
13.1593797298236 6.66e+7 1 2
infoConductor42 = 4 35.1377491901514 13.1593797298236 35.6713149370015
12.3136211390968 37.7062176873006 13.4161527096284 37.0709068029355
14.1884091956532 6.66e+7 1 2
infoConductor43 = 4 37.0709068029355 14.1884091956532 37.7062176873006
13.4161527096284 39.5409386486964 14.7011835360391 38.8138917162616
15.3877713003032 6.66e+7 1 2
infoConductor44 = 4 38.8138917162616 15.3877713003032 39.5409386486964
14.7011835360391 41.146572466879 16.1484684300314 40.3392438435351
16.738570534696 6.66e+7 1 2
infoConductor45 = 4 40.3392438435351 16.738570534696 41.146572466879
16.1484684300314 42.4978229712683 17.7352059501172 41.6229318227048
18.2195255534427 6.66e+7 1 2
infoConductor46 = 4 41.6229318227048 18.2195255534427 42.4978229712683
17.7352059501172 43.5734017068823 19.4363976299465 42.6447316215382
19.8073044546168 6.66e+7 1 2
infoConductor47 = 4 42.6447316215382 19.8073044546168 43.5734017068823
19.4363976299465 44.3563633261205 21.2252418199558 43.3885451598144
21.4768923652921 6.66e+7 1 2
infoConductor48 = 4 43.3885451598144 21.4768923652921 44.3563633261205
21.2252418199558 44.8343725564855 23.073555937504 43.8426539286612
23.2019855416704 6.66e+7 1 2
infoConductor49 = 4 43.8426539286612 23.2019855416704 44.8343725564855
23.073555937504 45 25 44 25 6.66e+7 1 2
infoConductor50 = 4 42 25 44 25 43.850330992166 26.7537804131175
41.8660856245696 26.5032403541007 2.89e-2 701 2
infoConductor51 = 4 41.8660856245696 26.5032403541007 43.850330992166
26.7537804131175 43.4036819488647 28.4799306605098 41.4664522700368
27.9827977090084 2.89e-2 701 2
infoConductor52 = 4 41.4664522700368 27.9827977090084 43.4036819488647
28.4799306605098 42.6670896615867 30.1512558795558 40.8073960129986
29.4153621824764 2.89e-2 701 2
infoConductor53 = 4 40.8073960129986 29.4153621824764 42.6670896615867
30.1512558795558 41.6521588710493 31.7414249558026 39.8993000425178
30.7783642478308 2.89e-2 701 2
infoConductor54 = 4 39.8993000425178 30.7783642478308 41.6521588710493
31.7414249558026 40.3748794387726 33.2253853599945 38.7564710767966
32.0503303085667 2.89e-2 701 2
```

```
infoConductor55 = 4 38.7564710767966 32.0503303085667 40.3748794387726
33.2253853599945 38.8553744326887 34.5797578414619 37.3969139660899
33.2112210069673 2.89e-2 701 2
infoConductor56 = 4 37.3969139660899 33.2112210069673 38.8553744326887
34.5797578414619 37.1175830956039 35.7832047596217 35.8420480329088
34.2427469368186 2.89e-2 701 2
infoConductor57 = 4 35.8420480329088 34.2427469368186 37.1175830956039
35.7832047596217 35.1888836912281 36.8167662506613 34.1163696184672
35.1286567862811 2.89e-2 701 2
infoConductor58 = 4 34.1163696184672 35.1286567862811 35.1888836912281
36.8167662506613 33.0996621696941 37.6641589332226 32.2470661518316
35.8549933713337 2.89e-2 701 2
infoConductor59 = 4 32.2470661518316 35.8549933713337 33.0996621696941
37.6641589332226 30.8828334480835 38.3120324470906 30.2635878219694
36.4103135260776 2.89e-2 701 2
infoConductor60 = 4 30.2635878219694 36.4103135260776 30.8828334480835
38.3120324470906 28.5733228480068 38.7501797832101 28.1971836008482
36.7858683856087 2.89e-2 701 2
infoConductor61 = 4 28.1971836008482 36.7858683856087 28.5733228480068
38.7501797832101 26.2075158600005 38.9716980913621 26.0804089273688
36.9757412211675 2.89e-2 701 2
infoConductor62 = 4 26.0804089273688 36.9757412211675 26.2075158600005
38.9716980913621 23.8226849034984 38.9730974320309 23.9466128083933
36.9769406560265 2.89e-2 701 2
infoConductor63 = 4 23.9466128083933 36.9769406560265 23.8226849034984
38.9730974320309 21.4564021135648 38.7543557591187 21.8294124174001
36.7894477935303 2.89e-2 701 2
infoConductor64 = 4 21.8294124174001 36.7894477935303 21.4564021135648
38.7543557591187 19.1459474057181 38.3189192672736 19.7621634682741
36.4162165148059 2.89e-2 701 2
infoConductor65 = 4 19.7621634682741 36.4162165148059 19.1459474057181
38.3189192672736 16.9277211445656 37.6736480983596 17.7774347082955
35.8631269414511 2.89e-2 701 2
infoConductor66 = 4 17.7774347082955 35.8631269414511 16.9277211445656
37.6736480983596 14.8366706694396 36.8287082624437 15.9064948094986
35.1388927963803 2.89e-2 701 2
infoConductor67 = 4 15.9064948094986 35.1388927963803 14.8366706694396
36.8287082624437 12.905739711913 35.7974114760439 14.178819742238
34.2549241223233 2.89e-2 701 2
infoConductor68 = 4 14.178819742238 34.2549241223233 12.905739711913
35.7974114760439 11.1653493794185 34.5960054409288 12.6216283921113
33.2251475207961 2.89e-2 701 2
infoConductor69 = 4 12.6216283921113 33.2251475207961 11.1653493794185
34.5960054409288 9.6429188818831 33.2434178675491 11.2594537364217
32.0657867436135 2.89e-2 701 2
infoConductor70 = 4 11.2594537364217 32.0657867436135 9.6429188818831
33.2434178675491 8.36243355215558 31.7609582759172 10.1137563361392
30.7951070936433 2.89e-2 701 2
infoConductor71 = 4 10.1137563361392 30.7951070936433 8.36243355215558
31.7609582759172 7.34406696590393 30.1719822719522 9.20258623265089
29.4331276616733 2.89e-2 701 2
infoConductor72 = 4 9.20258623265089 29.4331276616733 7.34406696590393
30.1719822719522 6.60386311434664 28.5015235884948 8.54029857599436
28.0013059329955 2.89e-2 701 2
infoConductor73 = 4 8.54029857599436 28.0013059329955 6.60386311434664
28.5015235884948 6.1534836370687 26.7758996880482 8.13732746474568
26.5221997326128 2.89e-2 701 2
```

```
infoConductor74 = 4 8.13732746474568 26.5221997326128 6.1534836370687
26.7758996880482 6.00002409717675 25.0222971408308 8.00002156063183
25.0191118349978 2.89e-2 701 2
infoConductor75 = 4 8.00002156063183 25.0191118349978 6.00002409717675
25.0222971408308 6.1459021933106 23.268343310356 8.13054406769896
23.515722837448 2.89e-2 701 2
infoConductor76 = 4 8.13054406769896 23.515722837448 6.1459021933106
23.268343310356 6.58881966968993 21.5416710944757 8.52683865182783
22.0357180809791 2.89e-2 701 2
infoConductor77 = 4 8.52683865182783 22.0357180809791 6.58881966968993
21.5416710944757 7.32179852428926 19.8694835792325 9.18266183752197
20.602414496485 2.89e-2 701 2
infoConductor78 = 4 9.18266183752197 20.602414496485 7.32179852428926
19.8694835792325 8.33329094469479 18.2781254642391 10.087681371569
19.2383932550621 2.89e-2 701 2
infoConductor79 = 4 10.087681371569 19.2383932550621 8.33329094469479
18.2781254642391 9.60736123964402 16.7926680116196 11.227639003892
17.9651440099597 2.89e-2 701 2
infoConductor80 = 4 11.227639003892 17.9651440099597 9.60736123964402
16.7926680116196 11.1239368999837 15.4365140574911 12.5845751210381
16.8027263349924 2.89e-2 701 2
infoConductor81 = 4 12.5845751210381 16.8027263349924 11.1239368999837
15.4365140574911 12.859124833673 14.2310293088837 14.1371116932864
15.7694536933289 2.89e-2 701 2
infoConductor82 = 4 14.1371116932864 15.7694536933289 12.859124833673
14.2310293088837 14.7855877926655 13.1952057348796 15.8607890776481
14.8816049156111 2.89e-2 701 2
infoConductor83 = 4 15.8607890776481 14.8816049156111 14.7855877926655
13.1952057348796 16.8729750612031 12.3453623551224 17.7284513705502
14.1531677329621 2.89e-2 701 2
infoConductor84 = 4 17.7284513705502 14.1531677329621 16.8729750612031
12.3453623551224 19.0884006201863 11.6948881396607 19.710674239114
13.5956184054235 2.89e-2 701 2
infoConductor85 = 4 19.710674239114 13.5956184054235 19.0884006201863
11.6948881396607 21.3969612543155 11.2540310706472 21.7762284907034
13.2177409176976 2.89e-2 701 2
infoConductor86 = 4 21.7762284907034 13.2177409176976 21.3969612543155
11.2540310706472 23.7622864394189 11.0297366891465 23.8925720773748
13.025488590697 2.89e-2 701 2
infoConductor87 = 4 23.8925720773748 13.025488590697 23.7622864394189
11.0297366891465 26.1471113466902 11.0255386706896 26.0263627838807
13.0218902891625 2.89e-2 701 2
infoConductor88 = 4 26.0263627838807 13.0218902891625 26.1471113466902
11.0255386706896 28.5138639363684 11.2415031535139 28.1439835220138
13.2070027030119 2.89e-2 701 2
infoConductor89 = 4 28.1439835220138 13.2070027030119 28.5138639363684
11.2415031535139 30.8252568914129 11.6742276965804 30.2120719554747
13.5779094542118 2.89e-2 701 2
infoConductor90 = 4 30.2120719554747 13.5779094542118 30.8252568914129
11.6742276965804 33.0448750654768 12.316894883781 32.1980461112161
14.1287670432409 2.89e-2 701 2
infoConductor91 = 4 32.1980461112161 14.1287670432409 33.0448750654768
12.316894883781 35.1377491901514 13.1593797298236 34.0706176964513
14.8508969112774 2.89e-2 701 2
infoConductor92 = 4 34.0706176964513 14.8508969112774 35.1377491901514
13.1593797298236 37.0709068029355 14.1884091956532 35.8002850342055
15.7329221677028 2.89e-2 701 2
```

```
infoConductor93 = 4 35.8002850342055 15.7329221677028 37.0709068029355
14.1884091956532 38.8138917162616 15.3877713003032 37.3597978513919
16.7609468288313 2.89e-2 701 2
infoConductor94 = 4 37.3597978513919 16.7609468288313 38.8138917162616
15.3877713003032 40.3392438435351 16.738570534696 38.7245865968472
17.9187747440251 2.89e-2 701 2
infoConductor95 = 4 38.7245865968472 17.9187747440251 40.3392438435351
16.738570534696 41.6229318227048 18.2195255534427 39.873149525578
19.1881647600937 2.89e-2 701 2
infoConductor96 = 4 39.873149525578 19.1881647600937 41.6229318227048
18.2195255534427 42.6447316215382 19.8073044546168 40.78739145085
20.5491181039572 2.89e-2 701 2
infoConductor97 = 4 40.78739145085 20.5491181039572 42.6447316215382
19.8073044546168 43.3885451598144 21.4768923652921 41.4529088272024
21.9801934559646 2.89e-2 701 2
infoConductor98 = 4 41.4529088272024 21.9801934559646 43.3885451598144
21.4768923652921 43.8426539286612 23.2019855416704 41.8592166730127
23.4588447500032 2.89e-2 701 2
infoConductor99 = 4 41.8592166730127 23.4588447500032 43.8426539286612
23.2019855416704 44 25 42 25 2.89e-2 701 2

infoConductor100 = 4 40 25 42 25 41.8660856245696 26.5032403541007
39.8818402569732 26.2527002950839 0.0269 20.1 2
infoConductor101 = 4 39.8818402569732 26.2527002950839 41.8660856245696
26.5032403541007 41.4664522700368 27.9827977090084 39.529222591209
27.485664757507 0.0269 20.1 2
infoConductor102 = 4 39.529222591209 27.485664757507 41.4664522700368
27.9827977090084 40.8073960129986 29.4153621824764 38.9477023644105
28.679468485397 0.0269 20.1 2
infoConductor103 = 4 38.9477023644105 28.679468485397 40.8073960129986
29.4153621824764 39.8993000425178 30.7783642478308 38.1464412139863
29.815303539859 0.0269 20.1 2
infoConductor104 = 4 38.1464412139863 29.815303539859 39.8993000425178
30.7783642478308 38.7564710767966 32.0503303085667 37.1380627148205
30.8752752571389 0.0269 20.1 2
infoConductor105 = 4 37.1380627148205 30.8752752571389 38.7564710767966
32.0503303085667 37.3969139660899 33.2112210069673 35.9384534994911
31.8426841724728 0.0269 20.1 2
infoConductor106 = 4 35.9384534994911 31.8426841724728 37.3969139660899
33.2112210069673 35.8420480329088 34.2427469368186 34.5665129702136
32.7022891140155 0.0269 20.1 2
infoConductor107 = 4 34.5665129702136 32.7022891140155 35.8420480329088
34.2427469368186 34.1163696184672 35.1286567862811 33.0438555457064
33.4405473219009 0.0269 20.1 2
infoConductor108 = 4 33.0438555457064 33.4405473219009 34.1163696184672
35.1286567862811 32.2470661518316 35.8549933713337 31.394470133969
34.0458278094447 0.0269 20.1 2
infoConductor109 = 4 31.394470133969 34.0458278094447 32.2470661518316
35.8549933713337 30.2635878219694 36.4103135260776 29.6443421958554
34.5085946050647 0.0269 20.1 2
infoConductor110 = 4 29.6443421958554 34.5085946050647 30.2635878219694
36.4103135260776 28.1971836008482 36.7858683856087 27.8210443536896
34.8215569880072 0.0269 20.1 2
infoConductor111 = 4 27.8210443536896 34.8215569880072 28.1971836008482
36.7858683856087 26.0804089273688 36.9757412211675 25.9533019947372
34.9797843509729 0.0269 20.1 2
```

```
infoConductor112 = 4 25.9533019947372 34.9797843509729 26.0804089273688
36.9757412211675   23.9466128083933   36.9769406560265   24.0705407132882
34.9807838800221 0.0269 20.1  2
infoConductor113 = 4 24.0705407132882 34.9807838800221 23.9466128083933
36.9769406560265   21.8294124174001   36.7894477935303   22.2024227212354
34.824539827942 0.0269 20.1  2
infoConductor114 = 4 22.2024227212354 34.824539827942 21.8294124174001
36.7894477935303   19.7621634682741   36.4162165148059   20.3783795308301
34.5135137623383 0.0269 20.1  2
infoConductor115 = 4 20.3783795308301 34.5135137623383 19.7621634682741
36.4162165148059   17.7774347082955   35.8631269414511   18.6271482720255
34.0526057845426 0.0269 20.1  2
infoConductor116 = 4 18.6271482720255 34.0526057845426 17.7774347082955
35.8631269414511   15.9064948094986   35.1388927963803   16.9763189495576
33.449077330317 0.0269 20.1  2
infoConductor117 = 4 16.9763189495576 33.449077330317 15.9064948094986
35.1388927963803   14.178819742238   34.2549241223233   15.4518997725629
32.7124367686028 0.0269 20.1  2
infoConductor118 = 4 15.4518997725629 32.7124367686028 14.178819742238
34.2549241223233   12.6216283921113   33.2251475207961   14.0779074048041
31.8542896006634 0.0269 20.1  2
infoConductor119 = 4 14.0779074048041 31.8542896006634 12.6216283921113
33.2251475207961   11.2594537364217   32.0657867436135   12.8759885909603
30.8881556196779 0.0269 20.1  2
infoConductor120 = 4 12.8759885909603 30.8881556196779 11.2594537364217
32.0657867436135   10.1137563361392   30.7951070936433   11.8650791201228
29.8292559113694 0.0269 20.1  2
infoConductor121 = 4 11.8650791201228 29.8292559113694 10.1137563361392
30.7951070936433   9.20258623265089   29.4331276616733   11.0611054993978
28.6942730513944 0.0269 20.1  2
infoConductor122 = 4 11.0611054993978 28.6942730513944 9.20258623265089
29.4331276616733   8.54029857599436   28.0013059329955   10.4767340376421
27.5010882774963 0.0269 20.1  2
infoConductor123 = 4 10.4767340376421 27.5010882774963 8.54029857599436
28.0013059329955   8.13732746474568   26.5221997326128   10.1211712924227
26.2684997771773 0.0269 20.1  2
infoConductor124 = 4 10.1211712924227 26.2684997771773 8.13732746474568
26.5221997326128   8.00002156063183   25.0191118349978   10.0000190240869
25.0159265291649 0.0269 20.1  2
infoConductor125 = 4 10.0000190240869 25.0159265291649 8.00002156063183
25.0191118349978   8.13054406769896   23.515722837448   10.1151859420873
23.76310236454 0.0269 20.1  2
infoConductor126 = 4 10.1151859420873 23.76310236454 8.13054406769896
23.515722837448   8.52683865182783   22.0357180809791   10.4648576339657
22.5297650674826 0.0269 20.1  2
infoConductor127 = 4 10.4648576339657 22.5297650674826 8.52683865182783
22.0357180809791   9.18266183752197   20.602414496485   11.0435251507547
21.3353454137375 0.0269 20.1  2
infoConductor128 = 4 11.0435251507547 21.3353454137375 9.18266183752197
20.602414496485   10.087681371569   19.2383932550621   11.8420717984433
20.1986610458851 0.0269 20.1  2
infoConductor129 = 4 11.8420717984433 20.1986610458851 10.087681371569
19.2383932550621   11.227639003892   17.9651440099597   12.84791676814
19.1376200082997 0.0269 20.1  2
infoConductor130 = 4 12.84791676814 19.1376200082997 11.227639003892
17.9651440099597   12.5845751210381   16.8027263349924   14.0452133420924
18.1689386124937 0.0269 20.1  2
```

```
infoConductor131 = 4 14.0452133420924 18.1689386124937 12.5845751210381
16.8027263349924   14.1371116932864   15.7694536933289   15.4150985528997
17.307878077774 0.0269 20.1  2
infoConductor132 = 4 15.4150985528997 17.307878077774 14.1371116932864
15.7694536933289   15.8607890776481   14.8816049156111   16.9359903626307
16.5680040963426 0.0269 20.1  2
infoConductor133 = 4 16.9359903626307 16.5680040963426 15.8607890776481
14.8816049156111   17.7284513705502   14.1531677329621   18.5839276798972
15.9609731108017 0.0269 20.1  2
infoConductor134 = 4 18.5839276798972 15.9609731108017 17.7284513705502
14.1531677329621   19.710674239114   13.5956184054235   20.3329478580418
15.4963486711862 0.0269 20.1  2
infoConductor135 = 4 20.3329478580418 15.4963486711862 19.710674239114
13.5956184054235   21.7762284907034   13.2177409176976   22.1554957270912
15.181450764748 0.0269 20.1  2
infoConductor136 = 4 22.1554957270912 15.181450764748 21.7762284907034
13.2177409176976   23.8925720773748   13.025488590697   24.0228577153307
15.0212404922475 0.0269 20.1  2
infoConductor137 = 4 24.0228577153307 15.0212404922475 23.8925720773748
13.025488590697   26.0263627838807   13.0218902891625   25.9056142210712
15.0182419076354 0.0269 20.1  2
infoConductor138 = 4 25.9056142210712 15.0182419076354 26.0263627838807
13.0218902891625   28.1439835220138   13.2070027030119   27.7741031076592
15.1725022525099 0.0269 20.1  2
infoConductor139 = 4 27.7741031076592 15.1725022525099 28.1439835220138
13.2070027030119   30.2120719554747   13.5779094542118   29.5988870195365
15.4815912118431 0.0269 20.1  2
infoConductor140 = 4 29.5988870195365 15.4815912118431 30.2120719554747
13.5779094542118   32.1980461112161   14.1287670432409   31.3512171569554
15.9406392027007 0.0269 20.1  2
infoConductor141 = 4 31.3512171569554 15.9406392027007 32.1980461112161
14.1287670432409   34.0706176964513   14.8508969112774   33.0034862027511
16.5424140927312 0.0269 20.1  2
infoConductor142 = 4 33.0034862027511 16.5424140927312 34.0706176964513
14.8508969112774   35.8002850342055   15.7329221677028   34.5296632654754
17.2774351397523 0.0269 20.1  2
infoConductor143 = 4 34.5296632654754 17.2774351397523 35.8002850342055
15.7329221677028   37.3597978513919   16.7609468288313   35.9057039865223
18.1341223573594 0.0269 20.1  2
infoConductor144 = 4 35.9057039865223 18.1341223573594 37.3597978513919
16.7609468288313   38.7245865968472   17.9187747440251   37.1099293501593
19.0989789533543 0.0269 20.1  2
infoConductor145 = 4 37.1099293501593 19.0989789533543 38.7245865968472
17.9187747440251   39.873149525578   19.1881647600937   38.1233672284512
20.1568039667448 0.0269 20.1  2
infoConductor146 = 4 38.1233672284512 20.1568039667448 39.873149525578
19.1881647600937   40.78739145085   20.5491181039572   38.9300512801617
21.2909317532977 0.0269 20.1  2
infoConductor147 = 4 38.9300512801617 21.2909317532977 40.78739145085
20.5491181039572   41.4529088272024   21.9801934559646   39.5172724945903
22.4834945466372 0.0269 20.1  2
infoConductor148 = 4 39.5172724945903 22.4834945466372 41.4529088272024
21.9801934559646   41.8592166730127   23.4588447500032   39.8757794173641
23.715703958336 0.0269 20.1  2
infoConductor149 = 4 39.8757794173641 23.715703958336 41.8592166730127
23.4588447500032 42 25 40 25 0.0269 20.1  2
```

```
infoConductor150  =  4  32  25  40  25  39.8818402569732  26.2527002950839
31.9448587865875 25.3758100885252 0.8 150  2
infoConductor151 = 4 31.9448587865875 25.3758100885252 39.8818402569732
26.2527002950839   39.529222591209   27.485664757507   31.7803038758975
25.7456994272521 0.8 150  2
infoConductor152 = 4 31.7803038758975 25.7456994272521 39.529222591209
27.485664757507   38.9477023644105   28.679468485397   31.5089277700582
26.1038405456191 0.8 150  2
infoConductor153 = 4 31.5089277700582 26.1038405456191 38.9477023644105
28.679468485397   38.1464412139863   29.815303539859   31.1350058998603
26.4445910619577 0.8 150  2
infoConductor154 = 4 31.1350058998603 26.4445910619577 38.1464412139863
29.815303539859   37.1380627148205   30.8752752571389   30.6644292669162
26.7625825771417 0.8 150  2
infoConductor155 = 4 30.6644292669162 26.7625825771417 37.1380627148205
30.8752752571389   35.9384534994911   31.8426841724728   30.1046116330958
27.0528052517418 0.8 150  2
infoConductor156 = 4 30.1046116330958 27.0528052517418 35.9384534994911
31.8426841724728   34.5665129702136   32.7022891140155   29.464372719433
27.3106867342047 0.8 150  2
infoConductor157 = 4 29.464372719433 27.3106867342047 34.5665129702136
32.7022891140155   33.0438555457064   33.4405473219009   28.753799254663
27.5321641965703 0.8 150  2
infoConductor158 = 4 28.753799254663 27.5321641965703 33.0438555457064
33.4405473219009   31.394470133969   34.0458278094447   27.9840860625189
27.7137483428334 0.8 150  2
infoConductor159 = 4 27.9840860625189 27.7137483428334 31.394470133969
34.0458278094447   29.6443421958554   34.5085946050647   27.1673596913992
27.8525783815194 0.8 150  2
infoConductor160 = 4 27.1673596913992 27.8525783815194 29.6443421958554
34.5085946050647   27.8210443536896   34.8215569880072   26.3164873650551
27.9464670964022 0.8 150  2
infoConductor161 = 4 26.3164873650551 27.9464670964022 27.8210443536896
34.8215569880072   25.9533019947372   34.9797843509729   25.4448742642107
27.9939353052919 0.8 150  2
infoConductor162 = 4 25.4448742642107 27.9939353052919 25.9533019947372
34.9797843509729   24.0705407132882   34.9807838800221   24.5662523328678
27.9942351640066 0.8 150  2
infoConductor163 = 4 24.5662523328678 27.9942351640066 24.0705407132882
34.9807838800221   22.2024227212354   34.824539827942   23.6944639365765
27.9473619483826 0.8 150  2
infoConductor164 = 4 23.6944639365765 27.9473619483826 22.2024227212354
34.824539827942   20.3783795308301   34.5135137623383   22.843243781054
27.8540541287015 0.8 150  2
infoConductor165 = 4 22.843243781054 27.8540541287015 20.3783795308301
34.5135137623383   18.6271482720255   34.0526057845426   22.0260025269452
27.7157817353628 0.8 150  2
infoConductor166 = 4 22.0260025269452 27.7157817353628 18.6271482720255
34.0526057845426   16.9763189495576   33.449077330317   21.2556155097935
27.5347231990951 0.8 150  2
infoConductor167 = 4 21.2556155097935 27.5347231990951 16.9763189495576
33.449077330317   15.4518997725629   32.7124367686028   20.5442198938627
27.3137310305808 0.8 150  2
infoConductor168 = 4 20.5442198938627 27.3137310305808 15.4518997725629
32.7124367686028   14.0779074048041   31.8542896006634   19.9030234555752
27.056286880199 0.8 150  2
```

```
infoConductor169 = 4 19.9030234555752 27.056286880199 14.0779074048041
31.8542896006634  12.8759885909603  30.8881556196779  19.3421280091148
26.7664466859034 0.8 150 2
infoConductor170 = 4 19.3421280091148 26.7664466859034 12.8759885909603
30.8881556196779  11.8650791201228  29.8292559113694  18.8703702560573
26.4487767734108 0.8 150 2
infoConductor171 = 4 18.8703702560573 26.4487767734108 11.8650791201228
29.8292559113694  11.0611054993978  28.6942730513944  18.4951825663857
26.1082819154183 0.8 150 2
infoConductor172 = 4 18.4951825663857 26.1082819154183 11.0611054993978
28.6942730513944  10.4767340376421  27.5010882774963  18.222475884233
25.7503264832489 0.8 150 2
infoConductor173 = 4 18.222475884233 25.7503264832489 10.4767340376421
27.5010882774963  10.1211712924227  26.2684997771773  18.0565466031306
25.3805499331532 0.8 150 2
infoConductor174 = 4 18.0565466031306 25.3805499331532 10.1211712924227
26.2684997771773  10.0000190240869  25.0159265291649  18.0000088779072
25.0047779587495 0.8 150 2
infoConductor175 = 4 18.0000088779072 25.0047779587495 10.0000190240869
25.0159265291649  10.1151859420873  23.76310236454  18.0537534396407
24.628930709362 0.8 150 2
infoConductor176 = 4 18.0537534396407 24.628930709362 10.1151859420873
23.76310236454  10.4648576339657  22.5297650674826  18.2169335625173
24.2589295202448 0.8 150 2
infoConductor177 = 4 18.2169335625173 24.2589295202448 10.4648576339657
22.5297650674826  11.0435251507547  21.3353454137375  18.4869784036855
23.9006036241213 0.8 150 2
infoConductor178 = 4 18.4869784036855 23.9006036241213 11.0435251507547
21.3353454137375  11.8420717984433  20.1986610458851  18.8596335059402
23.5595983137655 0.8 150 2
infoConductor179 = 4 18.8596335059402 23.5595983137655 11.8420717984433
20.1986610458851  12.84791676814  19.1376200082997  19.329027825132
23.2412860024899 0.8 150 2
infoConductor180 = 4 19.329027825132 23.2412860024899 12.84791676814
19.1376200082997  14.0452133420924  18.1689386124937  19.8877662263098
22.9506815837481 0.8 150 2
infoConductor181 = 4 19.8877662263098 22.9506815837481 14.0452133420924
18.1689386124937  15.4150985528997  17.307878077774  20.5270459913532
22.6923634233322 0.8 150 2
infoConductor182 = 4 20.5270459913532 22.6923634233322 15.4150985528997
17.307878077774  16.9359903626307  16.5680040963426  21.236795502561
22.4704012289028 0.8 150 2
infoConductor183 = 4 21.236795502561 22.4704012289028 16.9359903626307
16.5680040963426  18.5839276798972  15.9609731108017  22.0058329172854
22.2882919332405 0.8 150 2
infoConductor184 = 4 22.0058329172854 22.2882919332405 18.5839276798972
15.9609731108017  20.3329478580418  15.4963486711862  22.8220423337528
22.1489046013559 0.8 150 2
infoConductor185 = 4 22.8220423337528 22.1489046013559 20.3329478580418
15.4963486711862  22.1554957270912  15.181450764748  23.6725646726426
22.0544352294244 0.8 150 2
infoConductor186 = 4 23.6725646726426 22.0544352294244 22.1554957270912
15.181450764748  24.0228577153307  15.0212404922475  24.5440002671543
22.0063721476743 0.8 150 2
infoConductor187 = 4 24.5440002671543 22.0063721476743 24.0228577153307
15.0212404922475  25.9056142210712  15.0182419076354  25.4226199698332
22.0054725722906 0.8 150 2
```

```
infoConductor188 = 4 25.4226199698332 22.0054725722906 25.9056142210712
15.0182419076354   27.7741031076592   15.1725022525099   26.294581450241
22.051750675753 0.8 150  2
infoConductor189  =  4  26.294581450241  22.051750675753  27.7741031076592
15.1725022525099   29.5988870195365   15.4815912118431   27.1461472757837
22.1444773635529 0.8 150  2
infoConductor190 = 4 27.1461472757837 22.1444773635529 29.5988870195365
15.4815912118431   31.3512171569554   15.9406392027007   27.9639013399125
22.2821917608102 0.8 150  2
infoConductor191 = 4 27.9639013399125 22.2821917608102 31.3512171569554
15.9406392027007   33.0034862027511   16.5424140927312   28.7349602279505
22.4627242278194 0.8 150  2
infoConductor192 = 4 28.7349602279505 22.4627242278194 33.0034862027511
16.5424140927312   34.5296632654754   17.2774351397523   29.4471761905552
22.6832305419257 0.8 150  2
infoConductor193 = 4 29.4471761905552 22.6832305419257 34.5296632654754
17.2774351397523   35.9057039865223   18.1341223573594   30.0893285270437
22.9402367072078 0.8 150  2
infoConductor194 = 4 30.0893285270437 22.9402367072078 35.9057039865223
18.1341223573594   37.1099293501593   19.0989789533543   30.6513003634077
23.2296936860063 0.8 150  2
infoConductor195 = 4 30.6513003634077 23.2296936860063 37.1099293501593
19.0989789533543   38.1233672284512   20.1568039667448   31.1242380399439
23.5470411900234 0.8 150  2
infoConductor196 = 4 31.1242380399439 23.5470411900234 38.1233672284512
20.1568039667448   38.9300512801617   21.2909317532977   31.5006905974088
23.8872795259893 0.8 150  2
infoConductor197 = 4 31.5006905974088 23.8872795259893 38.9300512801617
21.2909317532977   39.5172724945903   22.4834945466372   31.7747271641422
24.2450483639912 0.8 150  2
infoConductor198 = 4 31.7747271641422 24.2450483639912 39.5172724945903
22.4834945466372   39.8757794173641   23.715703958336   31.9420303947699
24.6147111875008 0.8 150  2
infoConductor199 = 4 31.9420303947699 24.6147111875008 39.8757794173641
23.715703958336 40 25 32 25 0.8 150  2
infoConductor200  =  4  21.20  10.031  21.20  0  23.697  0  23.697  10.031
6.66e+7 1 2
infoConductor201  =  4  28.698  10.25  28.698  0  31.131  0  31.131  10.722
6.66e+7 1 2
infoConductor202 = 4 23.697 10.031 23.697 0 28.698 0 28.698 10.25 0 1 2
infoConductor203 = 4 25 25 25 24 26 24 26 25 6.66e+7 1 2
```

APPENDIX B

A SAMPLE *PROBLEM.G* FILE

```
222
 0  0 0 5.0
 1  21.2073276361216 0 1.0
 2  23.697143620441  0 1.0
 3   28.6988041435457 0 1.0
 4   31.131849359382  0 1.0
 5   48 0 5.0
 6   48 45  5.0
 7   0  45 5.0
 8  45  25 0.5
 9  44.8424536759642  26.8790504426259 0.5
 10  44.3722967882786  28.7284971362605 0.5
 11  43.5969364858807  30.5192027280955 0.5
 12  42.5285882853151  32.2229553097885 0.5
 13  41.1840836197606  33.8129128857084 0.5
 14  39.5846046659881  35.2640262587091 0.5
 15  37.7553506269515  36.5534336710233 0.5
 16  35.7251407276085  37.6608209828513 0.5
 17  33.5259601786254  38.5687417141671 0.5
 18  31.1924562611405  39.2628919075971 0.5
 19  28.7613924715861  39.7323354820109 0.5
 20  26.2710693263163  39.9696765264594 0.5
 21  23.7607209510509  39.9711758200331 0.5
 22  21.2698969616472  39.7368097419129 0.5
 23  18.8378393744401  39.2702706435074 0.5
 24  16.5028643627006  38.5789086768139 0.5
 25  14.3017585994101  37.6736159954754 0.5
 26  12.2691996967506  36.5686551529042 0.5
 27  10.4372098730721  35.2814344009951 0.5
 28  8.83465145461379  33.8322334295169 0.5
 29  7.48677216016377  32.2438838670541 0.5
 30  6.41480733253045  30.5414095770916 0.5
 31  5.63564538352278  28.7516324162444 0.5
 32  5.16156172323021  26.902749665766 0.5
 33  5.00002536544921  25.0238897937473 0.5
 34  5.15358125611642  23.14465354681 0.5
 35  5.61981017862097  21.2946476012239 0.5
 36  6.3913668676729  19.5030181206063 0.5
 37  7.45609573125767  17.7979915688277 0.5
 38  8.79722235752002  16.2064300124496 0.5
 39  10.3936177894565  14.7534079187405 0.5
 40  12.2201314038663  13.4618171166611 0.5
 41  14.2479871501742  12.3520061445139 0.5
 42  16.4452369065296  11.4414596662026 0.5
 43  18.7772638107224  10.7445230067794 0.5
 44  21.2073276361216  10.272176147122 0.5
 45  23.697143620441  10.0318607383713 0.5
 46  26.2074856280949  10.0273628614531 0.5
 47  28.6988041435457  10.2587533787649 0.5
 48  31.131849359382  10.7223868177647 0.5
 49  33.4682895426071  11.4109588040511 0.5
```

```
50  35.6713149370015  12.3136211390968 0.5
51  37.7062176873006  13.4161527096284 0.5
52  39.5409386486964  14.7011835360391 0.5
53  41.146572466879  16.1484684300314 0.5
54  42.4978229712683  17.7352059501172 0.5
55  43.5734017068823  19.4363976299465 0.5
56  44.3563633261205  21.2252418199558 0.5
57  44.8343725564855  23.073555937504 0.5
58  44  25 0.5
59  43.850330992166  26.7537804131175 0.5
60  43.4036819488647  28.4799306605098 0.5
61  42.6670896615867  30.1512558795558 0.5
62  41.6521588710493  31.7414249558026 0.5
63  40.3748794387726  33.2253853599945 0.5
64  38.8553744326887  34.5797578414619 0.5
65  37.1175830956039  35.7832047596217 0.5
66  35.1888836912281  36.8167662506613 0.5
67  33.0996621696941  37.6641589332226 0.5
68  30.8828334480835  38.3120324470906 0.5
69  28.5733228480068  38.7501797832101 0.5
70  26.2075158600005  38.9716980913621 0.5
71  23.8226849034984  38.9730974320309 0.5
72  21.4564021135648  38.7543557591187 0.5
73  19.1459474057181  38.3189192672736 0.5
74  16.9277211445656  37.6736480983596 0.5
75  14.8366706694396  36.8287082624437 0.5
76  12.905739711913  35.7974114760439 0.5
77  11.1653493794185  34.5960054409288 0.5
78  9.6429188818831  33.2434178675491 0.5
79  8.36243355215558  31.7609582759172 0.5
80  7.34406696590393  30.1719822719522 0.5
81  6.60386311434664  28.5015235884948 0.5
82  6.1534836370687  26.7758996880482 0.5
83  6.00002409717675  25.0222971408308 0.5
84  6.1459021933106  23.268343310356 0.5
85  6.58881966968993  21.5416710944757 0.5
86  7.32179852428926  19.8694835792325 0.5
87  8.33329094469479  18.2781254642391 0.5
88  9.60736123964402  16.7926680116196 0.5
89  11.1239368999837  15.4365140574911 0.5
90  12.859124833673  14.2310293088837 0.5
91  14.7855877926655  13.1952057348796 0.5
92  16.8729750612031  12.3453623551224 0.5
93  19.0884006201863  11.6948881396607 0.5
94  21.3969612543155  11.2540310706472 0.5
95  23.7622864394189  11.0297366891465 0.5
96  26.1471113466902  11.0255386706896 0.5
97  28.5138639363684  11.2415031535139 0.5
98  30.8252568914129  11.6742276965804 0.5
99  33.0448750654768  12.316894883781 0.5
100  35.1377491901514  13.1593797298236 0.5
101  37.0709068029355  14.1884091956532 0.5
102  38.8138917162616  15.3877713003032 0.5
103  40.3392438435351  16.738570534696 0.5
104  41.6229318227048  18.2195255534427 0.5
105  42.6447316215382  19.8073044546168 0.5
106  43.3885451598144  21.4768923652921 0.5
```

```
107  43.8426539286612  23.2019855416704 0.5
108  42  25 0.5
109  41.8660856245696  26.5032403541007 0.5
110  41.4664522700368  27.9827977090084 0.5
111  40.8073960129986  29.4153621824764 0.5
112  39.8993000425178  30.7783642478308 0.5
113  38.7564710767966  32.0503303085667 0.5
114  37.3969139660899  33.2112210069673 0.5
115  35.8420480329088  34.2427469368186 0.5
116  34.1163696184672  35.1286567862811 0.5
117  32.2470661518316  35.8549933713337 0.5
118  30.2635878219694  36.4103135260776 0.5
119  28.1971836008482  36.7858683856087 0.5
120  26.0804089273688  36.9757412211675 0.5
121  23.9466128083933  36.9769406560265 0.5
122  21.8294124174001  36.7894477935303 0.5
123  19.7621634682741  36.4162165148059 0.5
124  17.7774347082955  35.8631269414511 0.5
125  15.9064948094986  35.1388927963803 0.5
126  14.178819742238  34.2549241223233 0.5
127  12.6216283921113  33.2251475207961 0.5
128  11.2594537364217  32.0657867436135 0.5
129  10.1137563361392  30.7951070936433 0.5
130  9.20258623265089  29.4331276616733 0.5
131  8.54029857599436  28.0013059329955 0.5
132  8.13732746474568  26.5221997326128 0.5
133  8.00002156063183  25.0191118349978 0.5
134  8.13054406769896  23.515722837448 0.5
135  8.52683865182783  22.0357180809791 0.5
136  9.18266183752197  20.602414496485 0.5
137  10.087681371569  19.2383932550621 0.5
138  11.227639003892  17.9651440099597 0.5
139  12.5845751210381  16.8027263349924 0.5
140  14.1371116932864  15.7694536933289 0.5
141  15.8607890776481  14.8816049156111 0.5
142  17.7284513705502  14.1531677329621 0.5
143  19.710674239114  13.5956184054235 0.5
144  21.7762284907034  13.2177409176976 0.5
145  23.8925720773748  13.025488590697 0.5
146  26.0263627838807  13.0218902891625 0.5
147  28.1439835220138  13.2070027030119 0.5
148  30.2120719554747  13.5779094542118 0.5
149  32.1980461112161  14.1287670432409 0.5
150  34.0706176964513  14.8508969112774 0.5
151  35.8002850342055  15.7329221677028 0.5
152  37.3597978513919  16.7609468288313 0.5
153  38.7245865968472  17.9187747440251 0.5
154  39.873149525578  19.1881647600937 0.5
155  40.78739145085  20.5491181039572 0.5
156  41.4529088272024  21.9801934559646 0.5
157  41.8592166730127  23.4588447500032 0.5
158  32  25 1.0
159  31.6577400395485  26.2354620803957 1.0
160  30.6644292669162  27.3501101028556 1.0
161  29.1172021123196  28.2349442422125 1.0
162  27.1673596913992  28.8034378420259 1.0
163  25.0055742869751  28.9999987317273 1.0
```

```
164  22.8432437810541  28.8054055049353 1.0
165  20.891819360333  28.2386871531087 1.0
166  19.3421280091148  27.3552622478712 1.0
167  18.3457118132796  26.2415196386882 1.0
168  18.0000088779072  25.0063706116659 1.0
169  18.3388249952802  23.7705986117018 1.0
170  19.329027825132  22.6550480033199 1.0
171  20.8737868584959  21.768806874265 1.0
172  22.8220423337528  21.1985394684745 1.0
173  24.983277153214  21.0000114144491 1.0
174  27.1461472757837  21.1926364847373 1.0
175  29.0991487464297  21.7575781510707 1.0
176  30.6513003634077  22.6395915813417 1.0
177  31.6508194549914  23.7524259521897 1.0
178  25 25 1.0
179  25 24  1.0
180  26 24  1.0
181  26 25  1.0
182  40  25 1.0
183  39.8155119213864  26.5635581227525 1.0
184  39.2665857990324  28.0886552009893 1.0
185  38.3667243430199  29.5377762707555 1.0
186  37.1380627148205  30.8752752571389 1.0
187  35.610824037508  32.0682518110537 1.0
188  33.8225759549706  33.0873606055313 1.0
189  31.8173065275859  33.9075331841197 1.0
190  29.6443421958554  34.5085946050647 1.0
191  27.3571344283731  34.8757597128092 1.0
192  25.011944900661  34.9999968293183 1.0
193  22.6664615473792  34.8782499190031 1.0
194  20.3783795308301  34.5135137623383 1.0
195  18.2039820316728  33.9147602890231 1.0
196  16.1967557721421  33.0967178827716 1.0
197  14.4060753276999  32.0795090864843 1.0
198  12.8759885909603  30.888155619678 1.0
199  11.6441332635465  29.551962883958 1.0
200  10.7408110284563  28.1037990967204 1.0
201  10.1882421768258  26.5792867852487 1.0
202  10.0000190240869  25.0159265291649 1.0
203  10.1807715606129  23.4521745057791 1.0
204  10.7260535613146  21.9264965292544 1.0
205  11.6224519557105  20.4764218527204 1.0
206  12.84791676814  19.1376200082997 1.0
207  14.3723035121159  17.9430233933152 1.0
208  16.1581146967769  16.9220171856625 1.0
209  18.1614222055596  16.0997165151419 1.0
210  20.3329478580418  15.4963486711862 1.0
211  22.6192755748518  15.1267555436928 1.0
212  24.9641653283158  15.0000285361228 1.0
213  27.3099365577433  15.1192849314277 1.0
214  29.5988870195365  15.4815912118431 1.0
215  31.7747121706637  16.0780352187633 1.0
216  33.7838901709207  16.8939453776766 1.0
217  35.5769984351263  17.9092515955778 1.0
218  37.1099293501593  19.0989789533542 1.0
219  38.3449752521312  20.4338620490979 1.0
220  39.2517559749817  21.8810648804743 1.0
```

```
 221  39.8079661542729  23.404988558187 1.0
228
0    0      1
1    1      2
2    2      3
3    3      4
4    4      5
5    5      6
6    6      7
7    7      0
8    8      9
9    9      10
10    10      11
11    11      12
12    12      13
13    13      14
14    14      15
15    15      16
16    16      17
17    17      18
18    18      19
19    19      20
20    20      21
21    21      22
22    22      23
23    23      24
24    24      25
25    25      26
26    26      27
27    27      28
28    28      29
29    29      30
30    30      31
31    31      32
32    32      33
33    33      34
34    34      35
35    35      36
36    36      37
37    37      38
38    38      39
39    39      40
40    40      41
41    41      42
42    42      43
43    43      44
44    44      45
45    45      46
46    46      47
47    47      48
48    48      49
49    49      50
50    50      51
51    51      52
52    52      53
53    53      54
54    54      55
```

55	55	56
56	56	57
57	57	8
58	58	59
59	59	60
60	60	61
61	61	62
62	62	63
63	63	64
64	64	65
65	65	66
66	66	67
67	67	68
68	68	69
69	69	70
70	70	71
71	71	72
72	72	73
73	73	74
74	74	75
75	75	76
76	76	77
77	77	78
78	78	79
79	79	80
80	80	81
81	81	82
82	82	83
83	83	84
84	84	85
85	85	86
86	86	87
87	87	88
88	88	89
89	89	90
90	90	91
91	91	92
92	92	93
93	93	94
94	94	95
95	95	96
96	96	97
97	97	98
98	98	99
99	99	100
100	100	101
101	101	102
102	102	103
103	103	104
104	104	105
105	105	106
106	106	107
107	107	58
108	108	109
109	109	110
110	110	111
111	111	112

112	112	113
113	113	114
114	114	115
115	115	116
116	116	117
117	117	118
118	118	119
119	119	120
120	120	121
121	121	122
122	122	123
123	123	124
124	124	125
125	125	126
126	126	127
127	127	128
128	128	129
129	129	130
130	130	131
131	131	132
132	132	133
133	133	134
134	134	135
135	135	136
136	136	137
137	137	138
138	138	139
139	139	140
140	140	141
141	141	142
142	142	143
143	143	144
144	144	145
145	145	146
146	146	147
147	147	148
148	148	149
149	149	150
150	150	151
151	151	152
152	152	153
153	153	154
154	154	155
155	155	156
156	156	157
157	157	108
182	182	183
183	183	184
184	184	185
185	185	186
186	186	187
187	187	188
188	188	189
189	189	190
190	190	191
191	191	192
192	192	193

193	193	194
194	194	195
195	195	196
196	196	197
197	197	198
198	198	199
199	199	200
200	200	201
201	201	202
202	202	203
203	203	204
204	204	205
205	205	206
206	206	207
207	207	208
208	208	209
209	209	210
210	210	211
211	211	212
212	212	213
213	213	214
214	214	215
215	215	216
216	216	217
217	217	218
218	218	219
219	219	220
220	220	221
221	221	182
158	158	159
159	159	160
160	160	161
161	161	162
162	162	163
163	163	164
164	164	165
165	165	166
166	166	167
167	167	168
168	168	169
169	169	170
170	170	171
171	171	172
172	172	173
173	173	174
174	174	175
175	175	176
176	176	177
177	177	158
178	178	179
179	179	180
180	180	181
181	181	178
182	44	1
183	95	45
184	45	2
185	97	47

```
186     47        3
187     48        4
```

APPENDIX C

PERMISSION FROM IEEE TO REPRINT

Sent by: j.hansson@ieee.org
To: Ripan Das <rdas1@lsu.edu>
cc:
Subject: Re: Need permission to reproduce figures from IEEE journals

Dear Mr. Das:

This is in response to your letter of 14 July 2003 in which you have requested permission to reprint, in your upcoming thesis/dissertation, four IEEE copyrighted figures. We are happy to grant this permission.

Our only requirements are that you credit the original source (author, paper, and publication), and that the IEEE copyright line (© 2003 IEEE) appears prominently with each reprinted figure.

Sincerely yours,

Jacqueline Hansson
IEEE Intellectual Property Rights Office
445 Hoes Lane
Piscataway, NJ 08855-1331 USA
+1 732 562 3828 (phone)
+1 732 981 8062 (fax)
e-mail: j.hansson@ieee.org

VITA

The author, Ripan Das was born in January 1978, in Assam, India. He graduated from Scottish Church College, Calcutta, in 1996.

In May 1997, the author attended Indian Institute of Technology, Kanpur, India, with a major in electrical engineering. He obtained a Bachelor of Technology degree in Electrical Engineering in May 2001. He continued his graduate study in electrical and computer engineering at Louisiana State University where he is currently a candidate for the degree of Master of Science in Electrical Engineering.